PETE 407 - Capstone Design Project II

Field Development Planning for the Poseidon Offshore Gas Field in Australia

Department of Petroleum Engineering, Nazarbayev University

Spring 2025

Team B

Amir Khakimov

Diana Nurkassova

Aruzhan Oralkhanova

Aray Serikkali

Adil Serik

Almat Tuzelbay

Table of Contents

Part 1: Introduction

1.1 Team Members

Our enthusiastic team consists of 6 people, each sharing their own experience and vision of the project. All of us are senior students pursuing a Bachelor's Degree in Petroleum Engineering at Nazarbayev University, Astana, Kazakhstan.

Amir Khakimov - Role: Team Leader, Reservoir Simulation Engineer, Dynamic Model Developer

He has completed internships at KazMunayGas Engineering Company, Atameken National Chamber of Entrepreneurs, and Turgay Petroleum Company in departments like Geology and Enhanced Oil Recovery. Amir participated and was awarded in PetroCup games, Case Championship on university scope. His technical skills include CMG, Well Prospector, and Kappa.

Aray Serikkali - Role: Economist, HSE Specialist

She is a Research Assistant in Petroleum Engineering working on a project titled “Evaluation of Natural Chemicals for Enhanced Oil Recovery.” Aray contributed to the publishment of the paper “Revisiting Troubleshooted Drill Stem Test: Methodological Framework Incorporating Artificial Intelligence” She was also an active member of AIESEC and SPE at Nazarbayev University, completed an internships at North Caspian Operating Company in Production and Technical directorates. She participated in PetroCup games, Case Championship in Nazarbayev University, winning the prizes. Her technical skills include CMG, PETREL, ECLIPSE, Well Prospector, and Kappa.

Almat Tuzelbay - Role: Basic Reservoir Engineer

He is an active member of Society of Petroleum Engineers, occupying the position in the External Department, he organized guest lectures for students with the specialists in oil and gas industry. Almat did his internship at KCP-Kazakhstan-China Pipeline in Almaty, which is the part of KazTransOil company. Almat participated in both the PetroCup games and the Case

Championship at the university level, earning awards for his efforts. His technical skills include MATLAB, CMG, Eclipse, Prosper, GAP, Emeraude, and Saphir.

Aruzhan Oralkhanova - Role: Geologist, Static Model Developer

She is a Research Assistant in the Petroleum Engineering Department, working on a project "A comprehensive study on asphaltene characterization and screening asphaltene deposition inhibitors for Kazakhstan crude oils". Aruzhan also was a vice-president of SPE Student Chapter. In terms of her experience, she had an internship in KazMunayGaz Engineering in the department of digitalization of field development. She competed in the PetroCup games and the university-wide Case Championship, receiving accolades for his participation. Aruzhan's technical skills include CMG, Eclipse, Petrel, Eclipse, Saphir, Well Prospector.

Diana Nurkassova - Role: Petrophysicist, Production Engineer

She is a Research Assistant in a project titled "A comprehensive study on asphaltene characterization and screening asphaltene deposition inhibitors for Kazakhstan crude oils", at the Petroleum Engineering Department. Diana was a member of Society Petroleum Engineers. Diana was also an intern at Manul, and published the article named "Investigating Falsified Motor Oil with Spectrophotometry and Fractional Distillation". She competed in the PetroCup games and the university-wide Case Championship, receiving accolades for his participation. Her technical skills include CMG, PETREL, ECLIPSE, Well Prospector, and Kappa.

Adil Serik - Role: Drilling and Completion Engineer, Facilities Engineer

His experience includes an internship at KazMunayGaz Engineering at Analytical Research Service for Borehole Operations department. Adil took part in the PetroCup games and the university-level Case Championship, where he gained valid experience and awards.His technical skills include Python, CMG, Eclipse, Prosper, and Saphir.

All together we utilized our diverse expertise on a comprehensive capstone project, considered it from different angles, ensuring thorough analysis and research was conducted.

1.2 Background Information on the Oil and Gas Industry in Australia

Australia is a significant player in the global energy industry, primarily due to its vast reserves of natural gas, coal, and other resources, as well as its strategic location in the Asia-Pacific region. Australia is one of the leading exporters of liquefied natural gas (LNG) and coal globally, which forms a substantial part of its economy. The energy sector contributes significantly to Australia's GDP and government revenues, including taxes and royalties (IEA, 2020).

Most of Australia's natural gas reserves are located in the northwestern and eastern regions, with major basins such as the Carnarvon, Browse, and Bonaparte basins playing a critical role in LNG production. The North West Shelf and Gorgon projects are among the largest LNG operations, with the latter being notable for its extensive carbon capture and storage (CCS) initiatives. Australia’s proximity to key Asian markets has further boosted its LNG exports, making it a leading supplier to countries like Japan, China, and South Korea.

The Australian coal industry, concentrated in regions like Queensland and New South Wales, is another cornerstone of the energy sector. Australia is a top exporter of metallurgical coal, crucial for steel production, and thermal coal, used for power generation. The coal sector has attracted significant foreign direct investment, leading to advancements in extraction technology and production efficiency.

Australia is also rich in renewable energy resources, including solar, wind, and hydropower. The government is actively promoting renewable energy development to diversify the energy mix and reduce carbon emissions. In recent years, Australia has become a leader in rooftop solar installations and large-scale renewable energy projects, aligning with global trends toward cleaner energy solutions.

In addition to coal and natural gas, Australia has emerging hydrogen and critical minerals sectors, including lithium, essential for battery technologies. These resources position the country as a key player in the transition to a sustainable energy future.

1.3 Literature Review of the Poseidon Field

The Poseidon Field is a gas field, located in the Browse Basin in the Timor Sea, offshore of western Australia. The field contains extensive reserves of Australia's natural gas, playing an imperative role in the Liquefied Natural Gas (LNG) export and therefore, the country's energy sector. The exploration and development of the Poseidon Field have been pivotal in advancing offshore gas technology and infrastructure, supporting Australia's position as a leading global LNG exporter. This literature review explores the geological characteristics, exploration history, and ongoing development efforts within the Poseidon Field, providing insight into its role in the energy landscape and its economic significance for Australia's LNG export market.

Kuske et al. (2015) studied the geology and the tectonic development of the Browse Basin. It was determined that within the Browse Basin several petroleum systems, such as Poseidon, Torosa and Crown contain a vast amount of hydrocarbon accumulations, specifically, natural gas, some of which is rich in condensates. The tilted fault blocks of the Jurassic period in the Plover and Montara formations of the Poseidon field specifically are of interest. These accumulations have a spill point connected to the Torosa field with complex fluid compartmentalization. Based on the discovery and exploration of the Crown and Proteus fields, Kuske et al. were led to believe that there is a potential connectivity within the basin fields. Moreover, it was reported that a complex history of hydrocarbon charging can be assumed due to variations in the gas-water contact levels throughout the basin. Kuske et al. concluded that the intricate tectonic structures and migration trends suggest the existence of large reserves of untapped hydrocarbons.

Khan et al. (2024) reported that the depth of the basin increases from 200 meters in the east to 2,000 meters in the west. The Plover Formation was described to have formed in a fluvial-deltaic to shallow marine environment. It consists mainly of sands, silts, shales, and minor carbonates, with volcanic rocks at the top from Jurassic volcanic activity. The formation is bounded by unconformities at both its top (Triassic period) and base (Late Callovian period). The Plover Formation was said to mainly represent a transgressive system, although some parts are linked to higher sea levels and coastal progradation.

Farfour and Foster (2022) gave further insight into the Plover and Montara formations in the Browse basin, which have been the main target of the exploratory activities. It was reported that the basin extends over the area of approximately 140000 km2, and is formed through the duration of six tectonic phases, encompassing the time from the late Carboniferous to the late Miocene, including thermal subsidence during the Triassic and Permian. Farfour and Foster described the Plover formation as a synrift succession, the deposition of which took place during active Jurassic faulting. It is laterally continuous across Browse and has a variable thickness, owing to its tectonic history. Due to these complexities, seismic interpretation has been challenging, especially near the top of Plover. The low impedance contrast between the shale zones and reservoirs made the traditional Amplitude Versus Offset analysis with Intercept and Gradient (I x G) attributes inconclusive for this case. However, AVO analysis with Pseudo-Poseidon Reflectivity (SPR) and Gradient (G) attributes and their crossplot, proposed by Farfour and Foster, was successful in reservoir and fluid identification with high sensitivity.

Dixit and Mandal (2020) have addressed the issue of hydrocarbon seepage in the Poseidon field. It was emphasized that the Poseidon field suffers from gas , which poses various drilling and health and safety risks. Therefore, it was of interest to identify the migration pathways and the origin of the . Dixit and Mandal developed a multi-layer perceptron (MLP) neural network, which utilizes seismic data to create a chimney probability cube (CPC), visualizing gas flow channels. Combining the results of CPC, Lambda-Rho crossplot analysis and spectral decomposition, it was concluded that the leak is coming from the Jamieson horizon, followed by migration in the southwest direction, towards the seabed.

Farfour et al. (2021) explored the use of seismic attribute analysis for detecting hydrocarbons and characterizing reservoirs in the Plover Formation, which contains three gas-saturated sandstone layers alternated with shale and siltstone. This geological complexity, influenced by tectonic and stratigraphic factors, made it difficult to trace the sandstone layers. To address this challenge, spectral decomposition and amplitude decomposition to extract frequency and amplitude components, respectively were employed. These methods helped identify and map the varying thicknesses of the gas-bearing reservoirs. By combining these frequency and amplitude

components into a single composite attribute, Farfour et al. were able to improve the delineation and tracking of reservoir zones. Additionally, the integration of seismic attributes with petroleum system analysis allowed the identification of new prospective areas, providing valuable insights for potential future drilling targets in the Poseidon field.

Niță et al. (2023) conducted a detailed study of the Upper Eocene-Lower Oligocene formations in the Caswell sub-basin of the Browse Basin, aiming to identify new hydrocarbon reserves in this mature petroleum region. They integrated lithology, structural and depth maps, and seismic attributes to develop a sedimentological model for the Prion Formation, revealing the potential of separate submarine fan systems to host hydrocarbons. The study specifically highlighted the "Prometheus" prospect, estimated to contain significant oil and gas reserves, despite migration and sealing challenges, and emphasized the basin's underexplored potential for hydrocarbon recovery.

Dixit et al. (2024) presented a novel approach to mapping reservoir heterogeneity using an impedance-based texture analysis, integrating rock properties via a 3D acoustic impedance volume derived from deep convolutional network inversion. This method enhances lateral variation sensitivity and offers improved resolution of gas-bearing sands and fault-bound facies distributions in reservoirs. The study, applied to the Poseidon field, demonstrated that this approach more accurately delineates hydrocarbon zones than traditional amplitude-based methods, thus providing a more effective tool for identifying productive zones and managing reservoir complexity.

Farfour and Foster (2022) employed machine learning techniques to enhance prospect identification and risk assessment using seismic attributes in the Poseidon field, offshore Australia. Their study used feedforward artificial neural networks (ANN) to integrate seismic attributes, generating probability cubes for gas chimneys and gamma-ray, while convolutional neural networks (CNN) identified subtle faults that could facilitate hydrocarbon migration. Combining fluid-related attributes, such as Scaled Poisson Reflectivity and AVO-G, enabled the identification of new prospective zones and allowed risk ranking based on geological factors.

Islam et al. (2023) explored automated fault detection using a pre-trained Convolutional Neural Network (CNN) model applied to 3D seismic data from the Poseidon field. Their work aimed to address the time it takes to manually conduct seismic interpretation by leveraging a CNN model with a UNET architecture, which is a type of deep learning model that processes complex images by breaking them down into sections to observe and model features, such as faults, more clearly. Results demonstrated that this approach provided clearer fault probability volumes and greater efficiency than manual, variance-based interpretations, proving the model's potential to streamline fault detection in structurally complex reservoirs.

1.4 Problem Statement

The Poseidon Field obtained excellent discovery results and solid appraisal findings but development activities are delayed because the Field Development Plan (FDP) is missing. Although well tests and seismic studies have confirmed large volumes of gas, the reservoir is not connected very well, it may be divided by faults into isolated sections, and will produce over the long term. The absence of well placement optimization together with inadequate infrastructure development makes it challenging to finalize development choices for the field. A comprehensive strategy involving interdisciplinary data collection from geology and petrophysics and engineering fields must be used to analyze field performance dynamics and design suitable production solutions and maintain both technical strength and economic viability of the development plan which produces efficient gas outputs and limits operational risks.

1.5 Objectives and Scope of the Study

A Field Development Plan (FDP) is a company's strategy for developing a petroleum field and managing its influence on the environment and society by considering production and costs (Ogeer, 2022). A successful FDP involves (EPConsult Energies, n.d.):

- Data Collection, Scope Definition, and Demarcation of Development Planning;
- Development of a Robust Reservoir Model;
- Interpretation of 2D/3D Seismic Data and Reserves Estimation;

- Production Profiles and Engineering Strategy Development;
- Qualitative Evaluation;
- Quantitative Evaluation: Economic Evaluation, Uncertainty Analysis, Risk Analysis, Health, Safety and Environmental;

The FDP also addresses environmental and societal impacts, forecasts production and costs, and outlines measures for risk management and infrastructure development. Its objectives include (Ogeer, 2022):

- Maximize resource extraction and recovery;
- Ensure sustainable operations;
- Optimize production efficiency and techniques;
- Minimize risks and costs from an oil and gas project;

Part 2: Methodology and Data Gathering

2.1 Regional Geology

A successful FDP includes a detailed study of subsurface conditions and geological analysis of the field. The process starts with acquisition and collection of the required geological data. Accurate analysis of the geological structures and stratigraphic features of the subsurface can be performed using data obtained from 3D seismic surveys and drilled appraisal wells. These geologic data can provide a comprehensive understanding and interpretation of depositional environments, fault systems, and hydrocarbon traps. It is an important part of the well placement and reservoir management process.

2.1.1 Seismic Data

There are three main geophysical methods used in petroleum exploration. The magnetic surveying and gravity surveying methods are used only in the pre drilling exploration phase, while seismic surveying is used in both exploration and development phases.

Seismic surveying is the one of the most important geophysical methods that explore the subsurface structures of the Earth by initiating a a seismic pulse at or near the earth's surface and recording the amplitudes and travel times of waves as they return to the surface after being reflected or refracted from the interface of rock layers. Seismic surveying is more concerned with reflected ray paths than refracted ones. The depth to the interface can be calculated using the following equation:

$$D = \frac{\nu t}{2}$$

where ν is the acoustic velocity and t is the two-way travel time. Moreover, the velocity of a P wave can be estimated using the following equation:

$$\nu = \sqrt{(k + \frac{4}{3}h)/p}$$

where k is the bulk modulus, h is the shear modulus, and p is the density.

The seismic reflection technology is based on reflection of sound waves from rock and structural interfaces (Kundu, 2023). The time of arrival and intensity of the reflected waves at the receiver was helpful in detecting the depth of the rock interface where the acoustic contrast influences the reflection sound wave.

A pulse from a seismic source is initiated at or near the Earth's surface. The amplitudes and travel times of the reflected waves are recorded by an array of receivers. The compressional (P-wave) and shear waves (S-wave) are generated by seismic sources and travel through solid

rock. The sound waves travel between the layers with different velocities and at each interface shall refract, as per Snell's law:

$$\frac{sin\theta_1}{sin\theta_2} = \frac{V_2}{V_1}$$

where V1 and V2 are the velocities of sound in the first and second rock layer, Sinθ1 and Sinθ2 are the sines of the incident and refracted ray angles.

The velocity of sound in the two layers will be different as their densities are different. In such a case, a part of the sound wave shall be reflected back and the other part shall be refracted. The proportion of the sound energy reflected shall depend on the acoustic impedance of the rocks. Acoustic impedance is the product of density and acoustic velocity for a medium. The reflection coefficient (R) of a normally incident P-wave on a boundary is given by:

$$R = \frac{(\rho_2 V_2 - \rho_1 V_1)}{(\rho_2 V_2 + \rho_1 V_1)}$$

where ρ1 and ρ2 are the densities of the upper and lower layers, V1 and V2 are their respective P-wave velocities. Any event and contact between subsurface rock formations which causes a large contrast in impedance shall generate a strong reflection.

In a seismic survey, seismic traces are generated at fixed intervals, showing the ray path from the surface to the deepest subsurface point. Each trace reflects the acoustic impedance changes at rock interfaces, creating "wiggles" on the trace. A synthetic seismic trace, derived from known densities and seismic velocities, provides a model of this process and helps validate real seismic data. Since seismic surveys are done before drilling, rock properties are estimated, which can lead to processing artifacts. After drilling, synthetic seismograms based on actual well data help refine and reprocess seismic data to improve accuracy.

For the Poseidon field, 3D seismic survey data is available. As shown in **Figures 1 and 2**, it was carried out within exploration permits WA-315-P and WA-398-P between October 2009 and March 2010 by ConocoPhillips. The survey area covers a total of 2,828 km² and it aims to provide

detailed subsurface coverage of the northern portion of WA-398-P and the entirety of WA-315-P, targeting potential exploration prospects in Cretaceous and Jurassic formations.

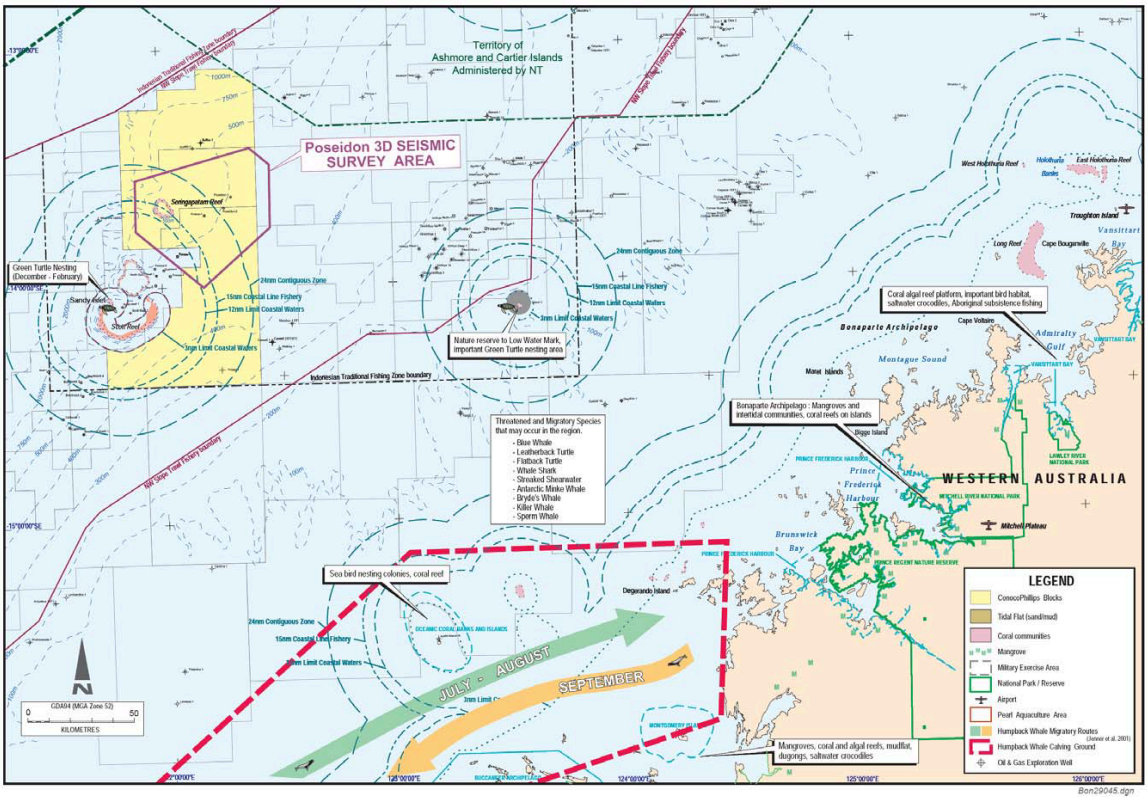

Figure 1. *WA-314-P, WA-315-P, WA-398-P and the Poseidon 3D Seismic Survey Regional Location (Le Poidevin, 2015).*

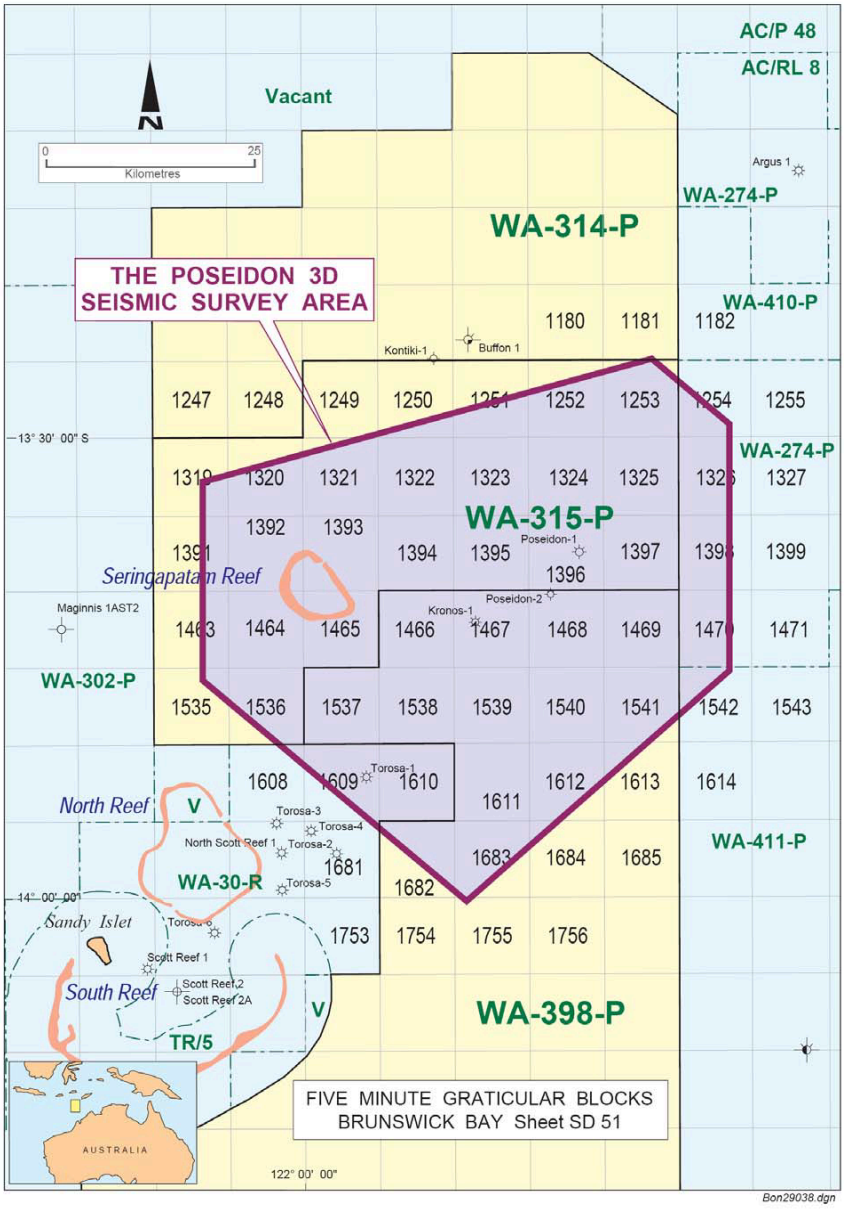

Figure 2. *Poseidon 3D Seismic Survey Location Map (Le Poidevin, 2015).*

2.1.2 Geological Setting

The Poseidon Gas Field is located in the Browse Basin, offshore of the Western Australia, in the Timor Sea (Figure 3). The Browse basin was formed as an intracratonic basin during the Carboniferous, containing more than 11 km of carboniferous to Cenozoic strata (Conocophillips,

2012). The Plover Formation from the Poseidon field is deposited as fluvial deltaic environment sediments in the syn-rift tectonic setting during the Early to Middle Jurassic. The formation comprises sandstone intercalated with shale, coal, and siltstone.

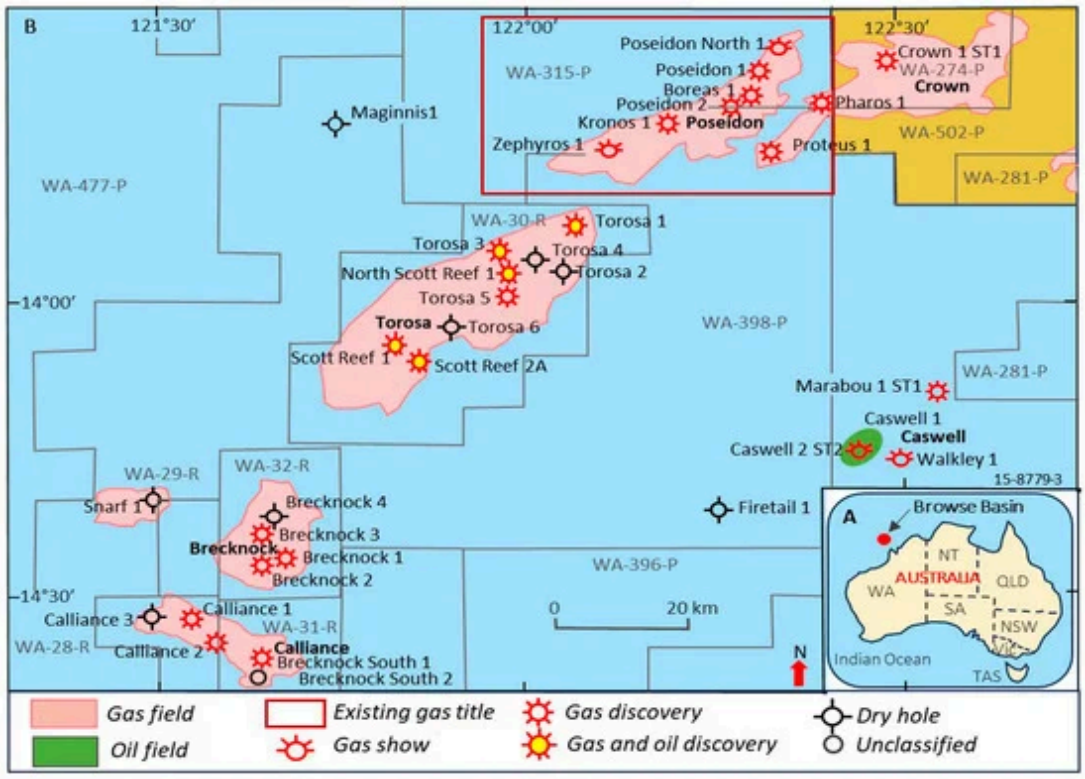

Figure 3. *Overview map of the Browse Basin and Poseidon field (Le Poidevin, 2015).*

The Browse Basin is a northeast-southwest trending passive continental margin basin covering approximately 140,000 km², with over 15 km of Paleozoic to Cenozoic sediments. It lies between the Scott Plateau and Argo Abyssal Plain to the northwest, and the Kimberley Block to the southeast, surrounded by the Yampi-Leveque shelves, the Rowley Sub-basin, and the Vulcan Sub-basin (Blevin, 1998).

2.2 Petrophysics

2.2.1 Well Log Analysis

The main tool of the Petrophysical analysis of the field are the well logs available for the two wells: Boreas and Poseidon - 2.

Well Logging is a method of indirectly measuring and recording rock and fluid properties in subsurface areas of oil and gas reservoirs. Although there are different ways of placing the logging tool and obtaining the measurements, most of the widely used well log techniques involve lowering a sonde at the end of a wireline into the wellbore until it reaches a certain depth, and pulling it back up towards the surface. The intended properties are measured and recorded as the tool is being lifted up (Baker, 2004).

The main logs used in the majority of the wells are the Caliper (CALI), Gamma Ray (GR), Neutron Porosity (NPHI), Bulk Density (RHOB), and Resistivity (RS, RD) logs, among many others.

Using the GR log generally helps differentiate the lithologies of interest from the non-productive shaly zones. GR logs produce high values in shale zones due to the gamma ray response of the radioactive isotopes found in shale (AAPG Wiki, n.d.). The values for different lithologies can be found in different ranges, and there is no set API value for the Gamma log for a certain rock type due to numerous factors like heterogeneity, fluids in place and so on. However, based on the literature and the field reports, the following GR ranges were used to differentiate the rock beds:

Table 2. GR ranges for different types of rocks (AAPG Wiki, n.d.)

Lithology	**GR range, API**
Sandstone	15-20
Silty Sandstone	20-30
Volcanics	30-90
Claystone	>90

Moreover, using the values of the GR log, shale volume, Vsh can be calculated using Larionov (1969) equation as follows:

$$V_{sh} = 0.083(23.7 \times IGR - 1) \quad (1)$$

Where

$$IGR = \frac{GR_{log} - GR_{min}}{GR_{max} - GR_{min}} \quad (2)$$

The next standard well log track used for analysis contains porosity logs. The overlap between NPHI and RHOB log curves helps estimate porosity in the measured depth intervals. The RHOB log tool emits gamma rays, and uses the Compton Scattering effect of electrons, to estimate the density of the encountered matter based on the amount of scattering and energy loss. The higher the intensity of the scattered gamma rays, the greater is the electron density, and therefore, the bulk density (Fanchi, 2010). Then, the porosity in the interval is estimated by the formula:

$$DPHI = \frac{\rho_{ma} - \rho_b}{\rho_{ma} - \rho_f} \quad (3)$$

Where

ρ_{ma} - density of the rock grain matrix;

ρ_{b} - bulk density;

ρ_{f} - fluid density;

The average ρ_{ma} for both of the wells was indicated as 2.65 gcc. The average ρ_{f} at reservoir conditions are equal to 0.2785 gcc in Boreas, and 0.245 gcc in Poseidon - 2 (Conocophillips, 2012).

Meanwhile, the NPHI log employs the process of emitting neutrons into the formation, and measuring the resulting energy loss of these neutrons after neutron capture takes place. Hydrogen atoms lead to the highest levels of energy loss, so the results of NPHI log measurements are strongly correlated with the hydrogen content of the fluids in place (Ward, 2003).

Analyzing the NPHI and the RHOB logs together can give insight into identification of zones of interest (see **Figure 4**). A phenomenon which is of particular interest to the Poseidon field is the “fluid effect” displayed by these two well logs. When a layer is saturated with gas, it shows an apparent high porosity via RHOB (low bulk density, since gas is lighter than water or oil), and an apparent low porosity via NPHI, because gasses are lighter and shorter chained hydrocarbons with less hydrogen atoms (Ward, 2003). These overlaps correspond to the “fluid effect", which can be helpful in identifying the type of hydrocarbon in pores.

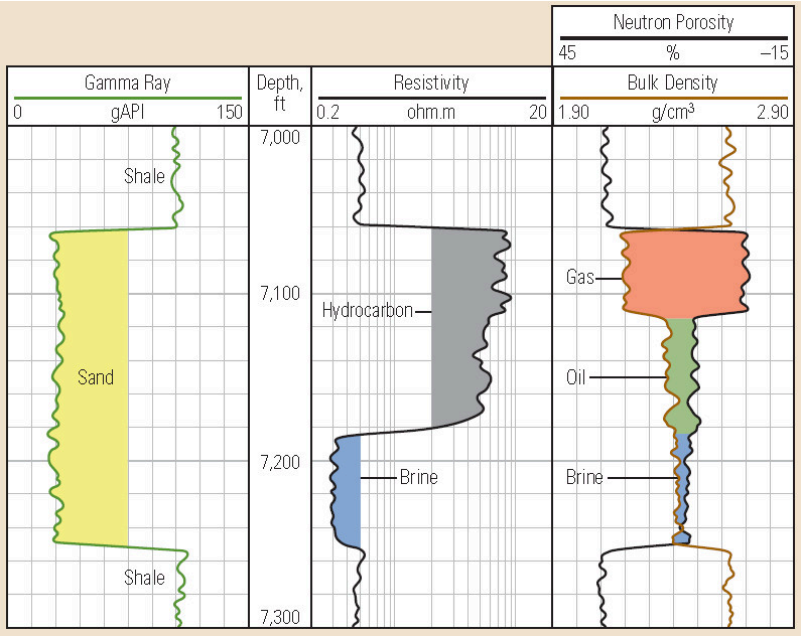

Figure 4. *GR, Resistivity logs, RHOB and CNL overlaps (Nazlan, 2016).*

Knowing the behavior of the RHOB and NPHI logs within gas zones, the porosity value for the gas zones should be corrected by accounting for both DPHI (porosity derived from RHOB) and NPHI (Neutron porosity). The gas-corrected porosity, GasPHI* can be calculated as:

$$GasPHI\ *= \sqrt{\frac{DPHI^2+NPHI^2}{2}} \tag{4}$$

Another important analysis tool is the Resistivity log, which has a varying range of depths of investigation. The main three groups are Shallow, Medium, and Deep resistivity logs. For the studied wells, Boreas and Poseidon - 2, Shallow and Deep resistivity logs (RS and RD, respectively) are available.

Majority of the resistivity logs either measure the resistivity directly, or derive it from the conductivity, but in general, all of them show the ability of the formation interval to carry electric current. The shallow logs carry out the measurements within the diameter closest to the borehole, where typically drilling mud invasion takes place, whereas deep resistivity logs provide information about the uninvaded zone's true resistivity (Khan & Islam, 2007). The discrepancies

between the different resistivity logs should be given attention to, such as the zones of separation illustrated in **Figure 5.** Especially, if there is a significant difference between the deep resistivity vs. medium and shallow, where the deep resistivity is noticeably greater, it could signify the presence of hydrocarbons, since their electrical conductivity is much smaller than that of the formation water (Baker et al., 2015).

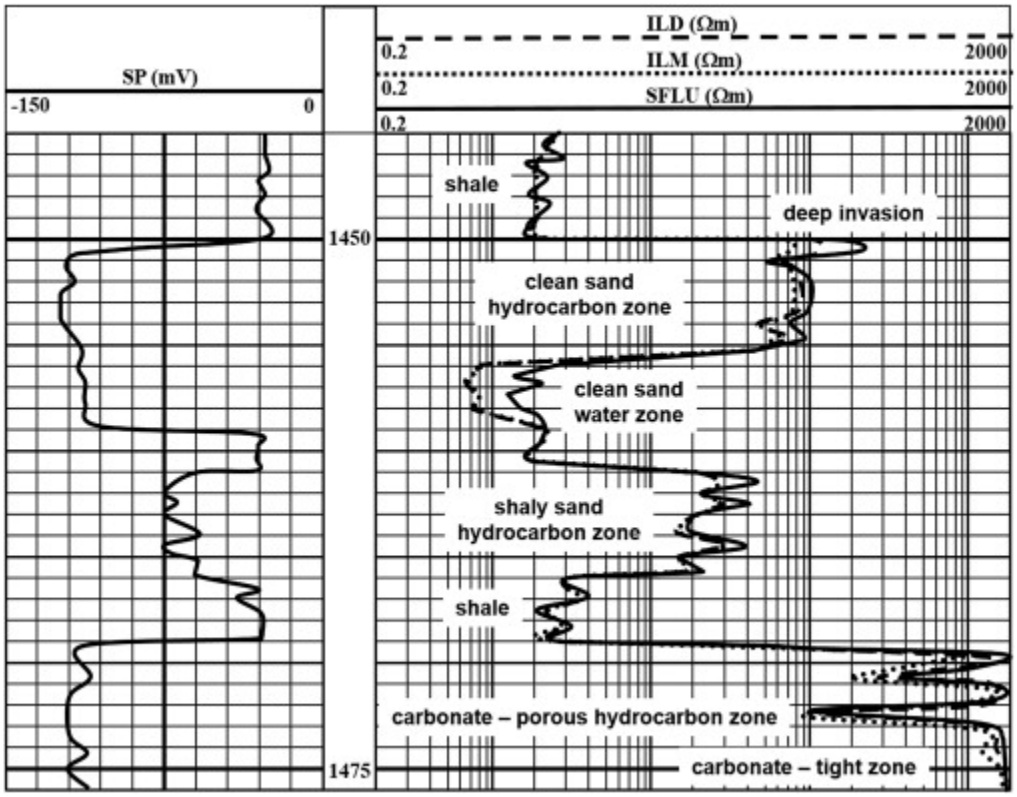

Figure 5. *Deep (ILD), Medium (ILM), and Shallow (SFLU) logs* (ScienceDirect, n.d.).

Also, considering porosity logs and resistivity logs, the water saturation values can be calculated along the logged depth interval using the Archie's equation:

$$S_w^{\ n} = \frac{aR_w}{\phi^m R_t} \tag{5}$$

The value of the cementation exponent "a" was taken as 1 as for standard calculations. The other parameters were available via Conocophillips, 2012:

Table 3. Input values for Sw calculations.

	Boreas - 1	Poseidon - 2
m	1.82	1.92
n	1.77	1.80
R_w, ohmm	0.14	0.08
R_t, ohmm	From the RD log	From the RD log

Well-log correlation was performed using Petrel™ software, to ensure an accurate interpretation of measured log-derived parameters for each well by depth. The final deliverables included petrophysical logs and interpreted reservoir properties (porosity, shale volume, and fluid saturations). These results were used to update the field development plan, optimizing well placement, and production strategies.

The available petrophysical data includes the aforementioned types of well logs and some additional coefficients and parameters for 2 wells across the depths of approximately 4000 - 5000 m. The performing company provides highly accurate well log measurements and interpretations, therefore, the reliability of data is sufficient.

2.2.2 Fluid Analysis

With the available chemical composition of the reservoir fluids, a Constant Composition Expansion test simulation was performed using WinProp by CMG. The fluid compositions for the Boreas - 1 and Poseidon - 2 wells are provided in Tables 4 and 5 below:

Table 4. Compositional analysis of the fluid sample in Boreas - 1.

Component	Reservoir Fluid Mole %	Reservoir Fluid Weight %
Carbon dioxide	17.148	31.396
Nitrogen	0.342	0.399
Methane	75.838	50.616
Ethane	3.406	4.261
Propane	0.97	1.78
i-Butane	0.226	0.546
n-Butane	0.283	0.685
neo-Pentane	0.009	0.026
i-Pentane	0.14	0.42
n-Pentane	0.127	0.382
Hexanes	0.179	0.663
Me-Cyclo-pentane	0.036	0.135
Benzene	0.048	0.168
Cyclo-hexane	0.053	0.199
C7+	1.193	8.324

Expectedly, the chemical composition is dominated by lighter hydrocarbons, especially Methane (>75 mol%). Some heavier chained, cyclic and saturated hydrocarbons are also present in small amounts. No H2S was found in the composition, pointing to a good quality and value of the reservoir fluid. Interestingly, the CO_2 content is significant (>17 mol% and >31 wt%). This indicates that the produced gas might need special treatment and projects for CO_2 sequestration.

Table 5. Compositional analysis of the fluid sample in Poseidon - 2.

Component	**Reservoir Fluid Mole %**	**Reservoir Fluid Weight %**
Carbon dioxide	10.511	21.666
Nitrogen	0.335	0.44
Methane	82.054	61.653
Ethane	4.089	5.758
Propane	1.176	2.43
i-Butane	0.276	0.751
n-Butane	0.291	0.792
neo-Pentane	0.008	0.026
i-Pentane	0.163	0.55
n-Pentane	0.105	0.355
Hexanes	0.174	0.704

Me-Cyclo-pentane	0.036	0.143
Benzene	0.064	0.239
Cyclo-hexane	0.062	0.249
C7+	0.634	2.743

The fluid in Poseidon - 2 has similar characteristics: high content of Methane (>82 mol%), trace amounts of heavier hydrocarbons, including straight and branched-chained hydrocarbons, cyclics, and aromatics. The CO_2 content of Poseidon - 2 is slightly lower than that in Boreas - 1, but still quite high (>10 mol% and >21 wt%).

Using the average values of the compositions from two wells, as well as the saturation pressure of the reservoir (5790 psi), and the temperature of 320 degF, CCE test was simulated in WinProp.

Constant Composition Expansion test is one of the standard laboratory tests conducted on a reservoir fluid sample. A PVT-cell, where a constant temperature is maintained, is initially filled with a fluid sample. The initial pressure is usually greater than the saturation pressure. Then the PVT-cell volume is gradually increased with decreasing pressure (Whitson Wiki, n.d.). The pressure and volume values are recorded at every step. Originally, the main parameters estimated in a CCE test were saturation pressure and volume changes with pressure. However, using WinProp simulation, other parameters of the fluid sample can also be estimated as a function of pressure, such as relative volume, fluid viscosities, Z-factor, density and compressibility.

2.3 Basic Reservoir Engineering

In the Poseidon Field of the Browse Basin, understanding the reservoir's physical properties is crucial for developing effective production strategies. The Boreas-1 Well Test

Interpretation and Boreas-1 WCR Volume 2 Interpretive Data offer detailed insights into key parameters such as permeability, porosity, water saturation. These data, derived from the Boreas-1 and Poseidon-2 wells, reveal the field's moderate permeability and porosity, along with a methane-dominated gas composition with significant CO_2 levels.

The Poseidon Field is a gas-dominated reservoir with estimated reserves of 7.6 trillion cubic feet (Tcf) of gas and liquids. The field is currently in the exploration phase, with ten wells drilled, including Poseidon-1, Poseidon-2, and Kronos-1, which have provided essential insights into the reservoir characteristics.

Well test interpretation was conducted in Sapphire by Cappa for Boreas-1 to assess permeability, reservoir pressure, and deliverability characteristics.

Table 6 . Reservoir data required for well test analysis.

Parameter	Boreas-1 Value
Initial Reservoir Pressure, psia	7141.5
Reservoir Temperature, °C	160
Net Pay, m	72
Distance to Faults, m	165 – 2034
DST Maximum Flow Rate, MMscf/d	30.2
Condensate/Gas Ratio (CGR), STB/MMscf	18

Monte Carlo simulation was used to estimate Gas Initially In Place (GIIP) considering uncertainties in reservoir parameters.

Table 7 . Reservoir data required for GIIP estimation.

Parameter	Value Range
Reservoir Area, km²	42.3
Net Pay, m	60 – 100
Porosity, %	8 – 25
Water Saturation, %	10 – 60
Bg (Gas Formation Volume Factor), ft³/SCF	0.00339 – 0.00513

Along with the main parameters, the normal distributions obtained from the Simulation software were used at the input data to estimate the GIIP value.

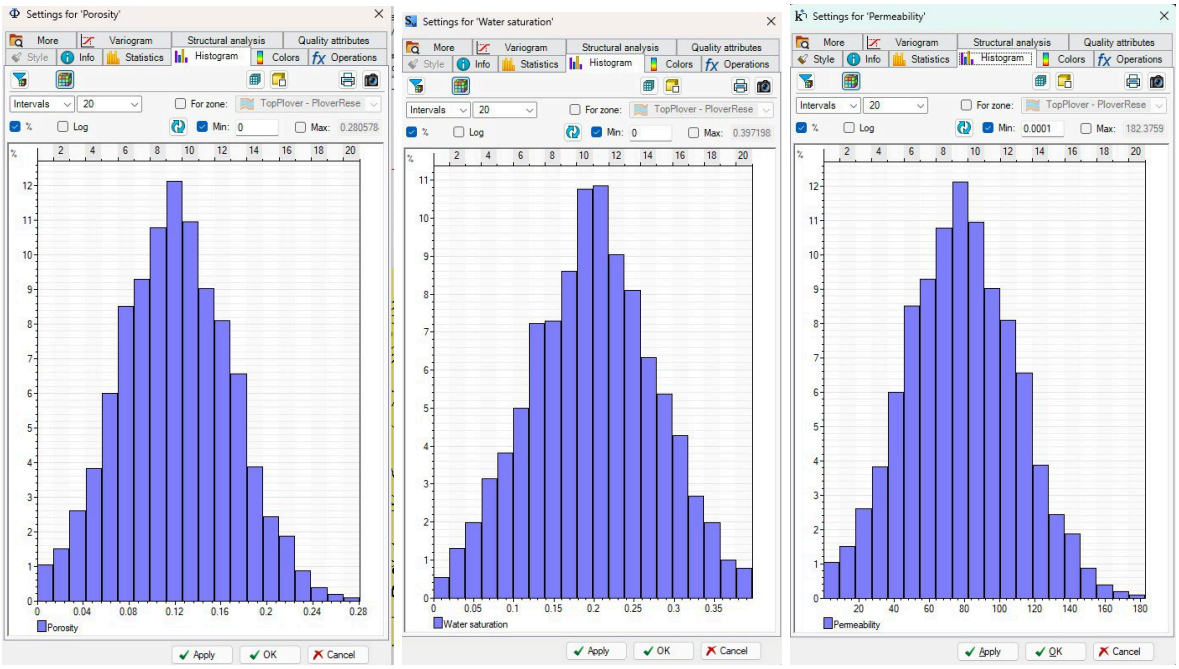

Figure 6. *Normal distributions for porosity, water saturation and permeability from the modeling.*

Below is a summary of the key reservoir properties derived from the data available for the Poseidon Field.

Table 8 . Key reservoir parameters summary.

Parameter	Range	Remarks
Porosity	8% – 18%	Moderate storage capacity with an average of 12%
Permeability	10 – 200 mD	Heterogeneous, with gas flow occurring through high-permeability streaks

Water Saturation	10% – 60%	Varies with lithology and depth, indicating zones of interest for fluid production
Drive Mechanism	Water Drive (Primary)	Supported by gas expansion initially with a water influx mechanism for long-term production

2.4 Drilling and Completion Engineering

One of the most prospective deepwater gas developments in Western Australia is the Poseidon gas-condensate field, which is located in the offshore Browse Basin. The field is located in a geologically complicated region with considerable resource potential and operating challenges, with water depths ranging from 400 to 500 meters. The field was found and evaluated using important wells like Poseidon-1, Poseidon-2, and Boreas-1. It has produced a wealth of data that is essential for creating the development plan for the future. The Callovian-aged sandstones in these wells have thick, gas-charged intervals with notable condensate yields. Operational experience from earlier drilling campaigns has brought several important lessons to light. Borehole instability, particularly in shale-rich intervals, was a consistent challenge. Pressure and temperature gradients in the deeper formations increased the risk of gas influx, highlighting the importance of accurate pressure control. Drilling operations also came upon weak formation zones that resulted in circulation losses, particularly between 2800 and 3000 meters. The engineering strategy for later well planning has been heavily influenced by these risks.

The proposed development of the Poseidon field will follow a five-spot configuration, comprising four production wells and one centrally placed injector well. This configuration minimizes the total number of wells needed while guaranteeing optimal reservoir drainage and

pressure support. In order to minimize inter-well interference and provide efficient reservoir coverage, each well will be placed around one to two kilometers apart.

2.4.1 Casing Design

The casing design will be tailored to accommodate geological hazards identified in previous drilling operations. The conductor casing will be set to depths around 570 meters to stabilize shallow formations and facilitate the installation of the blowout preventer (BOP). Surface casing will extend to 2300-2800 meters to isolate overburden zones and provide a foundation for intermediate sections. An intermediate casing string will be run to around 3900 to 4000 meters to manage unstable formations. The production zone will be completed using a 7-inch and 5-inch liner system, reaching total measured depths of up to 5200 meters. Described casing design with appropriate values for casing and hole sizes and depths illustrated further in **Table 9** and **Table 10**, for Boreas and Poseidon-2 wells respectively.

Table 9. *Boreas casing data*

Casing Type	Casing Diameter, in	Casing Depth, m	Hole Size, in	Hole Depth, m
Conductor	30	572.0	36	573.8
Surface Casing	13-3/8	2822.0	17.5	2829.0
Intermediate	9-5/8	4000.0	12.25	4009.0
Liner	7	4803.0	8.5	4805.0
Liner	4-1/2	5208.0	6	5210.0

Table 10. *Poseidon-2 casing data*

Casing Type	Casing Diameter, in	Casing Depth, m	Hole Size, in	Hole Depth, m
Conductor	30	577.7	36	581.8
Surface Casing	13-3/8	2287.5	17.5	2296.0
Intermediate	9-5/8	3890.8	12.25	3898.0
Exp Liner	7-5/8	3957.0	9.5	3965.0
Liner	7	4587.5	8.5	4588.0
Liner	5	5088.4	6	5112.1

Each part will have its own drilling bottom hole assembly (BHA). To increase drilling rates and hole cleaning in the tophole section, roller cone bits and traditional PDC bits, as shown in **Figure 7**, will be used. To guarantee accurate wellbore trajectory and real-time formation evaluation, the intermediate and production sections will make use of rotary steerable systems (**Figure 8**) in conjunction with Measurement While Drilling (MWD) and Logging While Drilling (LWD) instruments.

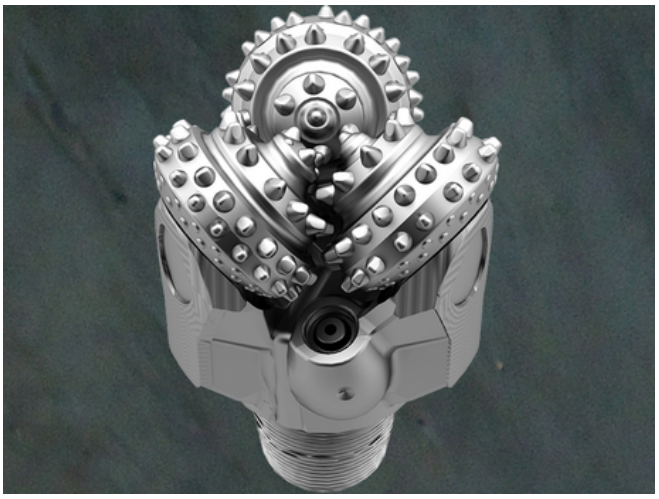

Figure 7. Roller cone bit for tophole section

Figure 8. Rotary Steerable System (RSS) for intermediate and production sections

2.4.2 Drilling mud selection

Mud system selection is critical in the context of Poseidon's high temperature, high pressure environment and reactive shale intervals. Water-based mud (WBM) will be utilized in the shallow sections due to their environmental compatibility and cost-effectiveness. Synthetic-based mud (SBM) will be adopted in deeper sections where their thermal stability, superior shale inhibition, and lubricity offer significant performance advantages.

According to the reports provided by ConocoPhillips, the operating company at the Poseidon gas field, the density of drilling mud that was used in Boreas well is 9.519 ppg. Based on the available data from drilling reports Mud Window, illustrated in **Figure 9**, for the future drilling operations is calculated further:

$$\rho = 8300/(0.052 * 16598.2) = 9.616\, ppg$$

$$Pressure\ gradient\ =\ 9.616\ *\ 0.052\ =\ 0.5\ psi/ft$$

$$S.G\ =\ 0.5/0.433\ =\ 1.155$$

$$Hydrostatic\ pressure\ =\ 9.519\ *\ 0.052\ *\ 16598.2\ =\ 8215.9\ psi$$

$$Maximum\ allowable\ MW\ (from\ LOT)\ =\ 13095.9/(0.052\ *\ 16598.2)\ =\ 15.173\ ppg$$

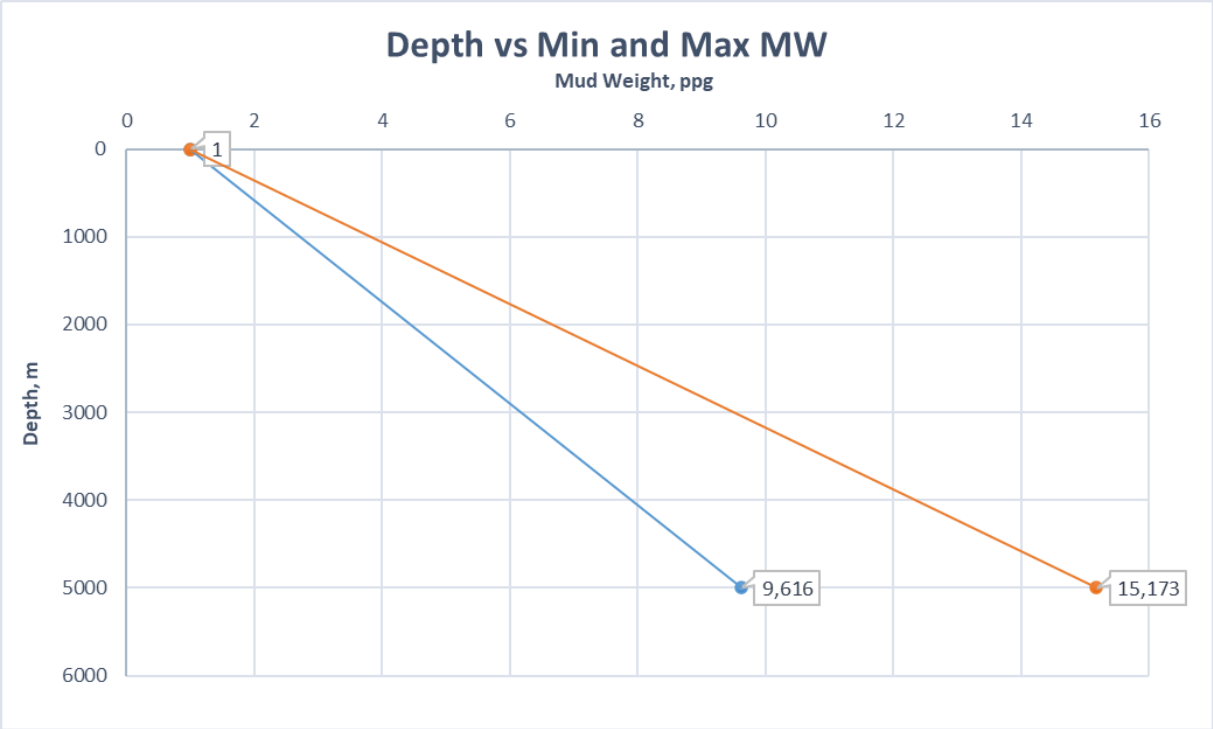

Figure 9. *Mud Window.*

Table 11 illustrates the comparison between mud density and other parameters of previous operations and planned drilling activities.

Table 11. *Comparison of provided and self calculated values of MD*

Parameter	Previous (report based)	Planned (our recalculation)
Mud density, ppg	9.519	9.616
Pressure gradient, psi/ft	0.494	0.5
Specific gravity	1.141	1.155
Hydrostatic pressure, psi	8300	8215.9

A multi-stage cementing system will be used to guarantee zonal isolation and cement integrity. A Class G cement slurry containing retarders and dispersants will be pumped for surface casing. This avoids early setting and guarantees placement at the desired depth. A lightweight lead slurry and a high-density tail slurry will be employed in a two-stage design for production liners. This method guarantees efficient drilling fluid displacement as well as top-of-liner coverage.

Real-time monitoring tools and lost circulation materials will be utilized to mitigate mud losses, especially in close proximity of previously identified weak formations. Optimizing pump rates and minimizing annular pressure losses, particularly during cementing operations, are key components of managing equivalent circulation density (ECD). Thorough laboratory testing is used to guarantee drilling and completion fluid compatibility in order to avoid formation damage and chemical instability.

2.3.2 Drilling rig selection

Given the Poseidon field's offshore and deepwater location, rig selection is a pivotal decision. Jack-up rigs are excluded due to their water depth limitations (<150 m). A comparison between drillships and semi-submersible rigs was made. Drillships are more costly and less stable in bad weather, despite their greater mobility and deeper drilling capabilities. The best option is determined to be the semi-submersible rig. These rigs are ideal for the 400–500 m water depth, have a bigger deck area for managing long risers, and provide good station-keeping. Additionally,

they have high-capacity marine risers that make well management easier and accommodate managed pressure drilling (MPD) systems.

The 18 3⁄4-inch, 15,000 psi-rated Blowout Preventer (BOP) system will be able to manage high-pressure formations while maintaining the highest level of safety. To improve pressure monitoring and function well in small mud windows, an MPD system will be incorporated. Dual derricks and sophisticated hoisting systems are additional rig capabilities that can enhance trip durations and overall operational effectiveness.

2.5 Reservoir Simulation

Reservoir simulation was conducted to build a predictive model of the gas production behavior which was then used as a tool to test various development scenarios and aid engineering decision making. This work combined the raw geological, petrophysical and fluid information available into a consistent numerical framework implemented into an industry-standard software which was then used.

The following softwares were used:

- Petrel – for creating a static model and defining the zones based on reservoir properties;
- WinProp – fluid property modeling and phase behavior definition;
- CMG GEM– dynamic simulation using a compositional modeling approach.

The process first consisted of building a relatively detailed static reservoir model in the Petrel environment. Based on petrophysical properties such as porosity, permeability and saturation a zone of interest was selected that exhibited favorable reservoir properties. That zone was designated to be the target interval input data to the dynamic.

The defined zone was exported to CMG GEM for simulation. By doing so, it was ensured that the most prolific and representative zone of the reservoir was simulated. The model was initialized with desired initial conditions of pressure, temperature and saturation. Fluid properties

were earlier defined in WinProp and these were imported to the present simulation model, allowing to capture the correct phase behaviour during the production.

Simulation scenarios were prepared in CMG GEM to simulate gas production from selected zones under different operational constraints. The model (well controls, boundary conditions and runtime settings) was set to enable high resolution modeling of the selected zone performance. This simulation scenario lays the groundwork for evaluating gas recovery efficiency, optimizing operational parameters, and assisting in future development planning.

2.5.1 Static Modeling

Static modeling is an approach in petroleum engineering that involves a three-dimensional representation of the structural, stratigraphic and petrophysical features and model of the subsurface reservoir geology (Noureldien and Merghany, 2015). Various data sources including geophysics, well logging, cores, well testing and production data are used in order to build the reservoir model.

The static modeling started with the collection of the relevant geological information in a suitable database or file format, considering geological contact points and orientation measurements. This information then required processing in the form of interpolation of lines between points, surfaces between lines, and finally geological volumes between surfaces. The geological model of the reservoir combines all available geological and geophysical data, presenting them in a consistent form, convenient for visualization and further use.

The Petrel software platform by Schlumberger was used for static modeling. The development of a static model of the Poseidon field aims to create a three-dimensional geological model reflecting the spatial distribution of the main reservoir properties, well placement, as well as a reliable assessment of volumes and development planning. Moreover, the static model can be further used as input for dynamic modeling.

The static model of the Poseidon field was constructed using the well headers, well deviations, well logs, well tops and seismic data gathered from the field. The **Table 12** presents the format and use of the input data:

Table 12. *Input data for Static Modeling in Petrel*

Data	Format	Use in Static Model
Well Header	.txt	Defines well locations in X-Y
Well Deviation	.dev	Tracks well trajectory
Well Log	.las	Provides petrophysical properties
Well Top	.txt	Marks formation boundaries
Seismic	SEG-Y	Offers subsurface structural information

2.5.2 Dynamic Modeling

Dynamic modeling was performed to predict the evolution of reservoir pressure, saturation and gas production performance in the zone of interest. It immediately follows the static modeling performed in Petrel and utilizes the deluxe fluid characterization in WinProp. The objective of the dynamic modeling process is assisting in the field development planning process by forecasting reservoir performance for multiple development scenarios.

Simulation was carried out in CMG GEM which is a compositional simulator calibrated model to multi-phase flow in gas-condensate and volatile oil reservoirs. The dynamic modelling was including the following steps:

Model Setup

The static geological model is exported from Petrel to GEM through a grid upscalling procedure preserving layer thicknesses, faults and structure geology. Petrophysical properties such

as porosity, permeability, net-to gross ratio and water saturation were distributed in each grid block. Local grid refinement (LGR) around wellbores is used to better resolve flow dynamics around wells and accurately capture early-time behavior.

Fluid characterization

The fluid model was generated in WinProp. PVT laboratory data was used to define the components and phase behaviour of the fluid. EOS were used in the compositional model for the hydrocarbon phases along with the matching of the saturation pressure and viscosity correlations. The fluid composition model was then imported into GEM and formed the compositional model which was used to model gas flow and condensate dropout and reservoir fluid and injection fluid interactions.

Initialization and Controls

The model was initialized with reservoir pressure and temperature gradients based on well test data and regional assumptions. Relative permeability and capillary pressure functions were incorporated based on core analysis and analog data.

Well controls, as existed in the models, were defined for the simulation as follows:

- Bottomhole pressure constraints to ensure realistic operating conditions;
- Maximum allowable production rates;
- Water or gas injection rate limitations where applicable.

Production Strategy Design

Several production scenarios were defined in order to investigate the effect of operating strategies on the reservoir performance. The production scenarios used were:

- Constant bottomhole pressure depletion to emulate natural depletion;

- Production is choked in order to study deliverability when surface facility limitations exist;
- Cyclic production to analyse recovery enhancement through pressure cycling;
- Injection-assisted case of pressure maintenance by water or gas.

Each scenario was run over a specified simulation period, with time-stepping being controlled by a combination of convergence criteria and reservoir response.

Output Monitoring and Validation

The simulation configuration was executed, tracking certain variables including average reservoir pressure, gas rate, gas-oil ratio, cumulative GOC production and more according to the different flow models. Several plots were generated in Petrel, including satellite well performance and fluid distribution variations with time gas breakthrough timing for multi-well simulation cases and also export them for diagnostic outside Petrel environment.

No calibration/history matching was done at this stage and the simulations were simply forward looking and scenario based. However, model structure was constructed in a manner that easily accommodates a history matching process in future work if production data become available.

Results of dynamic modeling are used as input to the technical assessment and comparison of field development options and are later combined with results of economical and surface facility evaluation.

2.6 Production Engineering

One of the standard methods used for flow assurance is Nodal analysis, which will be performed to evaluate the well's performance, considering both the reservoir inflow (IPR) and the outflow (TPR) through the wellbore and surface facilities (see **Figure 10**). The IPR curve characterizes the relationship between bottom-hole pressure and flow rate, indicating the well's ability to deliver fluids from the reservoir into the wellbore. The TPR curves represent the pressure

which is needed to lift a specific amount of fluid to the surface at a certain wellhead pressure. By simultaneously expressing IPR and TPR curves on the same plot, it is possible to establish the optimum operating conditions to maximize well production. Using correlations and approximations selected based on the reservoir characteristics, a production engineer simulates the performance of one well, and the obtained results dictate what surface pressure, inflow, sizes of tubing and choke etc. are optimal for that particular well (Lea & Rowlan, 2019).

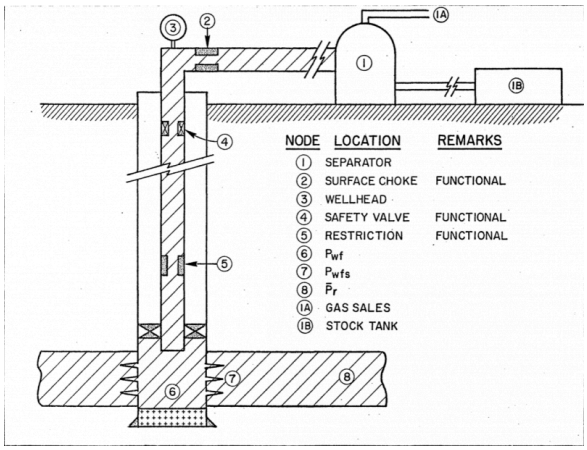

Figure 10. *Locations of the main nodes (PengTools, n.d.).*

Selecting one of the nodes, calculations can be carried out to evaluate the performance and the productive capacity of the well. Since the studied formation layer contains water with free gas and negligible amount of oil, the used correlations have to account for the two-phase flow, which complicates the calculations.

Nodal analysis can be carried out via Pipesim by SLB. Darcy's equation for inflow performance was chosen for the IPR estimation. The equation can be altered to account for the specifics of gas flow, thereby providing a more accurate estimation of the inflow for the Poseidon gas field. The Darcy equation for gas inflow performance can be derived as:

$$q_{gas} = \frac{kh}{1422\times10^{3}T_{R}}(P - P_{wf})J_{D} \quad ()$$

Where

$$q_{gas} = gas\ flow\ rate$$

$$k = permeability,\ mD$$

$$h = thickness,\ ft$$

$$P = reservoir\ pressure,\ psi$$

$$P_{wf} = well\ flowing\ pressure,\ psi$$

$$T_R = reservoir\ temperature,\ R^o$$

$J_D = dimensionless\ productivity\ index,\ dimensionless.$

TPR curves were computed by the Pipesim algorithms based on the input data, presented in **Table 13** below:

Table 13. Input data summary for the Production Engineering analysis.

	Boreas - 1	**Poseidon - 2**
Reservoir pressure, psi	7141	7320
Temperature, degF	329	363.2
Thickness, ft	213.3	203.4
Borehole diameter, in	11	9
Permeability, mD	70	50

2.7 Economics

Prior to making an investment choice, the economic evaluation is the last phase of the technical and financial assessments. For all economic evaluation the currency will be in US dollars ($). The economic evaluation plan consists of three key aspects: generating forecasts of key technical and economic parameters, modeling of the fiscal system, and calculation of economic indicators (Ganat, 2020).

1. **Making Predictions for Key Technical and Economic Factors**
    - Collect the data of the annual oil and gas production forecast from the reservoir engineering department. The predictions are estimated for 20 years, and the forecasting will be achieved through machine learning ARIMA model.
    - A forecast of the oil and gas prices per year at which production is expected to be sold.
    - The anticipated yearly capital expenditures needed for oil and gas project exploration and development.
    - The anticipated yearly operating costs necessary to sustain the oil and gas output.
2. **Fiscal System Modeling**

The ways in which petroleum corporations are required to pay the government a share of their profits are governed by the tax laws and contract terms of each nation.

These are collectively referred to as a nation's budgetary system. It is necessary to develop a model that will ultimately determine the yearly after-tax cash flow that the oil and gas company will receive from the project as a whole. Accordingly, production pooling agreements and royalty or

tax regimes are the two main categories of fiscal systems from the standpoint of economic evaluation.

3. **Economic Indicator Calculation**

Condensing future cash flow projections into a variety of economic indicators that will aid in project investment decision-making is the last step in the economic appraisal process. The time value of money is one of the most important components. The most accurate indicator of a project's true monetary worth is its net present value (NPV). The corporate discount rate is developed using a variety of techniques. There are three additional economic metrics in addition to NPV:

a. The only discount rate that requires the NPV to be precisely equal to zero is the internal rate of return, or IRR.

b. Payout, often known as payback, is a key metric that shows how long it will take the project's income to cover its capital expenses.

Depending on its own advantages and disadvantages, a wide range of additional economic indicators may be employed. However, when combined, they typically provide a very clear indicator of whether the project should move forward or not.

2.8 Health, Safety, and Environment (HSE)

Overview of Regulation Internationally and in Australia

In this thorough investigation, the Poseidon field development project site's Health, Safety, and Environment (HSE) component is crucial. It is a manifestation of our proactive commitment to the welfare of the ecosystem and the local communities, as well as our responsible stewardship of the

natural resources. Therefore, complying with the strict standards is significant. The standards can be divided into three groups: International Laws and Regulations, Australian Commonwealth, and State and Territory.

1. International laws and regulations:

London Protocol and convention

Hong Kong Convention

OSPAR (North Sea)

IMO's Resolution A.672 (16)

2. Australian Commonwealth:

Australia Offshore Petroleum and Greenhouse Gas Storage Act 2006

Radiation Protection and Nuclear Safety Act 1998

Environment Protection (Sea Dumping) Act 1981

Environment Protection and Biodiversity Conservation Act 1999

National Environment Protection (Movement of Controlled Waste between States and Territories) Measure 1998

3. State and Territory:

WA Petroleum (Submerged Lands) Act 1982

WA Environmental Protection (Controlled Waste) Regulations 2004

WA Environmental Protection Act 1986

WA Radiation Safety Act 1975

2.9 Software Procedures

2.9.1 Petrel Procedure

The geomodeling and property modeling step in the Poseidon Field was performed using Schlumberger's Petrel software. The aim of this section was to build a high-resolution static model that was imported into CMG for dynamic simulation.

The first step begins with creating a new project and selecting the coordinate reference system (CRS) for the field as shown in Figure **11.**

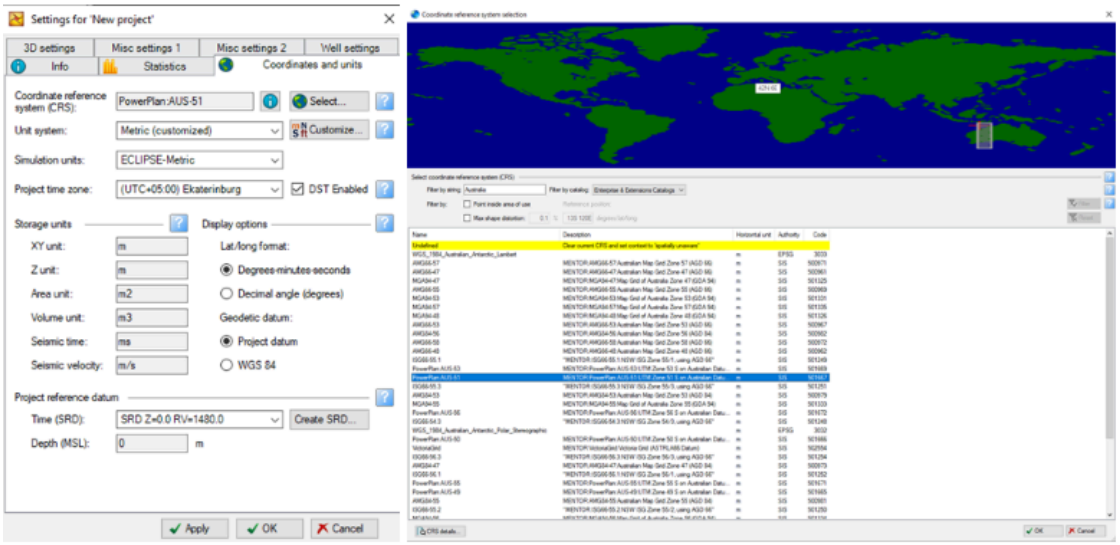

Figure 11. *CRS window.*

Once the new project was created, various types of data were imported into Petrel. The Well Headers file was imported by opening a .txt file containing information about the well name, well path length, and top position of the well.

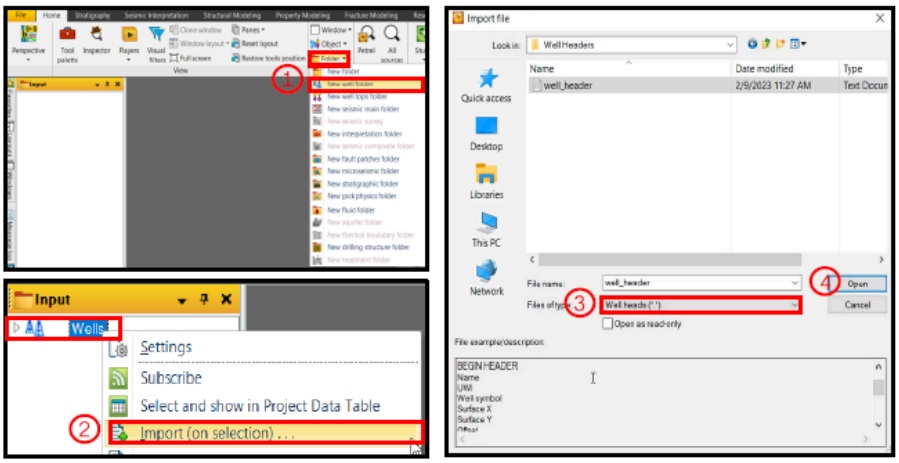

Figure 12. *Data Import: Well Header.*

The well deviations were imported by opening a .dev file containing information about the well path description, while well logs and well tops were imported by opening a .las file and a .txt file respectively. On the well section window, data on each well can be scaled, flattened, and correlated.

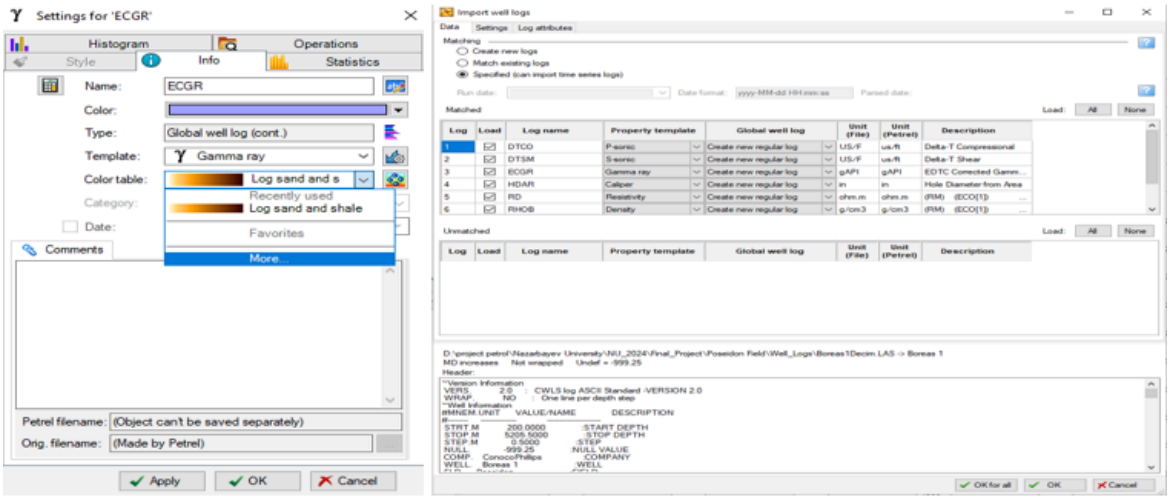

Figure 13. *Data Import: Well Logs.*

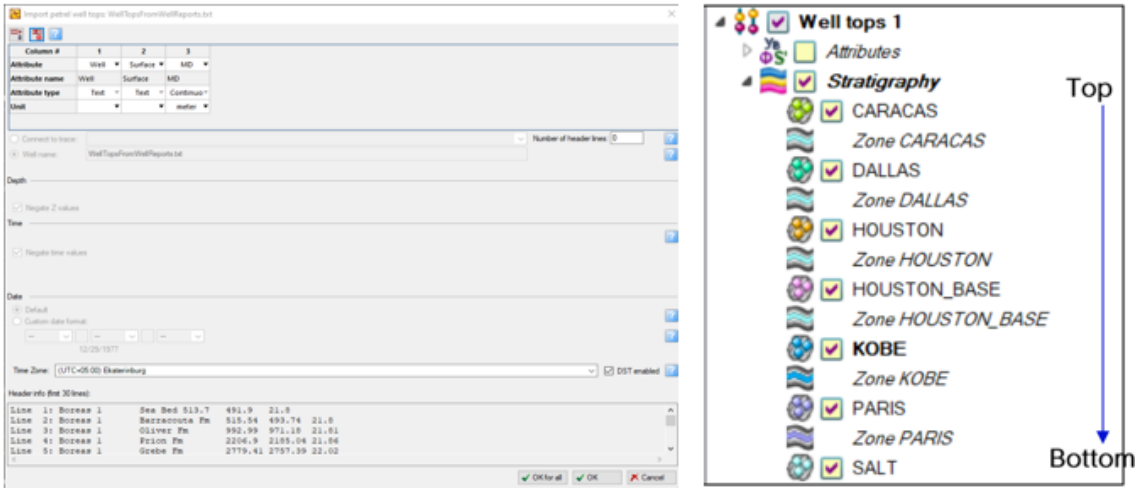

Figure 14. *Data Import: Well Tops.*

The seismic data was imported by opening a SEG-Y file. By choosing the required seismic data file, the seismic cube can be imported too.

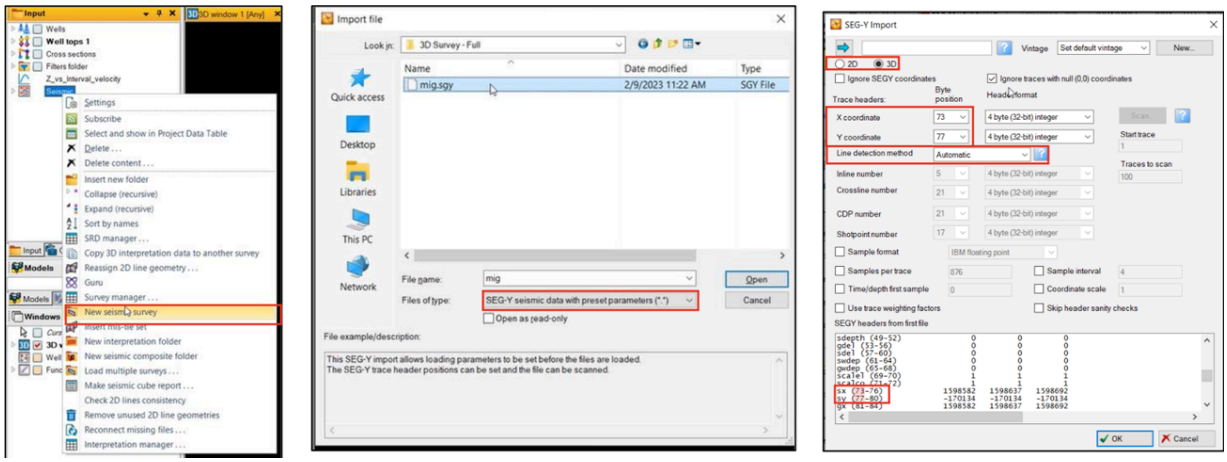

Figure 15. *Data Import: Seismic Data.*

Moreover, the seismic section across the well was visualised using intersection player move across inline/crossline and time slice.

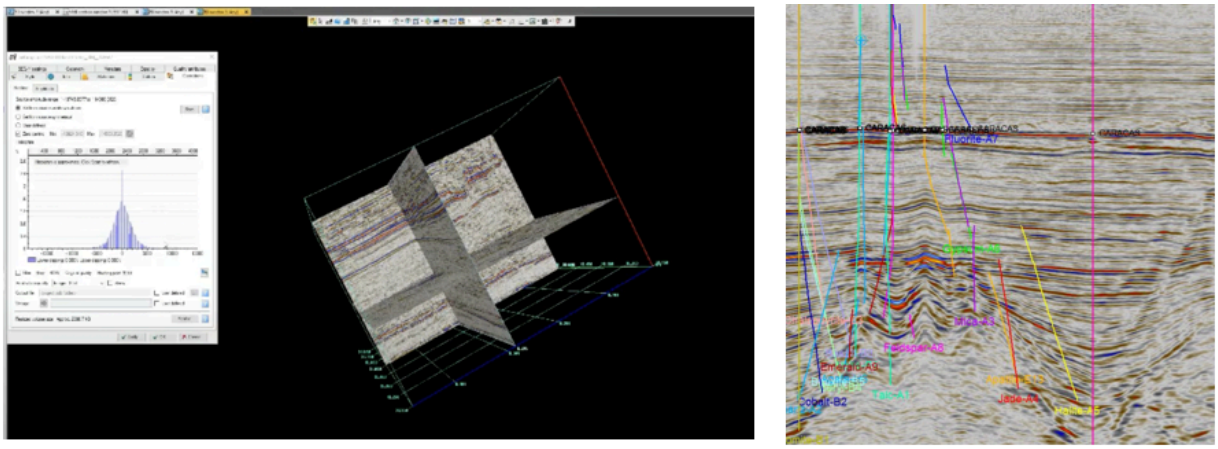

Figure 16. *Visualisation of the Seismic Data.*

The next step was the import of the check shot surveys. It is important for the identifying time depth relationship (TDR) for detailed subsurface interpretation.

Horizons and faults can be interpreted on the interpretation window by displaying well with well tops and using sticks. Tool palette for seismic interpretation contains manual interpretation, guided autotracking, seeded 2D autotracking, seeded 3D autotracking, paintbrush select, and fault interpretation buttons. During the fault interpretation, the projection of faults were displayed and direction of the faults were analysed.

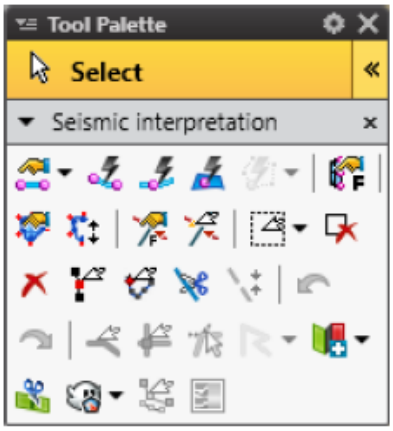

Figure 17. *Tool palette for seismic interpretation.*

Structural modeling started from the creating and visualising simple grid. During this step, the faults and horizons applied. However, they were edited to more accurately visualize the reservoir model.

Seismic and Structural Interpretation

Seismic and Structural Interpretation was carried out to define three key stratigraphic surfaces, which were the Top Plover, Plover Reservoir and Nome Formation, which bounded the structural framework of the reservoir and were considered the key elements necessary for the construction of grid. The three defined horizons are shown in **Figure 18**, which show the structural layering throughout the selected region.

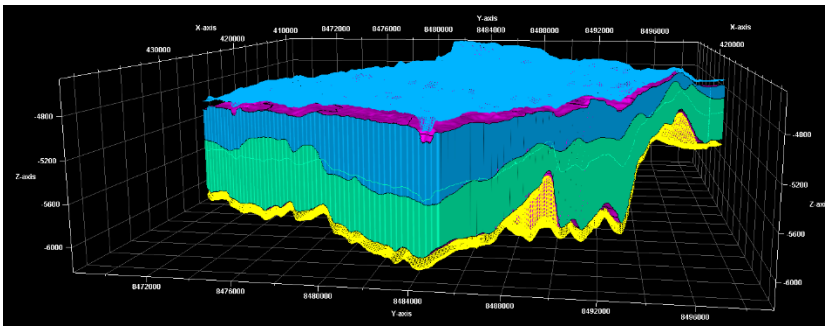

Figure 18. *Full-field static model with selected sub-region for dynamic simulation.*

Fault Modeling and Grid Construction

Faults intersecting the Poseidon Field were interpreted in Petrel, modeled, and merged into a singular 3D corner-point grid which honored both the fault geometries and the stratigraphic surfaces. A smaller zone of interest was then selected from the full-field model due to the simulation cell number limit of CMG. This smaller sub-region is shown in **Figure 19** which shows the portion of the extracted portion of the reservoir selected for dynamic simulation.

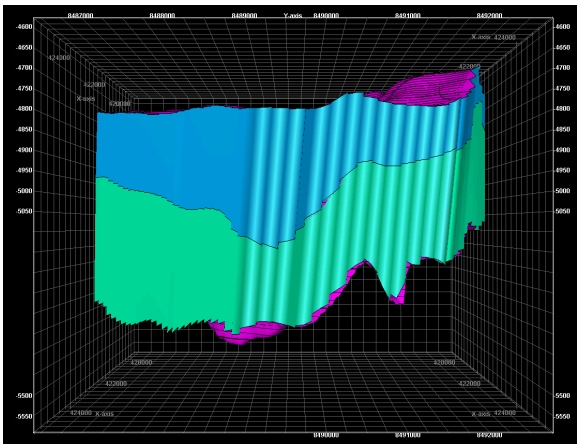

Figure 19. *3D Stratigraphic Model of the Selected Simulation Region.*

Zone choose based on reservoir quality

The dynamic modeling zone was selected from the petrophysics results of the well log data. The maps of key reservoir quality properties such as resistivity in **Figure 20**, solution gas–oil ratio and neutron porosity **(Figure 21)** were used in determining areas of high reservoir quality. These properties were derived from the upscaled well log properties. Visualising these properties aided in determining the petroleum quality within the dynamic modeling zones, thus ensuring efficient modeling efforts.

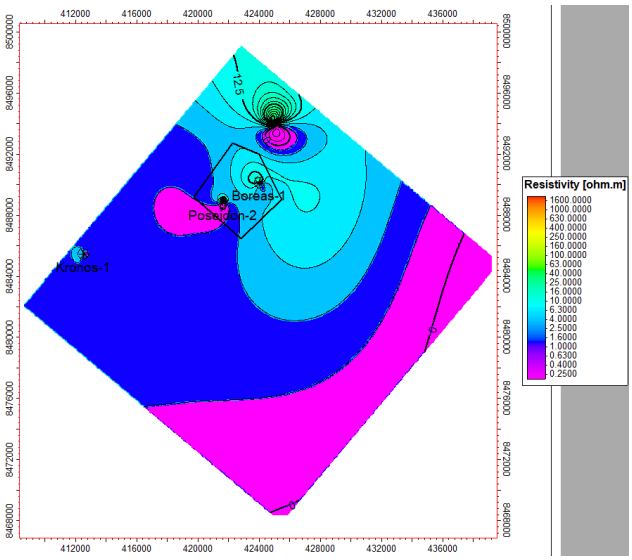

Figure 20. *Resistivity map indicating high gas saturation zones.*

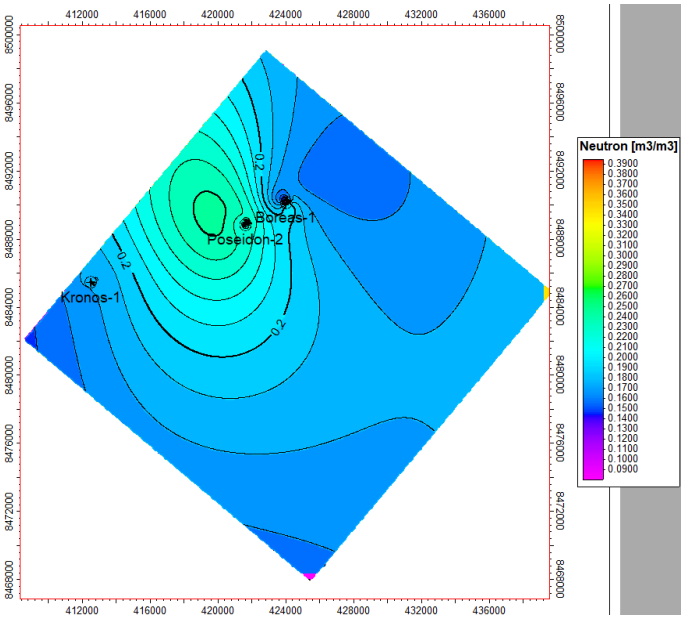

Figure 21. *Neutron porosity distribution identifying high-porosity areas.*

Fault modeling and surface creation

Surface modeling within Petrel was conducted using the surface creation window**.** Structural horizons were subsequently produced from the input boundary definitions, and fault centerlines were incorporated into appropriate positions on the horizon to identify geological settings prior to grid creation. Major intersecting faults within the Poseidon Field were interpreted and imported into the model to attempt to capture reservoir compartmentalization. All imported faults were defined in line with stratigraphic boundaries and incorporated into the surface creation methodology.

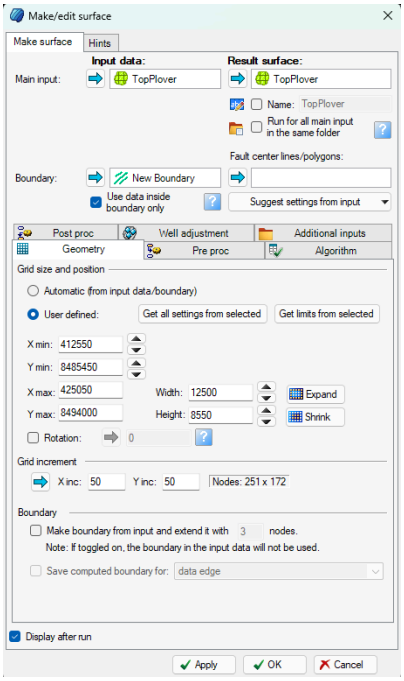

Figure 22. *Surface Creation Setup for Top Plover Horizon in Petrel.*

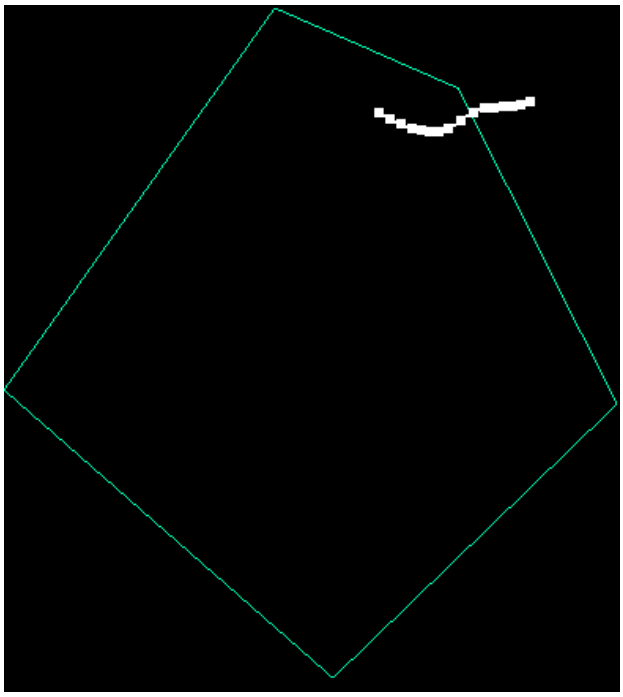

Figure 23. *Defined Boundary and Fault Line for the Simulation Region.*

3D Grid Construction

The conformable stratigraphic horizons and associated structural framework surfaces were used to build a corner-point 3D grid, which was the model suitable for simulation. As indicated in **Figure 24**, the corner-point 3D grid was built by assigning the conformable stratigraphic horizons to the corresponding layers of the 3D grid, Top Plover, Plover Reservoir and Nome Formation. The geometry of the stratigraphy and the internal faults are resolved by the 3D grid hence distribution of rock and fluid properties is achievable.

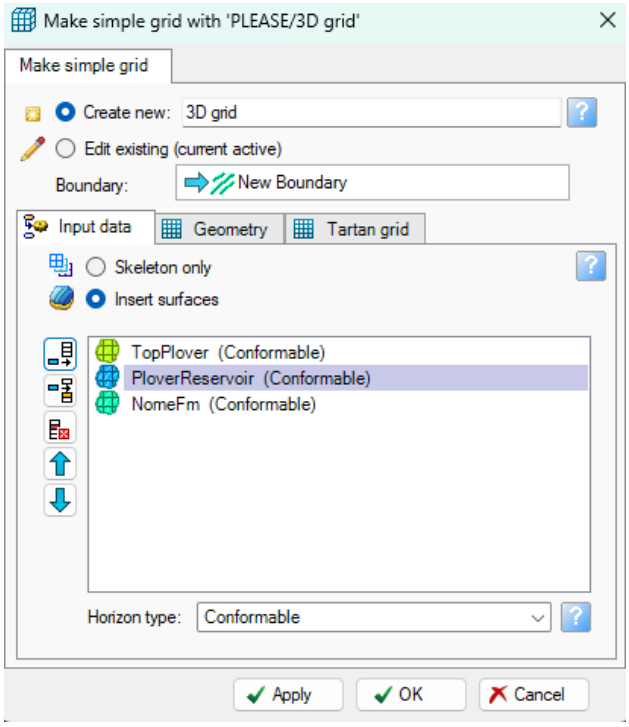

Figure 24. *Horizon Selection for 3D Grid Construction in Petrel.*

Property Modelling

Upscaled petrophysical data was used to populate the simulation grid with:

- Porosity , based on gas-corrected neutron porosity logs (**Figure 25**);
- Permeability is derived from the log-core correlation and the distribution geostatistically (**Figure 26**);
- Water saturation and gas saturation, which are used to determine initial distributions of fluids within the grid (**Figures 27 and 28** respectively).

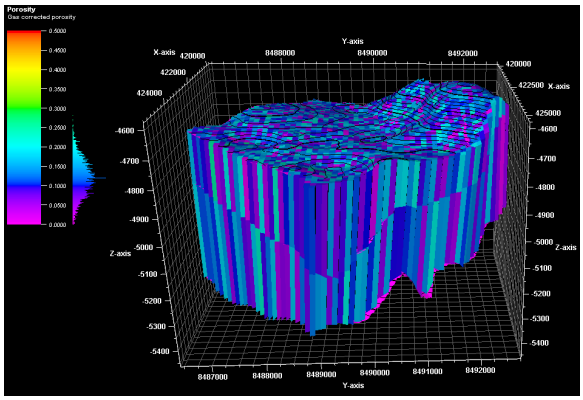

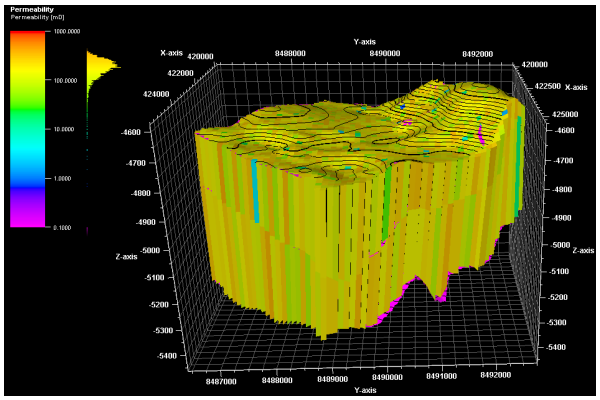

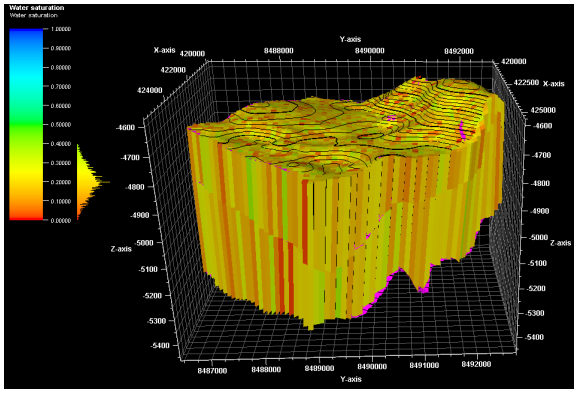

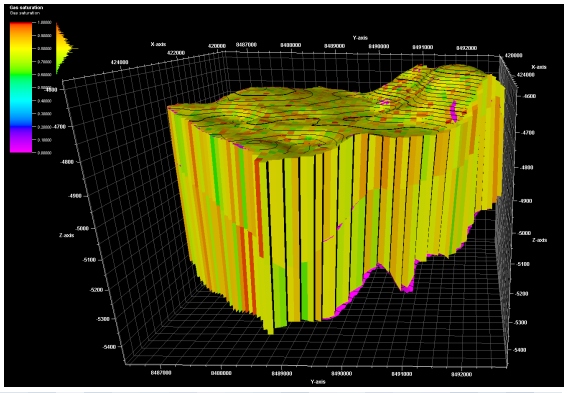

These models preserved the spatial heterogeneity of the reservoir and were critical for dynamic flow simulations with greater accuracy.

Export to CMG Format The resultant static model (surfaces, faults, grids, and property distributions) were exported into CMG Builder in RESCUE format (**Figure 29**). This is the final stage in the static geological modeling in Petrel and sets up the dynamic simulation preparation in CMG.

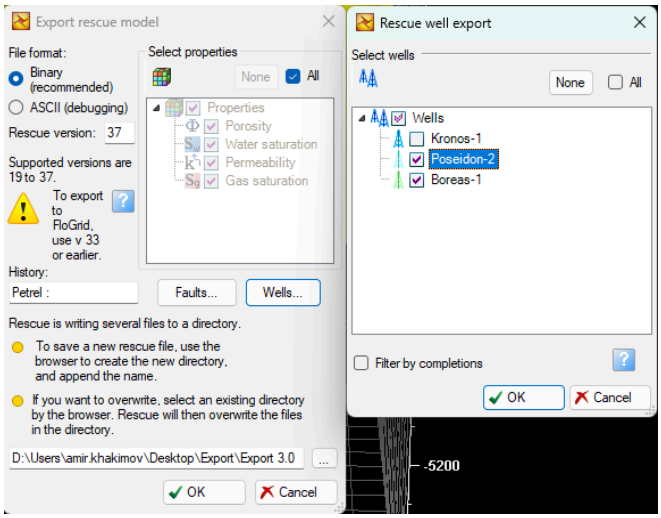

Figure 29. *3D Model Export in Rescue format.*

2.9.2 PIPESIM Procedure

Pipesim Software was utilized to design the well casings and create a surface facility network according to the drilling plan, with a further possibility to conduct the Nodal Analysis.

Casing Design

First of all, from the “Insert” section of the main menu the “Casing” was selected to create a production well. Well name and type are specified in the “General” section.

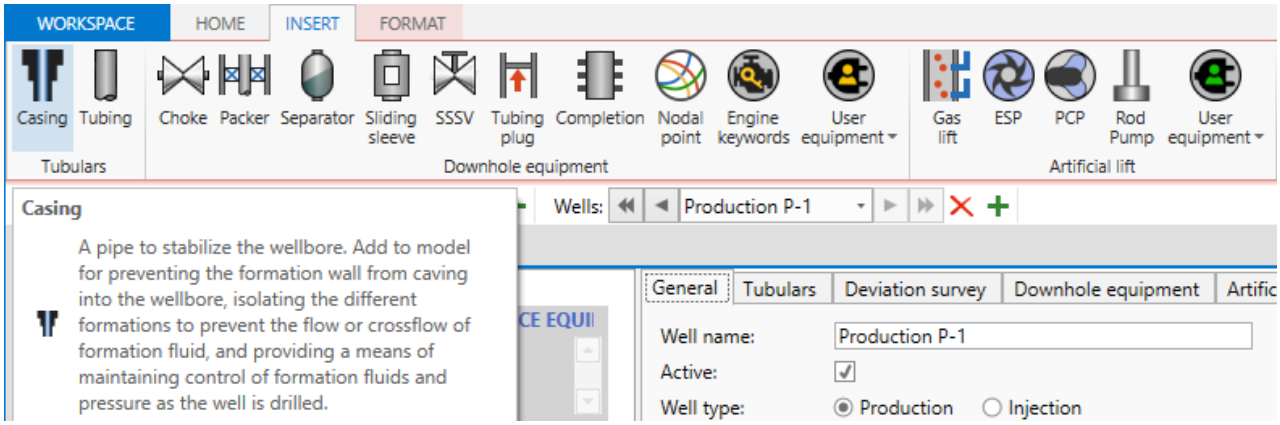

Figure 30. *Insertion of Casing.*

In the similar manner, 4 more casings are added, and two of them further will be converted into the liners. In order to finish the visual part of the design tubing is added, also from the "Insert" section of the main menu.

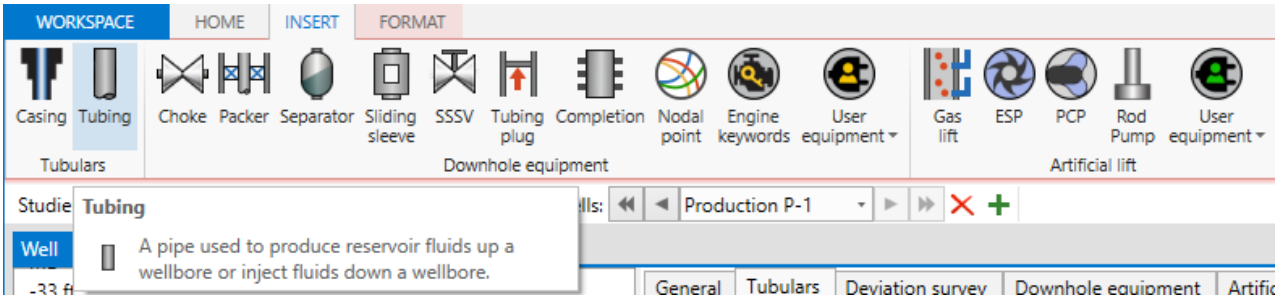

Figure 31. *Insertion of Tubing.*

Next, by proceeding to the "Tubulars" window it is possible to change the casing types, set values for depth and internal diameter. As it was mentioned earlier, the last two added casings are converted into the liners by opening the drop down menu of casing in the "Section type" column, and then selecting "Liner". After changing the section type, depths of each tubular and internal diameters are set.

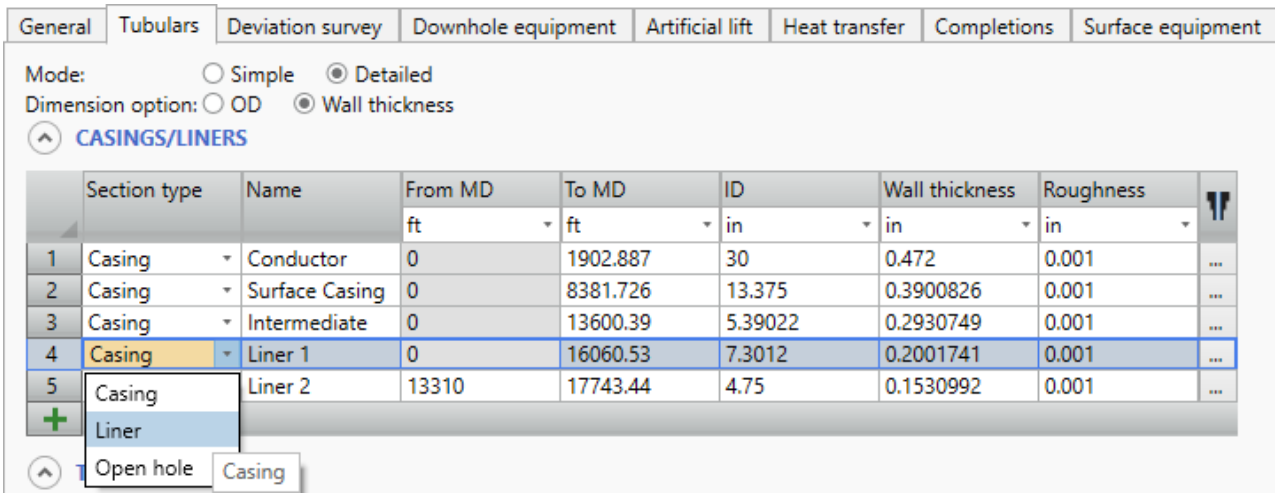

Figure 32. *Changing section type to Liner.*

Then, in the main menu “Completion” is selected and located at the depth of perforation.

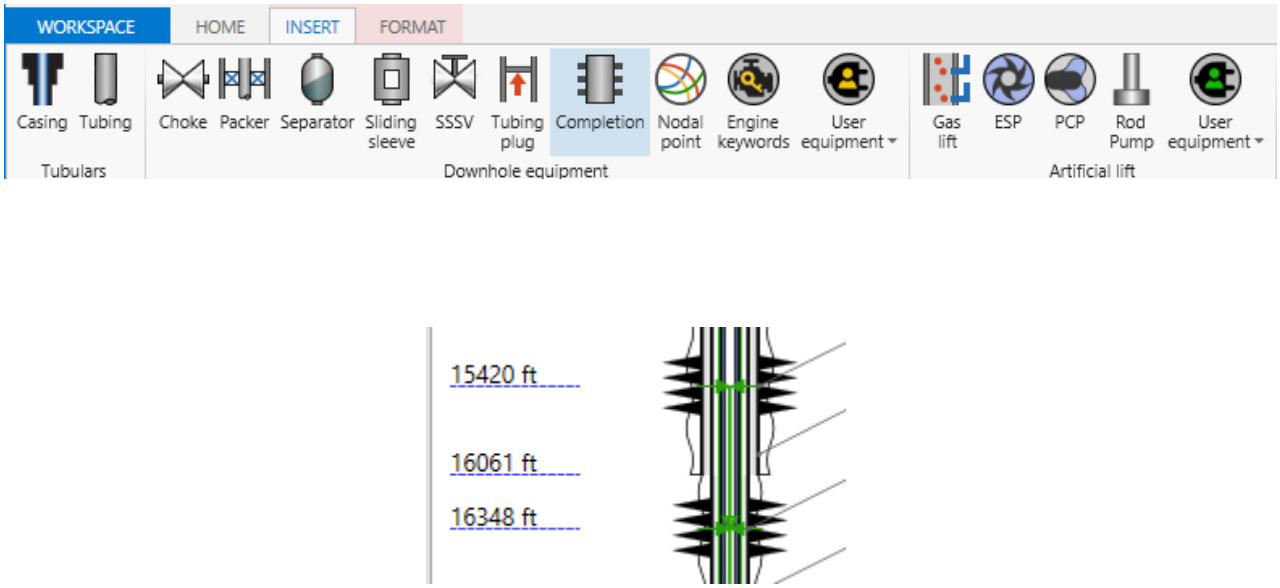

Figure 33. *Insertion of Completion (Perforation).*

It is possible to manually input the desired depth of perforations in the “Completion” section of the window.

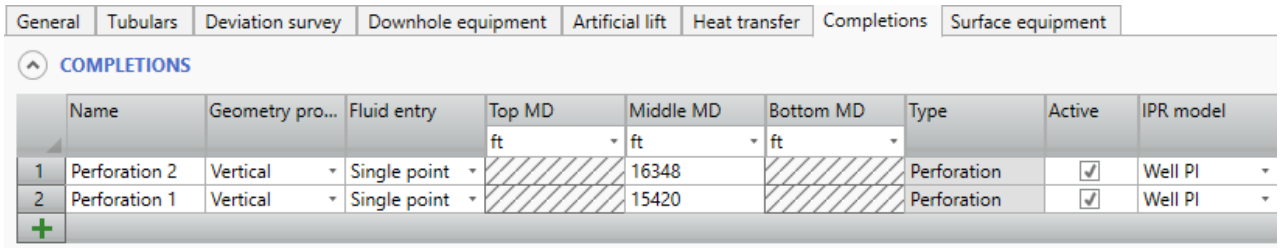

Figure 34. *Manually setting perforation depths.*

To mitigate the problem of converging flowpaths for multiple perforations the “Packer” is inserted.

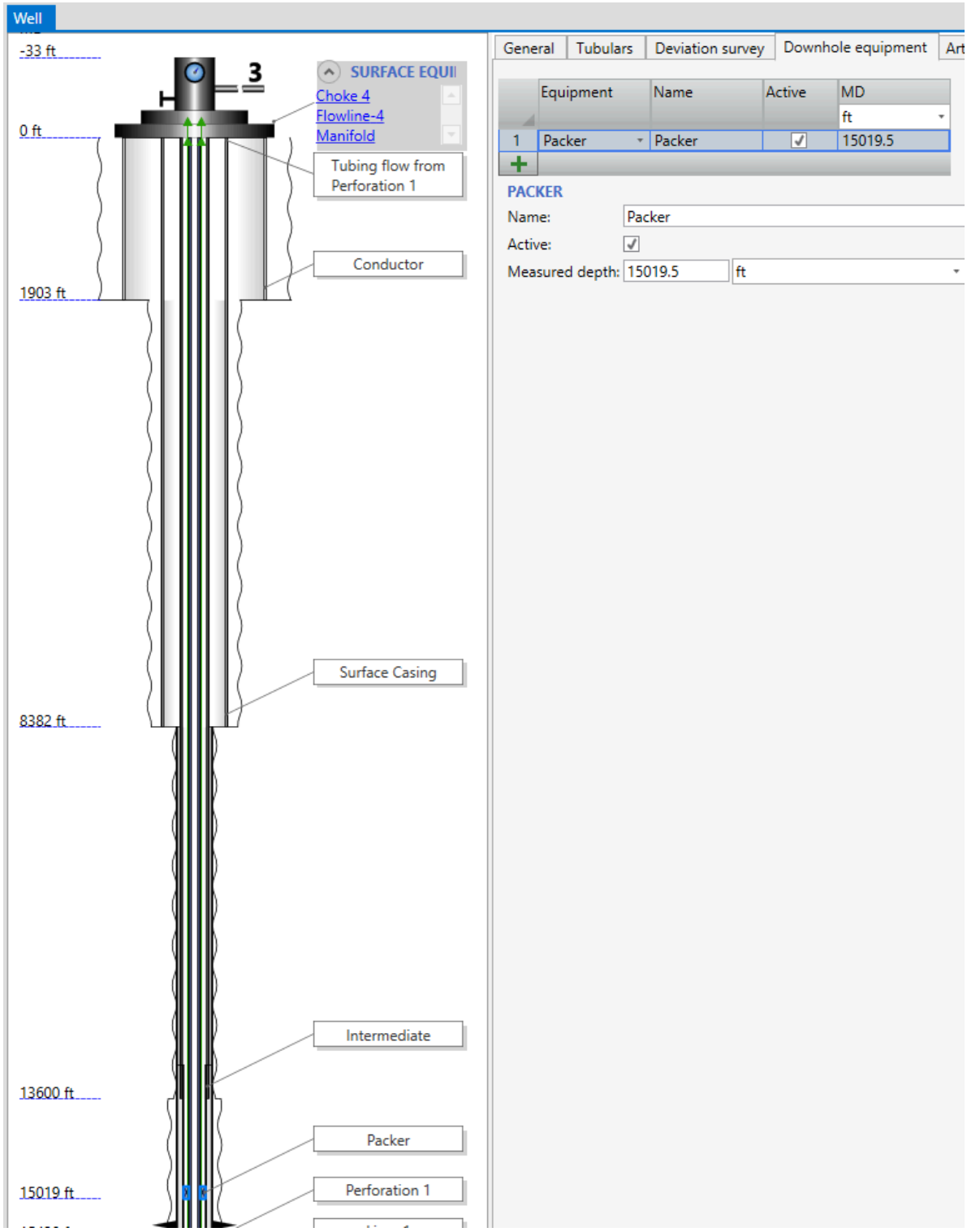

Figure 35. *Installation of Packer.*

The whole process is repeated several times for each well.

Design of Surface facility network

After successfully designing the 5 wells (4 production and 1 injection), from the "Home" section on the main menu change the "Perspective" to network to proceed to designing a surface facility.

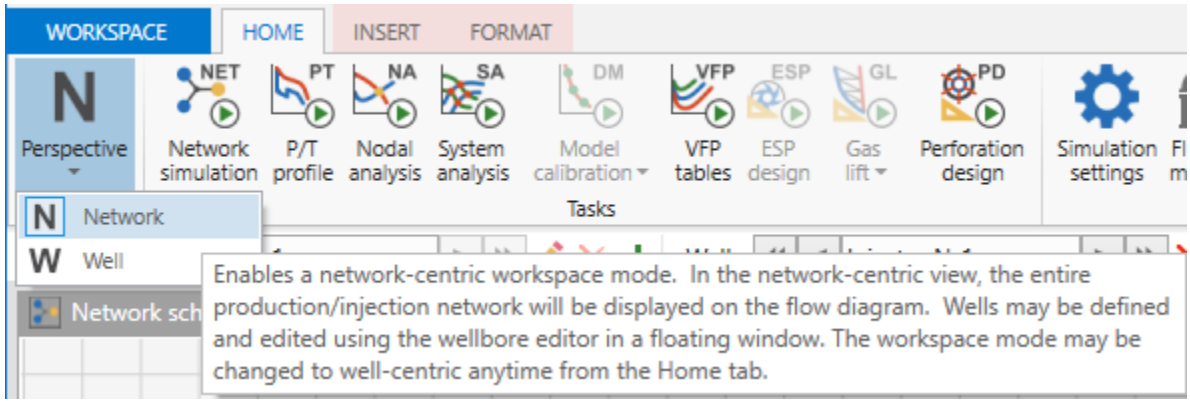

Figure 36. *Changing the Perspective to Network.*

From network tools select "Choke" and add for every production well. And using a "Connector" links the production wells to the chokes.

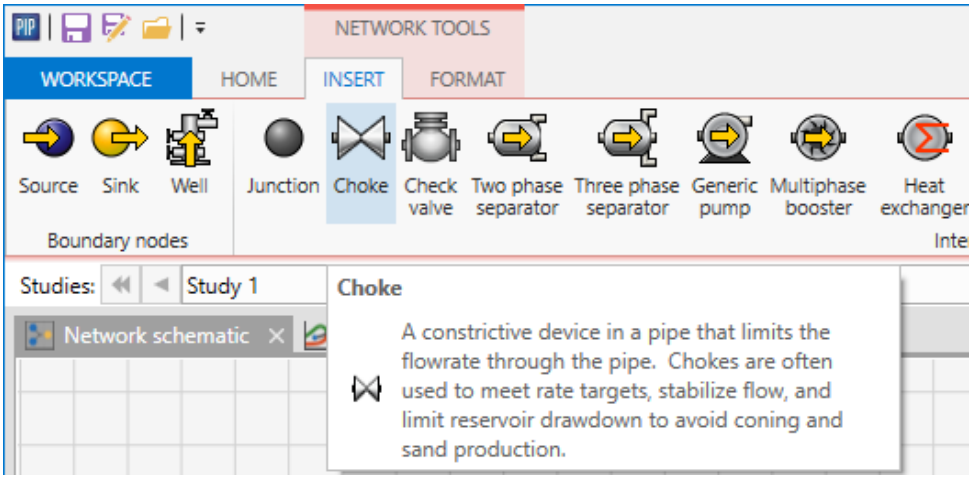

Figure 37a. *Addition of choke.*

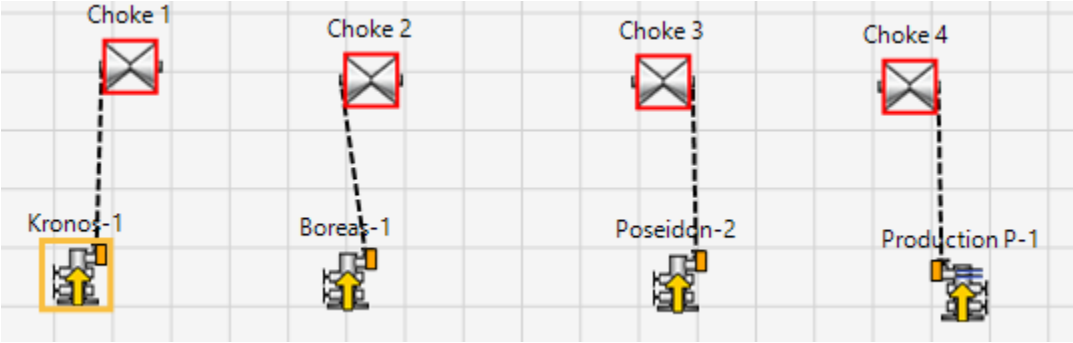

Figure 37b. *Connecting the production wells with choke.*

By double clicking on the choke an edit panel is opened on "Bean size" needs to be specified

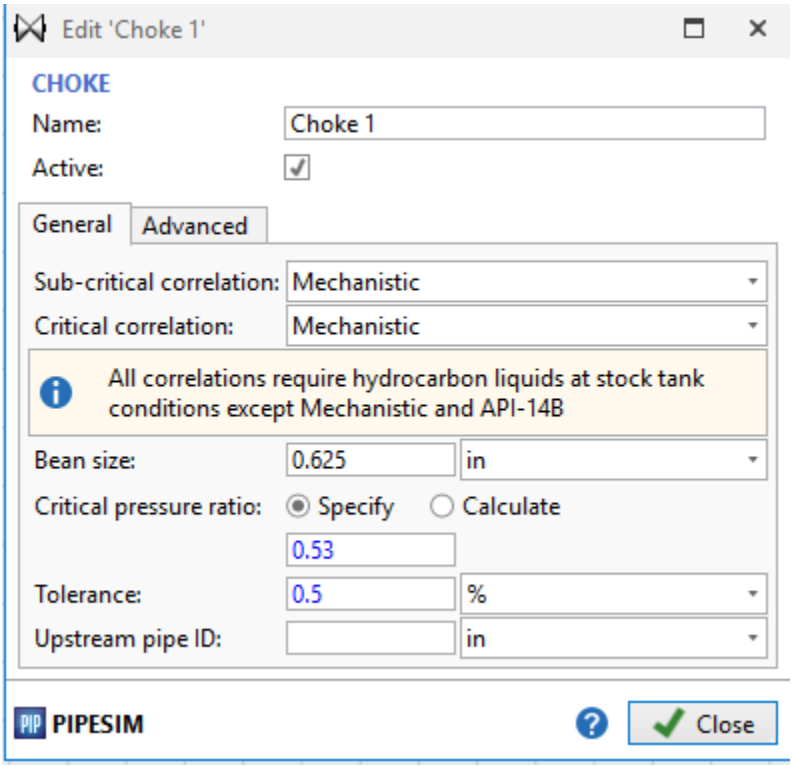

Figure 38. *Setting bean size value.*

Next step is to add flowlines, in order to connect the production wells in the manifold. Similar to choke, set the necessary parameters for flowlines (environment, inside diameter, horizontal distance, and depth at start) in the edit panel by double clicking on each flowline.

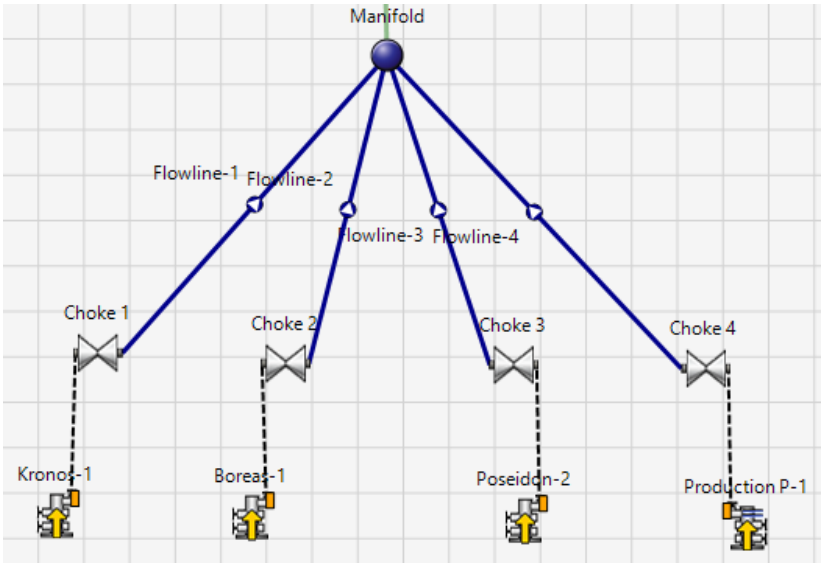

Figure 39. *Connecting the wells in the manifold via flowlines.*

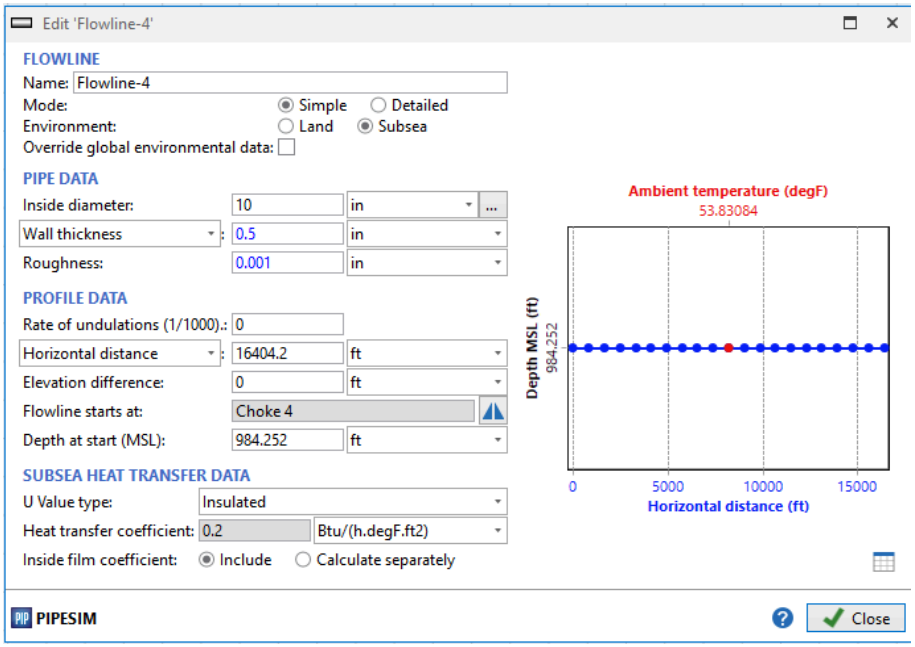

Figure 40. *Setting essential parameters for flowlines.*

Following step is to connect the manifold to 3-phase separator by export riser, and further linking the separator to two generic pumps and one compressor.

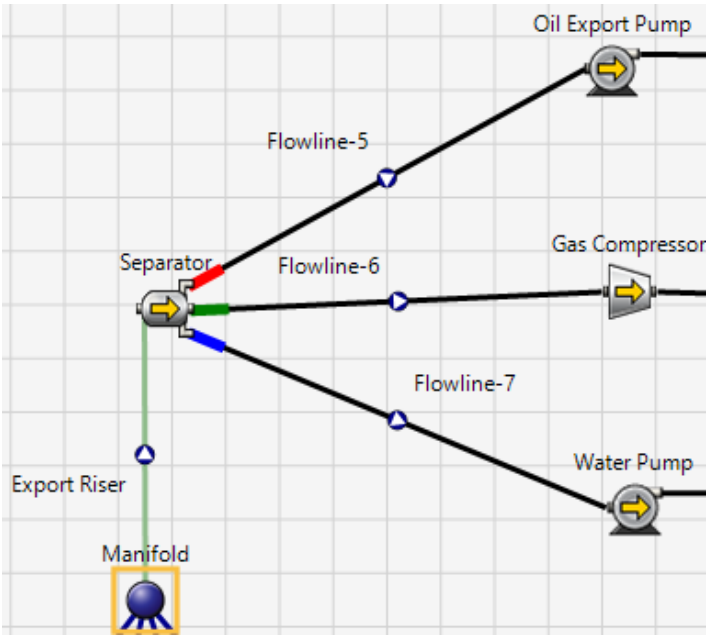

Figure 41. *Connecting manifold, separator and generic pumps.*

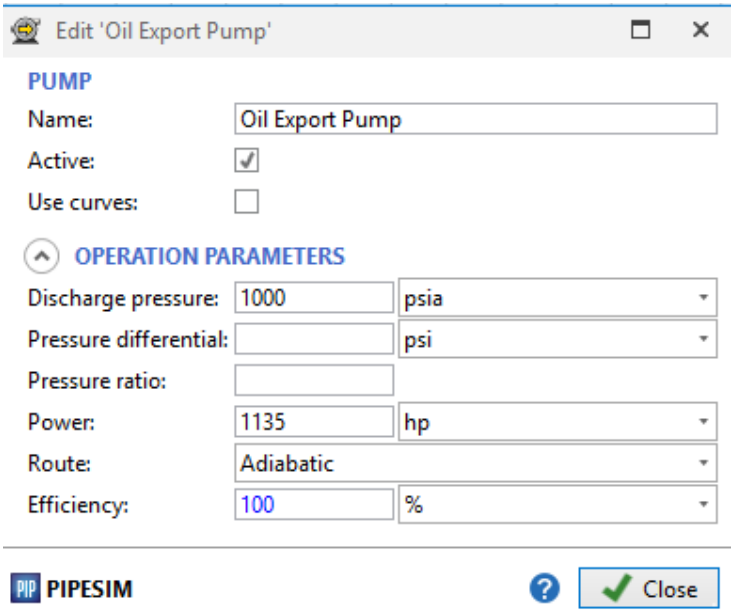

Figure 42. *Setting power of generic pumps.*

After inputting values for power of generic pumps and compressor, they are connected to sinks by flowline.

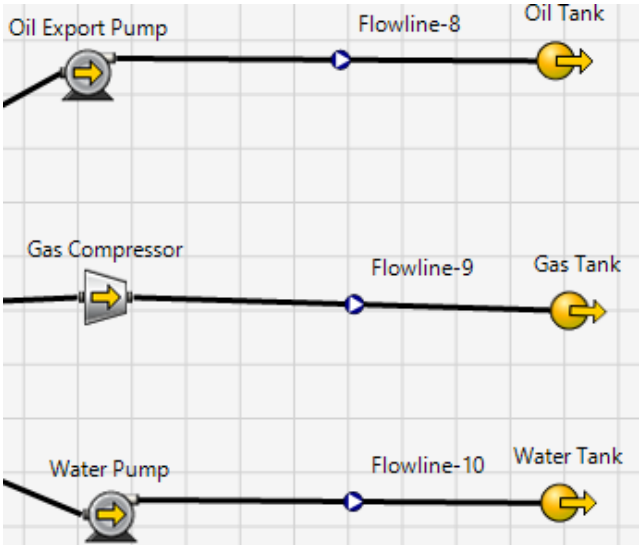

Figure 43. *Connecting pumps to sinks.*

Last step is to add an external source for CO_2 injection and connect it with the injection well via flowline.

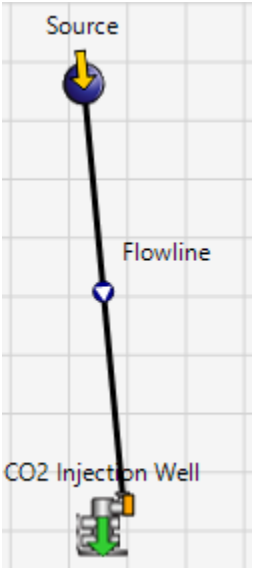

Figure 44. *Connection of injection well.*

After having successfully designed and described the characteristics of the surface facilities, Pipesim was also used to carry out the study of the production data with Nodal Analysis.

Importing the Well Fluid Data

To begin with, from the menu above, the Fluid manager module was selected to upload the chemical composition and characteristics of the fluids in place for each well.

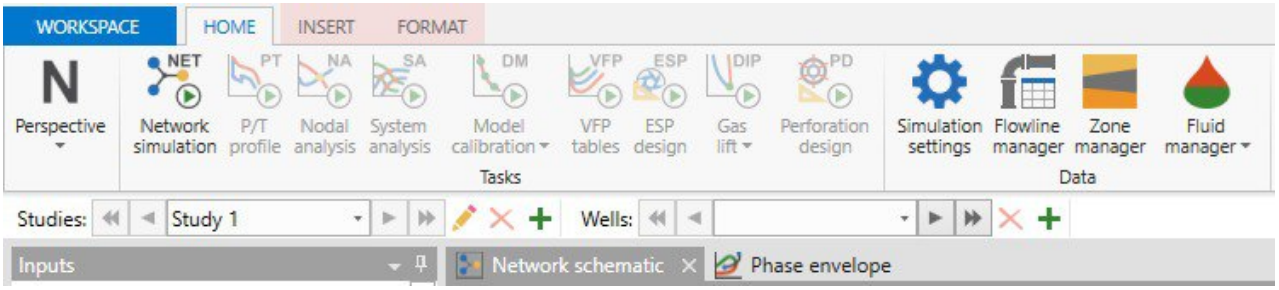

Figure 45. *The main menu of Pipesim.*

In the drop down menu, "Compositional" Fluid manager option was chosen, because it allows manually defining the specific molecular composition of the pore fluids. It is also the appropriate choice for working with gas reservoirs.

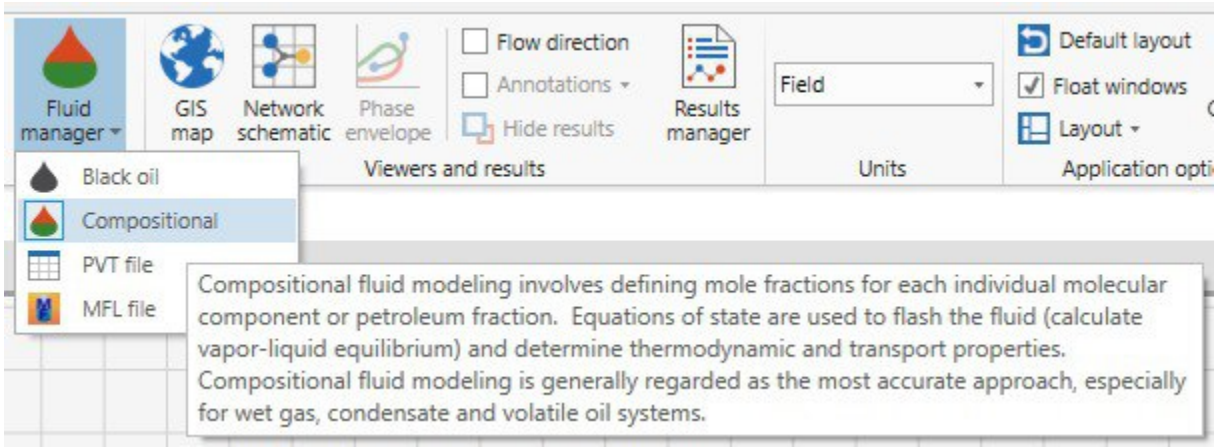

Figure 46. *Choosing the Compositional Fluid manager.*

After the Fluid manager was opened, a specific chemical composition could be defined for each well. The chemical components were chosen from the existing catalogue and their mole fractions were manually entered into the table.

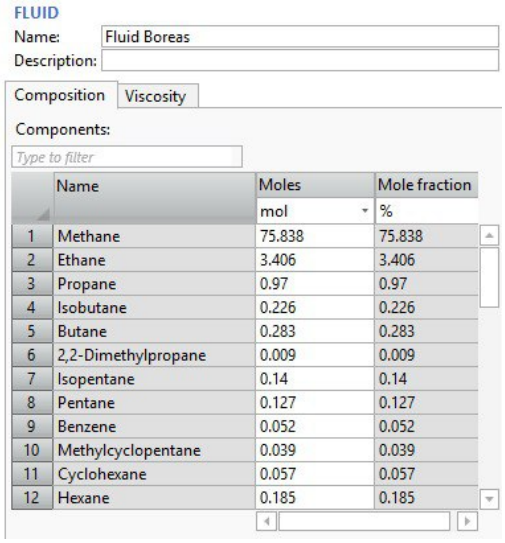

	Name	Moles	Mole fraction
		mol	%
1	Methane	75.838	75.838
2	Ethane	3.406	3.406
3	Propane	0.97	0.97
4	Isobutane	0.226	0.226
5	Butane	0.283	0.283
6	2,2-Dimethylpropane	0.009	0.009
7	Isopentane	0.14	0.14
8	Pentane	0.127	0.127
9	Benzene	0.052	0.052
10	Methylcyclopentane	0.039	0.039
11	Cyclohexane	0.057	0.057
12	Hexane	0.185	0.185

Figure 47 . *Filling in the chemical composition.*

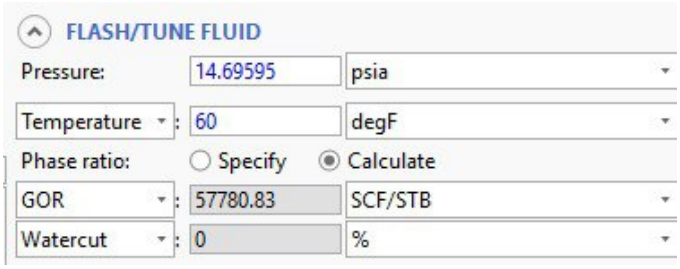

Figure 48 . *Automatically calculated GOR value.*

Inflow Performance Relationship

By clicking on the well from the general workspace, and opening the “Completions” folder, a specific model should be chosen from the available options. As previously mentioned, for the

Poseidon field, Nodal analysis was carried out based on the Darcy equation for gas inflow. After selecting this option, the following parameters were required to be filled out.

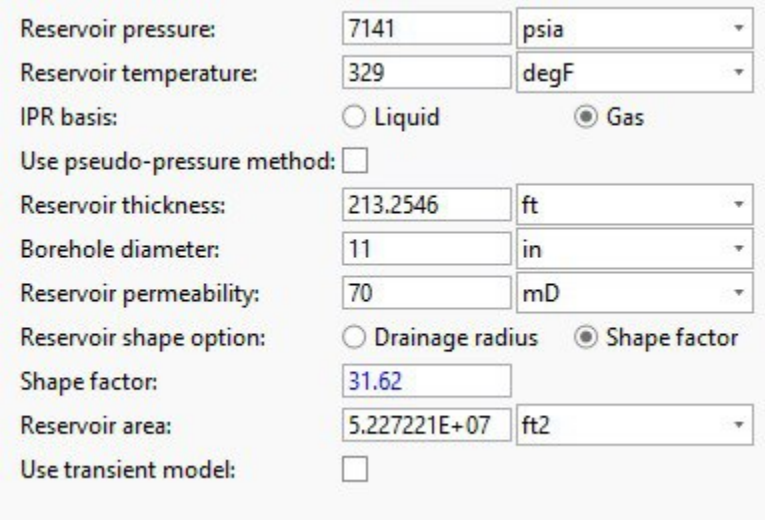

Figure 49 . *Utilizing the Darcy equation for gas inflow in Pipesim.*

Nodal Analysis

Provided that all the necessary information about the well characteristics is filled out, the "Nodal Analysis" module in the main menu above becomes available.

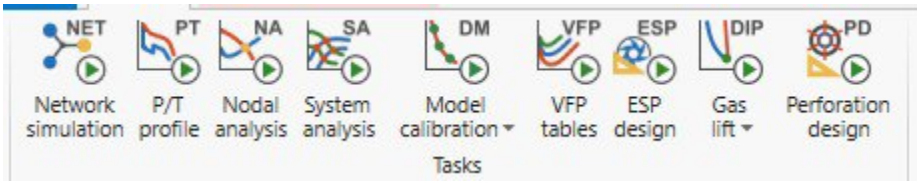

Figure 50 . *Available modules for constructed wells.*

By clicking on the "Nodal Analysis" icon, the following window was opened with other input information to be filled out according to the reported data.

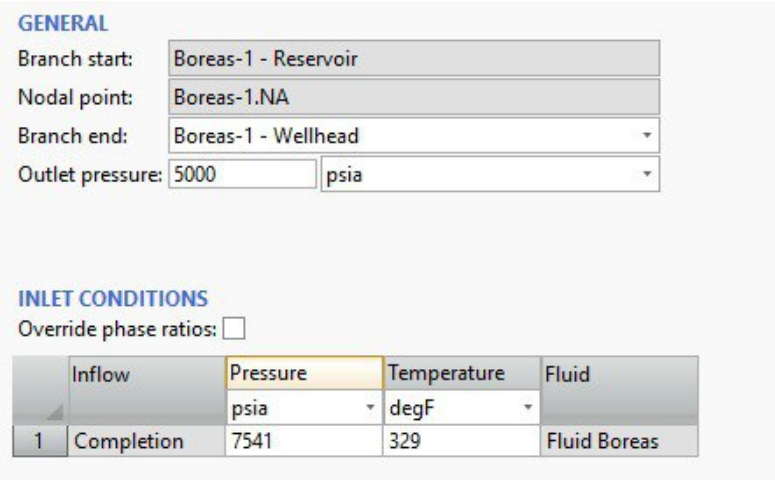

Figure 51. *Completing the General information and the Inlet conditions for a well.*

In the same window, it was also possible to enter the information for sensitivity analysis on various parameters including both inflow and outflow sensitivities. The values could be entered manually, or by specifying a range and the step between values.

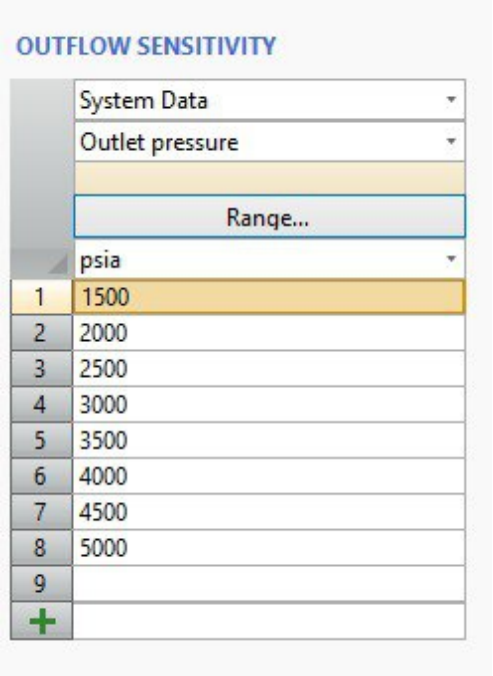

Figure 52. *Filling out the range for outflow sensitivity analysis.*

When all the necessary information was entered without any validation errors, the "Run" button was pressed to produce the results of the IPR and TPR curves, as well as the sensitivity analysis, when it was required.

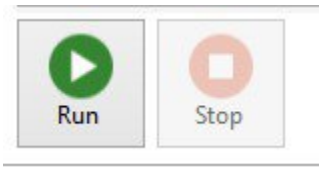

Figure 53. *The "Run" button for building the IPR and TPR curves.*

The Injection Well

When it comes to the injection well, similar steps were taken as for the production wells. However, for the chemical composition of the fluid, a pure injection of CO_2 was defined in the Fluid manager.

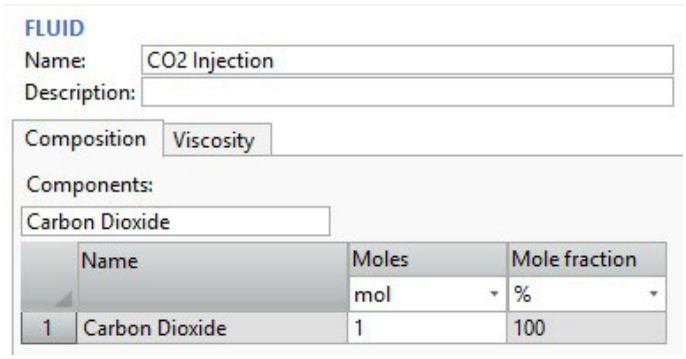

Figure 54. *Defining 100% CO_2 gas as the injection fluid.*

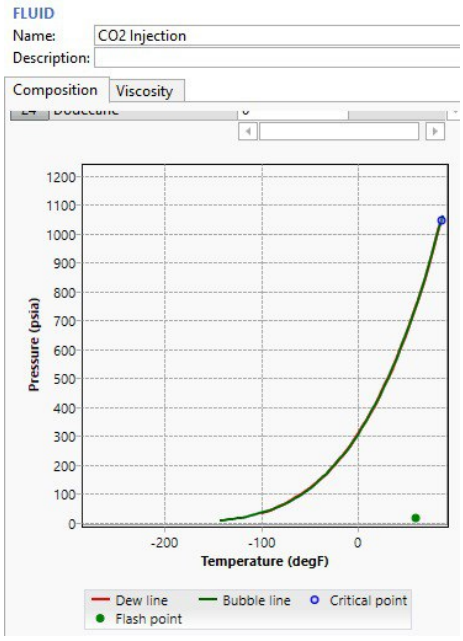

Figure 55. *The automatically computed Phase diagram of the injection fluid.*

Nodal Analysis for the Injection Well

First the Inlet conditions were defined for the Injection well. The values were selected by studying the literature for similar cases and their designs for CO_2 injection in high pressure gas reservoirs.

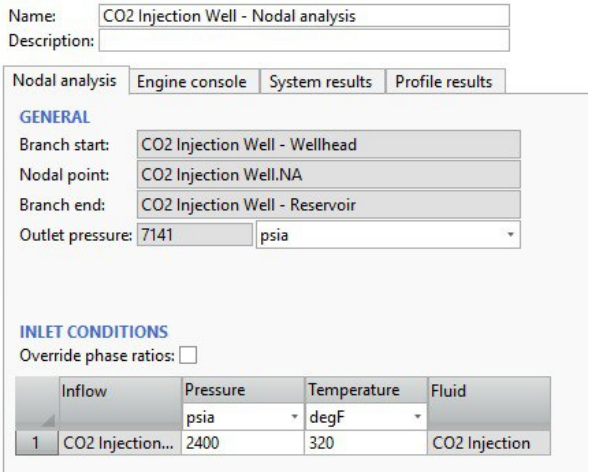

Figure 56. *Injection well Nodal analysis.*

Similar to the production wells, any range of values can be manually entered or calculated via a set number of steps to conduct sensitivity analysis. For the Injection well, sensitivity analysis was performed for the Inflow values.

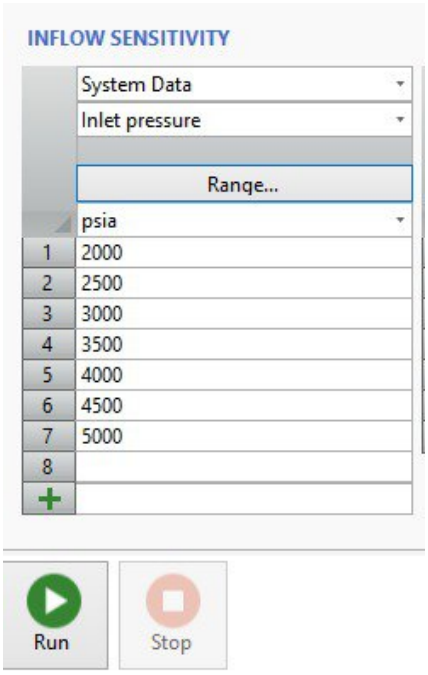

Figure 57. *Injection well sensitivity analysis for inlet pressure.*

2.9.3 CMG Procedure

After the static model was built in Petrel the dynamic reservoir simulation was done in CMG Builder and CMG WinProp. In the dynamic model-building process the geological model has been imported and set up along with the appropriate parameters such as fluid properties, wells, and initial condition to simulate scenarios that reflect reality.

Importing 3D Property Models

The first step taken in CMG Builder was to import the static model (grid, stratigraphy and upscaled property model) exported from Petrel in RESCUE format (property model contains:

porosity, permeability, water saturation and gas saturation). CMG established, matched and mapped the imported properties to the correct simulation properties as in below **Figure 58** using the RESCUE Property Importer. Importing these properties ensures all geological and petrophysical heterogeneity of the reservoir are preserved in the dynamic model.

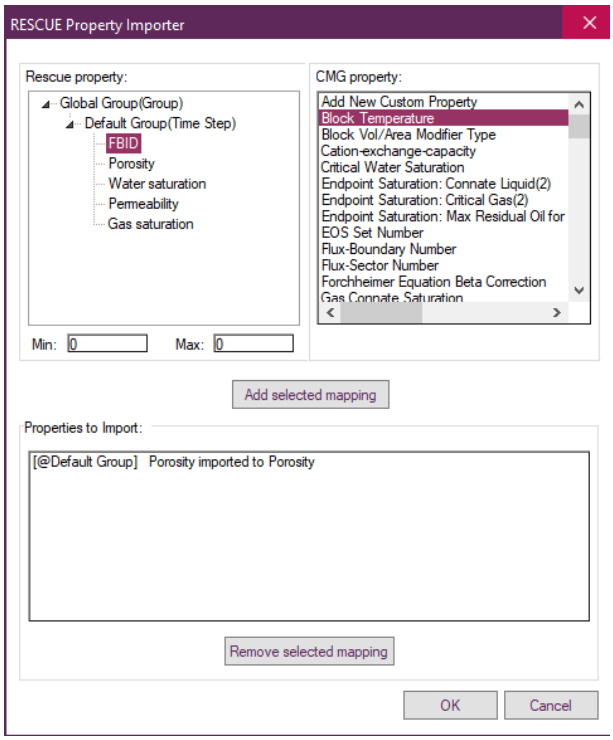

Figure 58. *RESCUE Property Importer in CMG.*

Perforation Intervals Import

The well perforations, created in Petrel, were imported into CMG to replicate the connectivity between the reservoir and the wellbore. The Trajectory Perforation Intervals interface (**Figure 59**) allows the user to load the measured depth (MD) starting and ending points for each well (e.g. Boreas-1, Poseidon-2, Cratos-1) and set the options to keep existing completions and also limit completions in selected wells. This enabled the uploaded well entry points to align correctly with productive reservoir zones.

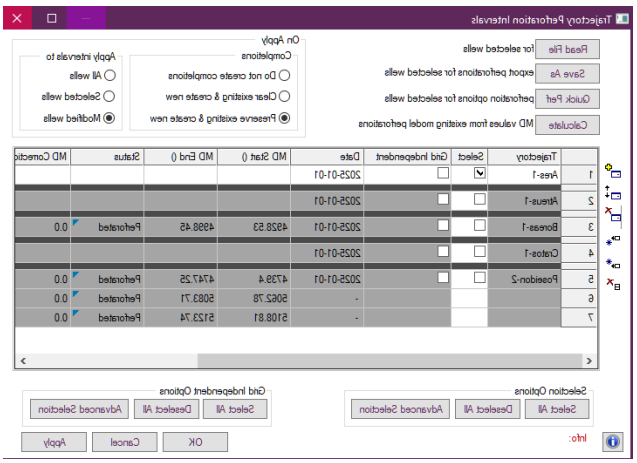

Figure 59. *Trajectory Perforation Intervals Interface.*

Imported Fluid Model From WinProp

The compositional fluid model was created in compositional reservoir simulation software CMG WinProp on the basis of PVT data obtained by laboratory analysis. The crucial components such as CO_2, CH_4, and heavy hydrocarbons were developed using Peng–Robinson component model and the model was verified and imported into CMG Builder by model export in Components section (**Figure 60**). On this basis, the effect of the injected gas on the phase behavior of the reservoir fluids, including the retrograde condensation, was simulated.

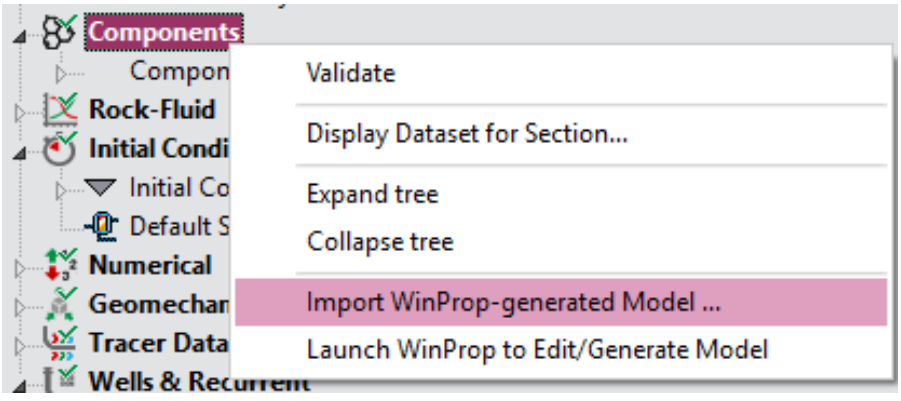

Figure 60. *Fluid Model Import via Components Section.*

Initialization of Reservoir Conditions

Initial pressure, depth, water-gas contact (WGC), and gas composition were defined in the Initial Conditions Panel of CMG builder, as shown in **Figure 61**. Initialization was done based on depth. Reference depth and reference pressure were established based on the well logs. Gas cap composition was assigned based on mole fraction of component gases CO 2 , CH 4 and other Hydrocarbon gases as recorded in the model. These data were inputs that were required to initialize the distribution of fluids prior to production.

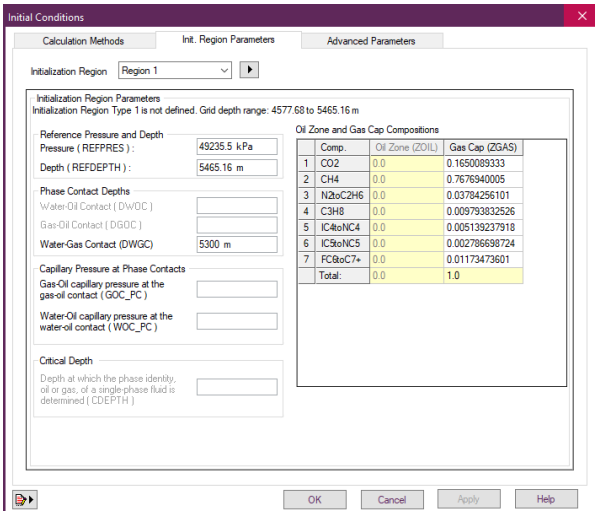

Figure 61. *Initialization Parameters and Gas Composition Input.*

Setting Well Constraints Based on Nodal Analysis

Well operating constraints were imposed on the model using nodal analysis results, which has been conducted in PipeSim. These constraints included minimum bottomhole pressure and maximum gas production rates for production wells (e.g. Boreas-1), and injection pressure and flow rate limits for injectors (e.g. Cratos-1), to ensure safe and controlled gas injection. **Figure 62** shows the Well Events interface set up for Boreas-1. The following constraints were set as:

- BHP: Minimum = 34,473.8 kPa
- STG: 1,066,007 m^3/day

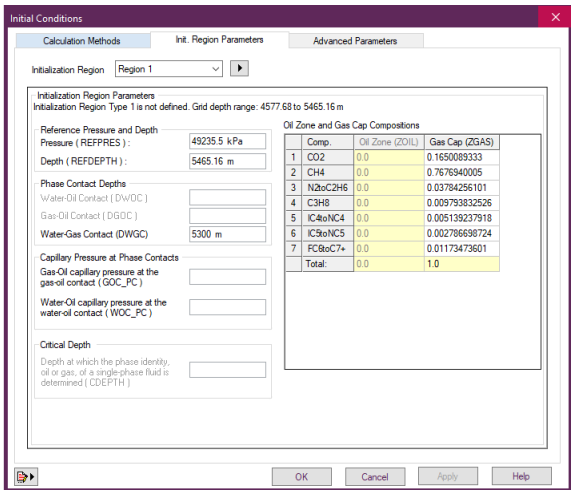

Figure 62. *Well Events: Production Constraints for Boreas-1.*

These restrictions ensured production conditions were consistent with mechanical limitations and reservoir contingency.

With the geological model, fluid behaviour, well completions, initial conditions and operating constraints completely defined the model was ready for dynamic simulations and performance forecasting under multiple scenarios (such as, natural depletion, CO_2 injection and optimized production strategies).

2.9.4 WinProp Procedure

The fluid model implemented in the dynamic simulation was modeled and constructed in CMG WinProp. This step of the software application defines the fluid's compositional behavior as well as generates the required equation of state (EOS) model that will be input into the CMG Builder. The procedure guarantees accurate representation of the fluid phase behavior for the ranges of pressure and temperature expected during reservoir depletion and injection.

Initialization and Setup

After opening the CMG facility, the fluid modeling process was initialized by selecting the Equation of state (EOS) model as Peng – Robinson (PR 1978) as shown in **Figure 63** with units defined as psia and Fahrenheit.

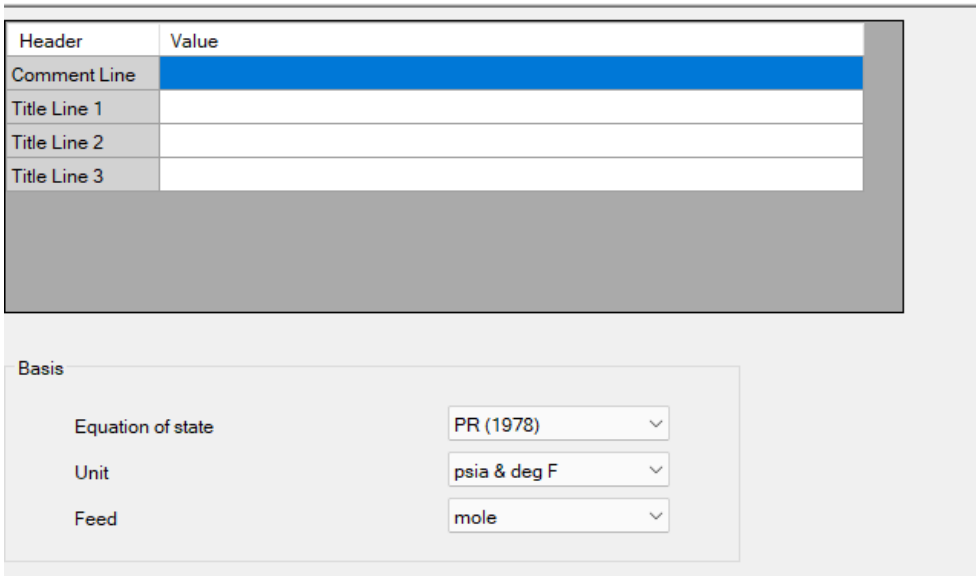

Figure 63. *WinProp EOS Specification Panel – Equation of State and Unit Setup.*

Component Selection and Composition

From input data, primary composition of gas was defined in **Table 14**

Table 14. Original Gas Composition.

Component	Molar Fraction, %	Component	Molar Fraction, %
CO_2	17.17685712	FC15	0.043072362
N2	0.342575527	FC16	0.056094238
CH4	75.96562225	FC17	0.029048802

C2H6	3.411731709	FC18	0.038063947
C3H8	0.971632342	FC19	0.023038705
IC4	0.226380319	FC20	0.020033657
NC4	0.28347624	FC21	0.017028608
IC5	0.149250741	FC22	0.015025242
NC5	0.127213719	FC23	0.013021877
FC6	0.185311323	FC24	0.012020194
BENZENE	0.052087507	FC25	0.010016828
TOLUENE	0.062104335	FC26	0.008013463
CYCLO-C6	0.057095921	FC27	0.006010097
FC7	0.111186794	FC28	0.005008414
FC8	0.10617838	FC29	0.004006731
FC9	0.082137992	FC30	0.003005048
FC10	0.080134626	FC31	0.003005048
FC11	0.069116115	FC32	0.002003366
FC12	0.066111067	FC33	0.002003366
FC13	0.056094238	FC34	0.001001683
FC14	0.10617838	FC35	0.001001683

The modified reservoir composition is presented in **Figure 64**. The fluid system was mainly methane (76.5%) with a large proportion of CO_2 (16.4%). Heavy fractions (C7+) were

added to account for the heavier hydrocarbons present in the fluid system, and lumping was used to group components according to the molecular weight in order to facilitate the EOS Tuning and avoid convergence issues at the simulation stage.

Table 15. New Gas Composition.

Component	Primary	Secondary
CO2	16.5008933275	0.0
CH4	76.7694000542	0.0
N2toC2H6	3.78425610056	0.0
C3H8	0.979383252621	0.0
IC4toNC4	0.513923791752	0.0
IC5toNC5	0.278669872386	0.0
FC6toC7+	1.17347360096	0.0
Sum	99.999999999979	0

.

Phase Envelope and Saturation Conditions

From the Calculations list select the Two-Phase Envelope section. In the Specification window set the minimum and maximum pressure and temperature for plot x and y axis range specification (**Figure 64**).

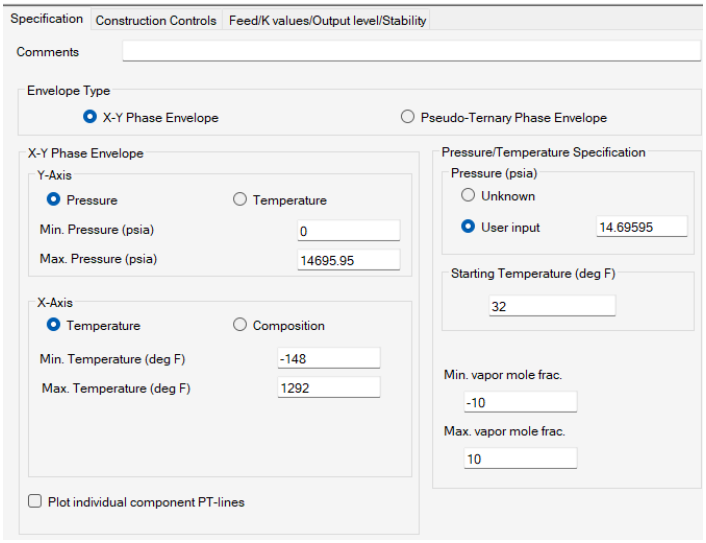

Figure 64. *XY Phase Envelope Setup – Pressure-Temperature Limits for Phase Behavior.*

The saturation pressure calculation was then performed at the reservoir temperature, 320°F (**Figure 65**). The saturation pressure was approximately 5790 psia. The saturation pressure check was critical for providing the initial state of the model in the reservoir as well as phase behavior tuning.

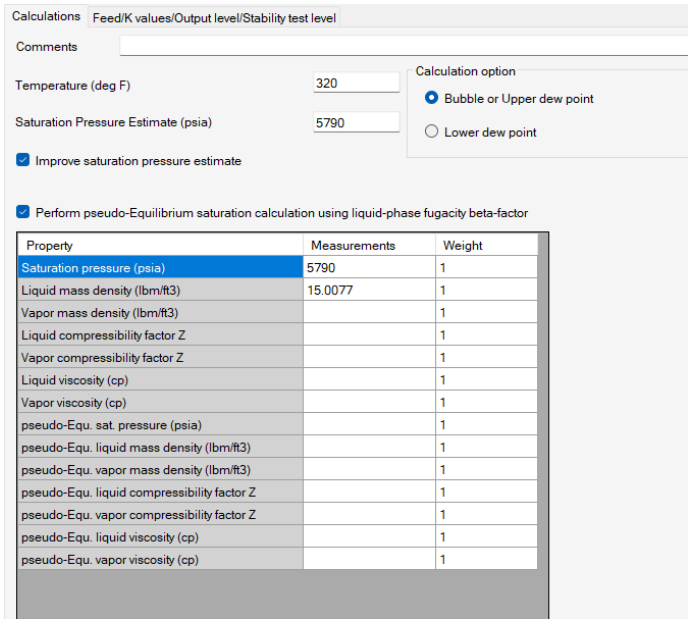

Figure 65. *Saturation Pressure Estimate.*

Constant Composition Expansion Test

A CCE test was conducted at 320°F and 5790 psia saturation pressure, as shown in **Figure 66**. The expansion ratio, liquid volume, viscosities, and Z-factors were measured at 24 pressure steps. This demonstrated the EOS expansion response.

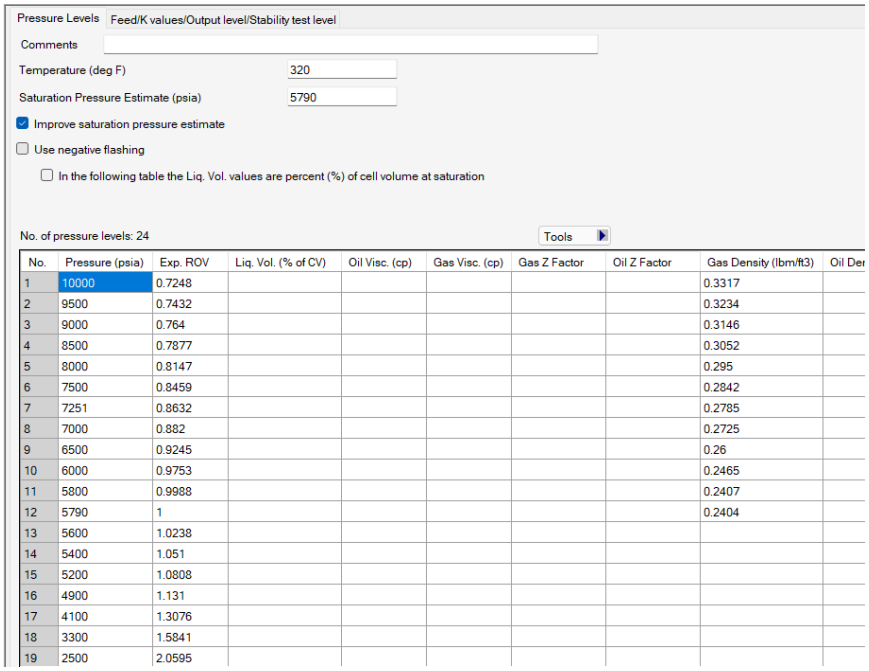

Pressure Levels | Feed/K values/Output level/Stability test level

Comments

Temperature (deg F) 320

Saturation Pressure Estimate (psia) 5790

☑ Improve saturation pressure estimate

☐ Use negative flashing

☐ In the following table the Liq. Vol. values are percent (%) of cell volume at saturation

No. of pressure levels: 24 Tools

No.	Pressure (psia)	Exp. ROV	Liq. Vol. (% of CV)	Oil Visc. (cp)	Gas Visc. (cp)	Gas Z Factor	Oil Z Factor	Gas Density (lbm/ft3)	Oil Der
1	10000	0.7248						0.3317	
2	9500	0.7432						0.3234	
3	9000	0.764						0.3146	
4	8500	0.7877						0.3052	
5	8000	0.8147						0.295	
6	7500	0.8459						0.2842	
7	7251	0.8632						0.2785	
8	7000	0.882						0.2725	
9	6500	0.9245						0.26	
10	6000	0.9753						0.2465	
11	5800	0.9988						0.2407	
12	5790	1						0.2404	
13	5600	1.0238							
14	5400	1.051							
15	5200	1.0808							
16	4900	1.131							
17	4100	1.3076							
18	3300	1.5841							
19	2500	2.0595							

Figure 66. *CCE Test Input Data.*

Constant Volume Depletion

Test Results of CVD, which simulates gas liberation and fluid shrinkage behavior during constant volume depletion, are shown in **Figure 67**. Liquid saturation and z-factors were tracked as a function of depletion so that appropriate EOS is capable of calculating these multi-phase transitions accompanied with shrinkage behaviour.

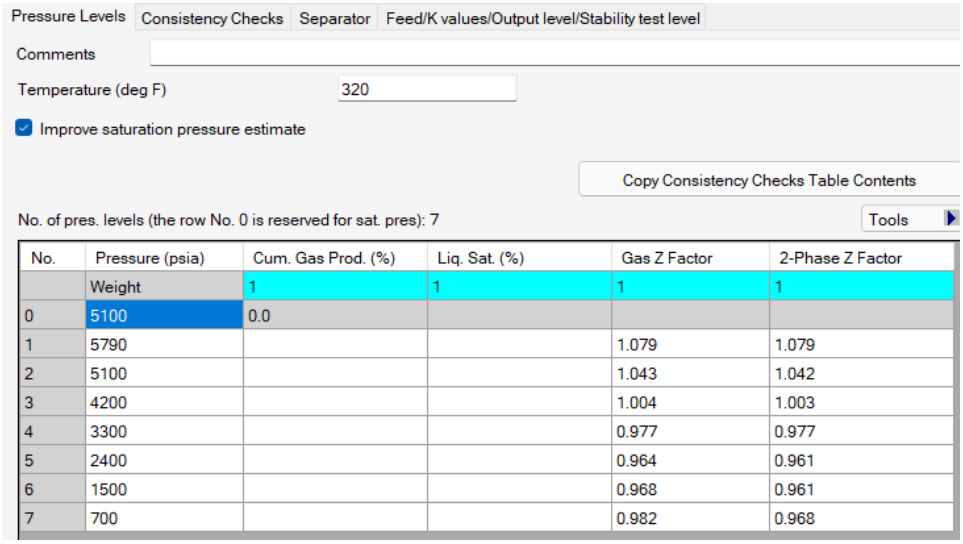

No.	Pressure (psia)	Cum. Gas Prod. (%)	Liq. Sat. (%)	Gas Z Factor	2-Phase Z Factor
	Weight	1	1	1	1
0	5100	0.0			
1	5790			1.079	1.079
2	5100			1.043	1.042
3	4200			1.004	1.003
4	3300			0.977	0.977
5	2400			0.964	0.961
6	1500			0.968	0.961
7	700			0.982	0.968

Figure 67. *CVD Input Data.*

Differential Liberation Test

The DL test, illustrated in **Figure 68**, is a laboratory experiment designed to capture the flash separation behavior during the depressurization process. In the DL test, variation of formation volume factor (FVF), GOR, gas/oil Z-factors, and oil viscosity are determined at different pressures. In this study, the DL test was performed at six pressure levels to simulate the actual experiment as close as possible and to ensure accurate simulation of the flash behavior

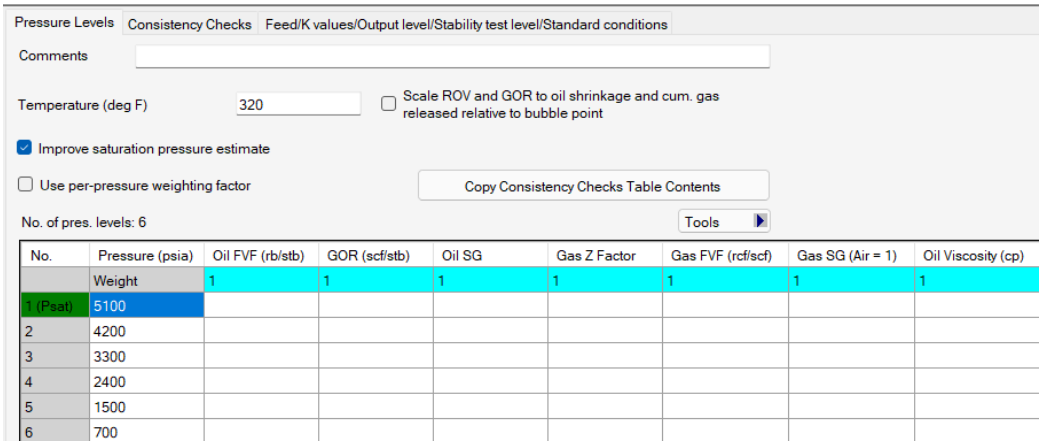

Figure 68. *Differential Liberation Test Setup.*

EOS Export to Gem

The EOS model was exported to CMG GEM format after EOS tuning and successful fluid property validation. The "Print component properties for GEM to pvt modelling.gem" was selected, as shown in **Figure 69**. The reservoir temperature was set as 320°F.

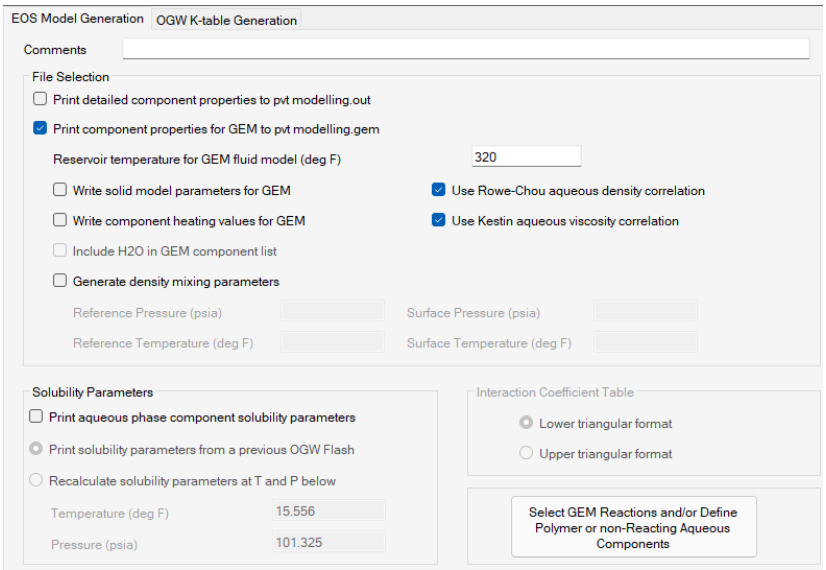

Figure 69. *Exporting GEM Fluid Model File from WinProp.*

Other options such as Rowe–Chou aqueous density correlation and Kestin aqueous viscosity correlation were activated so as to ensure the right behavior of the water components for the next CO_2 injection scenarios. The interaction coefficient tables were generated in the lower triangular format. The above settings guaranteed a seamless and unchanged implementation of the compositional fluid model in the dynamic model in CMG Builder.

2.9.5 Monte Carlo Simulation Procedure

A Monte Carlo simulation, in Python with Python Jupyter Notebook environment, was conducted to estimate the Gas Initially In Place (GIIP) of the Poseidon field. It provides a way to model reservoir parameters probabilistically in order to reflect uncertainty in volumetric calculations. The process was implemented as follows:

Setting Up the Simulation Environment

Python 3 was used along with the Jupyter Notebook that gives a web based interface to run and visualize Python code to run the Monte Carlo simulation. First thing to do is to launch the Jupyter notebook console and copy a link which is a secure, temporary access link to this URL. To open the Jupyter interface, a link is copied and pasted into the browser's address bar.

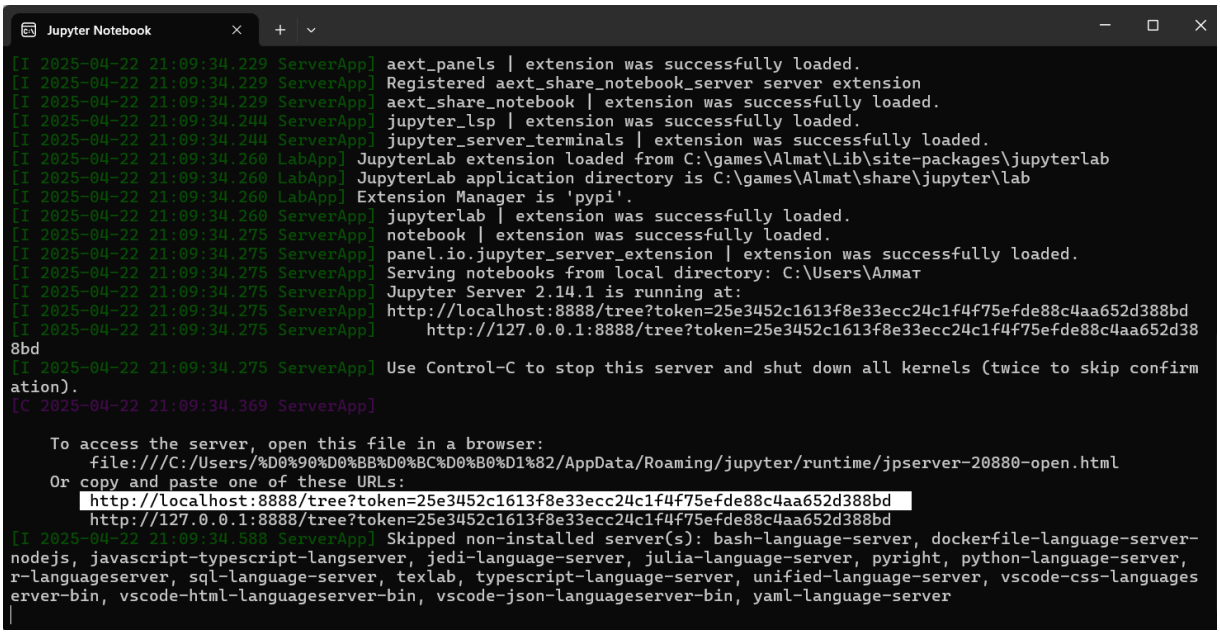

Figure 70. *Copying the URL from the Python console.*

After opening the link The “New” button on the top right of the Jupyter home page is clicked followed by ‘Python 3’ selection in the dropdown menu. Then, another tab opens, and a new notebook is opened. The notebook title is as GIIP_MonteCarlo_Poseidon.ipynb and the coding can commence now.

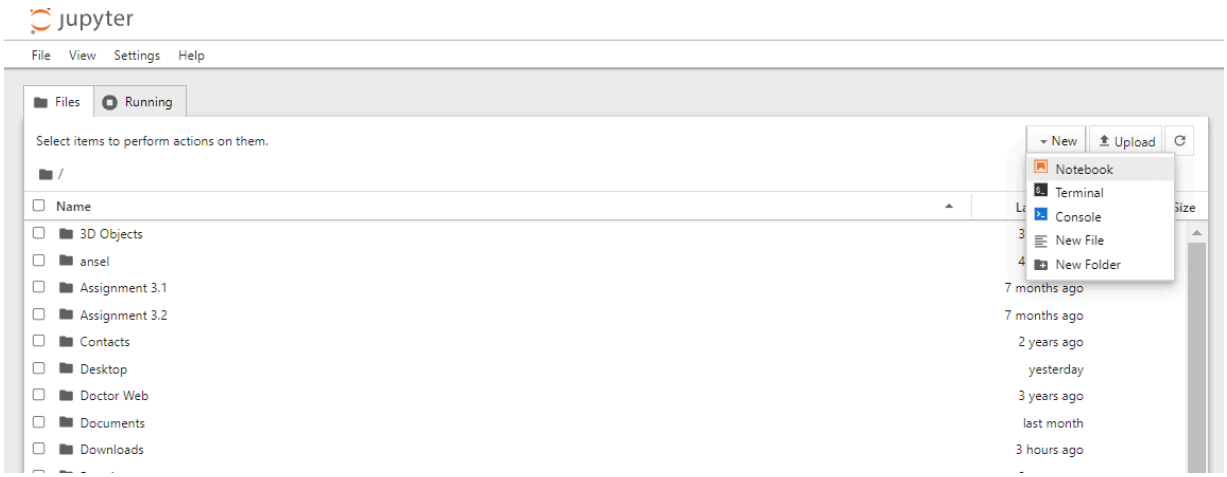

Figure 71. *Creating the new notebook in Jupyter main page.*

The Python libraries needed for the task are imported through import numpy as np followed by import matplotlib.pyplot as plt and finally import seaborn as sns. The system establishes an environment that allows numerical simulation and plotting to occur.

```
import numpy as np
import matplotlib.pyplot as plt
import seaborn as sns
```

Figure 72. *Importing the main libraries.*

Defining Input Distributions

The system generates input parameters by using the np.random.normal() function for realistic variation across 10,000 cases. The simulation model includes five reservoir characteristics named area, net pay, porosity, water saturation, and Bg which receive their values using specific mean and standard deviation pairs from data-based distributions. A restriction using the np.clip() function maintains physical limitations to prevent unrealistic extreme values in the dataset.

```
# Number of simulations
num_simulations = 10000

area = np.random.normal(loc=60e6, scale=2e6, size=num_simulations) * 10.764  # m² → ft²
net_pay = np.random.normal(loc=90, scale=3, size=num_simulations) * 3.28084  # m → ft
porosity = np.random.normal(loc=0.14, scale=0.01, size=num_simulations)
sw = np.random.normal(loc=0.22, scale=0.015, size=num_simulations)
bg = np.random.normal(loc=0.0041, scale=0.00005, size=num_simulations)  # in ft³/SCF

# Clip to keep values within physical limits
porosity = np.clip(porosity, 0.12, 0.16)
sw = np.clip(sw, 0.18, 0.26)
bg = np.clip(bg, 0.0040, 0.0042)
```

Figure 73. *Defining the input parameters for Monte Carlo simulation.*

GIIP Calculation

To estimate the Gas Initially In Place (GIIP), the volumetric method is used, which calculates the total gas volume in the reservoir based on key geological and petrophysical parameters. This method accounts for reservoir area, net pay thickness, porosity, water saturation, and gas formation volume factor. The general equation for GIIP is expressed as follows:

$$GIIP = \frac{A \times h \times \varphi \times (1 - Sw)}{Bg}$$

Where:

A = Reservoir area (m²)

h = Net pay thickness (m)

ϕ = Porosity (fraction)

S w= Water saturation (fraction)

Bg= Gas formation volume factor (m³/Sm³)

```
# GIIP calculation in SCF
giip_scf = (area * net_pay * porosity * (1 - sw)) / bg

# Convert SCF → standard m³ (1 SCF = 0.0283168 std m³)
giip_std_m3 = giip_scf * 0.0283168
```

Figure 74. *Defining the formula for GIIP calculation.*

The np.percentile() function determines P90, P50 and P10 values in the GIIP simulation outputs. These represent the conservative, median, and optimistic estimates respectively. The display of calculated values together with mean GIIP occurs through the print() function.

```
# Compute percentiles
p90 = np.percentile(giip_std_m3, 10)
p50 = np.percentile(giip_std_m3, 50)
p10 = np.percentile(giip_std_m3, 90)
mean_giip = giip_std_m3.mean()

# Print results
print(f"P90 (Conservative): {p90:.2e} std m³")
print(f"P50 (Median):       {p50:.2e} std m³")
print(f"P10 (Optimistic):   {p10:.2e} std m³")
print(f"Mean GIIP:          {mean_giip:.2e} std m³")
```

Figure 75. *Writing the function for P90, P50 and P10 determination.*

Visualization

The GIIP distribution receives a plot using sns.histplot() which adds vertical lines to indicate P90, P50 and P10 through plt.axvline(). The visual presentation of GIIP estimates allows one to understand the distribution width and positioning.

```
# Plot histogram
plt.figure(figsize=(10, 6))
sns.histplot(giip_std_m3 / 1e9, bins=50, kde=True, color="skyblue")
plt.axvline(p90 / 1e9, color='red', linestyle='--', label='P90')
plt.axvline(p50 / 1e9, color='orange', linestyle='--', label='P50')
plt.axvline(p10 / 1e9, color='green', linestyle='--', label='P10')
plt.xlabel("GIIP (Billion std m³)")
plt.ylabel("Frequency")
plt.title("Monte Carlo GIIP Distribution – Poseidon Field")
plt.legend()
plt.grid(True)
plt.tight_layout()
plt.show()
```

Figure 76. *Functions used for creating the plot of distribution.*

2.10 Machine Learning

Machine Learning (ML) has a wide range of applications in petroleum engineering including the production forecasting, well placement optimization, and gas injection optimization. Through the accurate analysis of the Poseidon field features, the gas injection optimization using the ML was chosen as the improvement for the FDP.

At first, the pandas library and dataset were imported into the Jupyter Notebook. The first rows of the dataset can be presented using the following set of the code.

```
import pandas as pd
```

```
df=pd.read_excel(r"D:/Simulation Results (1) (1).xlsx")
```

```
df.head()
```

	Date	FIELD-Gas Prod Rate SCTR (m3/day)	FIELD-Gas Prod Cum SCTR (m3)	FIELD-Gas Oil Ratio SCTR (m3/m3)	FIELD-Ave Pres POVO SCTR (kPa)	FIELD-Water Cut SCTR - %	FIELD-Gas Inje Rate SCTR (m3/day)

Figure 77. *Data Import into the Jupyter Notebook.*

Then the Matplotlib library was imported and the gas injection rate over time was created using another segment.

```
import matplotlib.pyplot as plt
```

```
df.sort_values('Date', inplace=True)

plt.figure(figsize=(14, 6))
plt.plot(df['Date'], df['FIELD-Gas Inje Rate SCTR (m3/day)'], linewidth=2)
plt.title('Gas Injection Rate Over Time', fontsize=16)
plt.xlabel('Date', fontsize=12)
plt.ylabel('Gas Injection Rate (m3/day)', fontsize=12)
plt.grid(True)
plt.tight_layout()
plt.show()
```

Figure 78. *Gas Injection over time plotting process.*

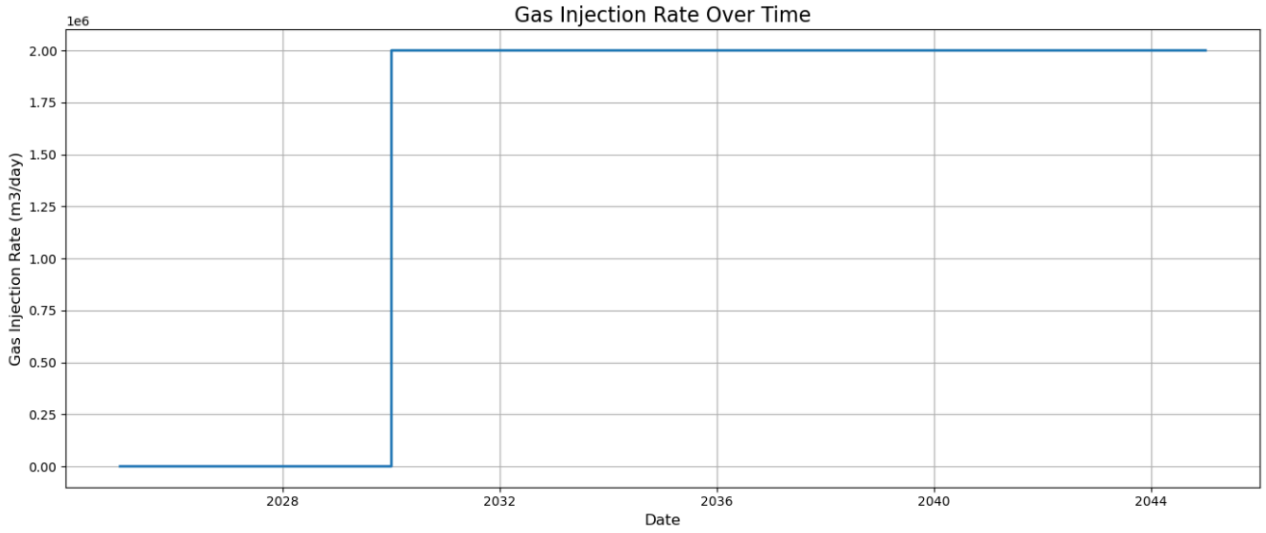

Figure 79. *Gas Injection over time plot.*

The correlations between features can be made in descending order as it can be seen from the following part of the code and results.

```
target = 'FIELD-Gas Prod Rate SCTR (m3/day)'

numeric_cols = df.select_dtypes(include='number').columns.tolist()
features = [col for col in numeric_cols if col != target]

correlation_matrix = df[features + [target]].corr()

target_correlations = correlation_matrix[target].drop(target).sort_values(ascending=False)

plt.figure(figsize=(10, 6))
target_correlations.plot(kind='barh')
plt.title('Correlation of Features with Gas Production Rate', fontsize=14)
plt.xlabel('Correlation Coefficient', fontsize=12)
plt.grid(True)
plt.tight_layout()
plt.show()
```

Figure 80. *Code for the correlations between features and target.*

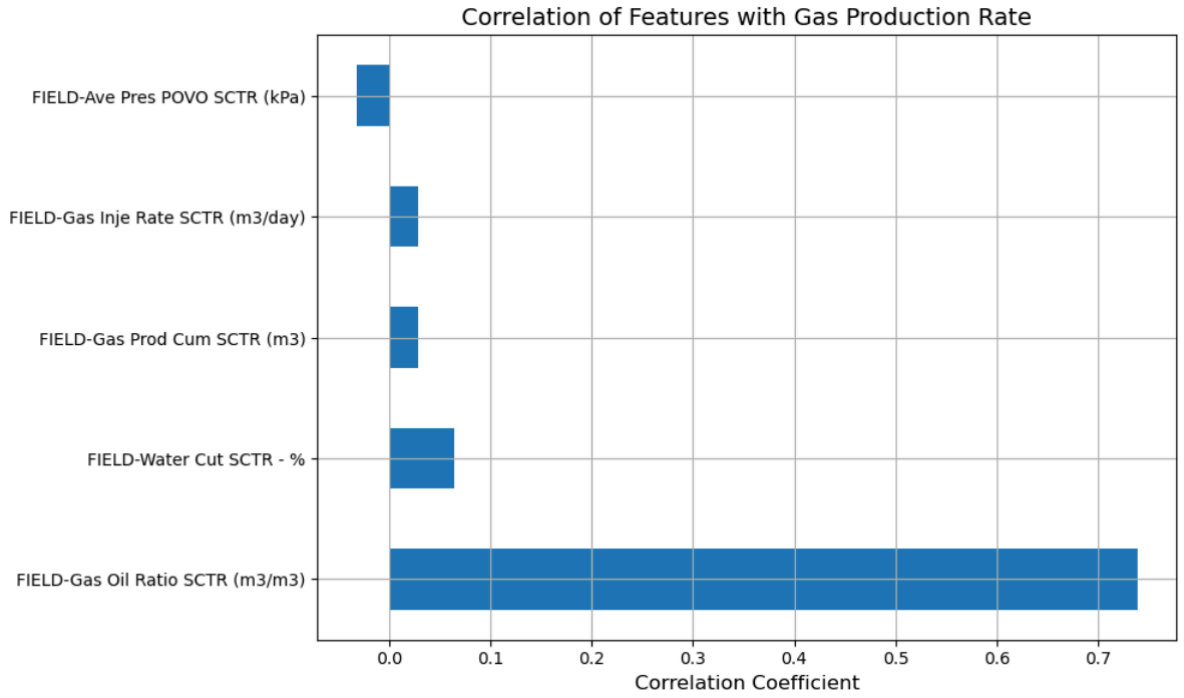

Figure 81. *Correlations between features and target.*

The regression models such as the Linear Regression (LR), Decision Tree (DT), Random Forest (RF), Gradient Boosting, XGBoost, Support Vector Regressor (SVR), and K-Nearest Neighbors (KNN) were used during this step.

```
models = {
    "Linear Regression": LinearRegression(),
    "Decision Tree": DecisionTreeRegressor(random_state=42),
    "Random Forest": RandomForestRegressor(random_state=42),
    "Gradient Boosting": GradientBoostingRegressor(random_state=42),
    "XGBoost": xgb.XGBRegressor(random_state=42, verbosity=0),
    "Support Vector Regressor": SVR(),
    "K-Nearest Neighbors": KNeighborsRegressor(),
}
```

Figure 82. *Machine learning models used in the project.*

The best results were achieved by the RF regression model showing the highest accuracy. Moreover, the sensitivity test revealed the improvement after the use of the ML model as it can be clear from the following **Figures**.

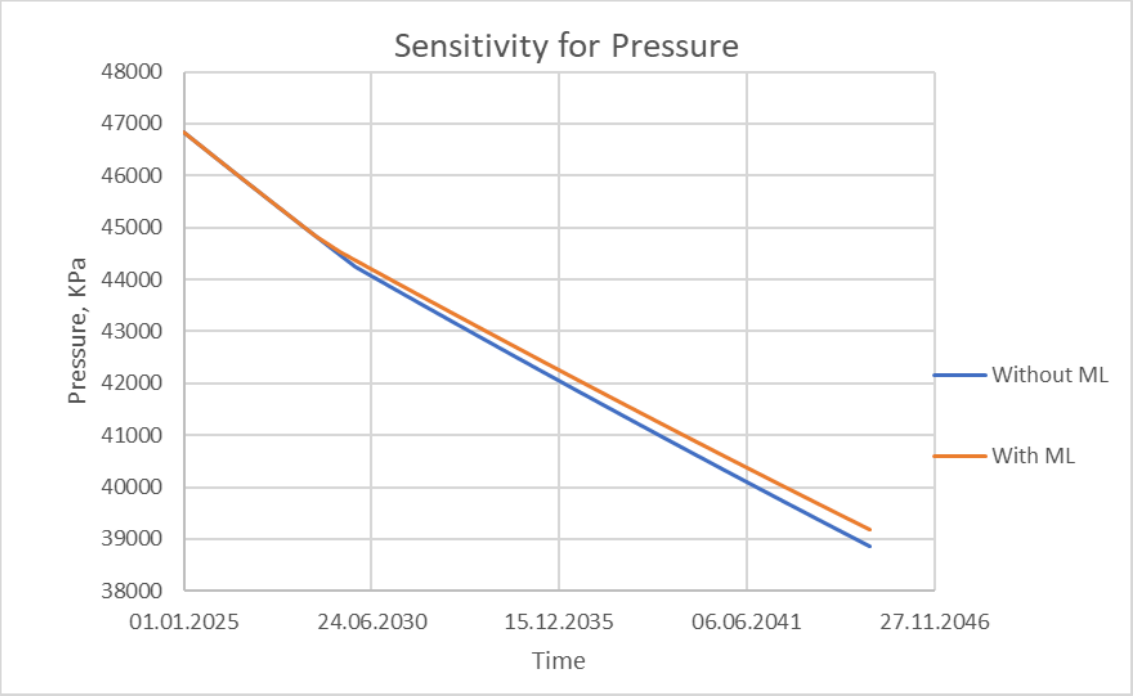

Figure 83. *Sensitivity for Pressure without ML and with ML.*

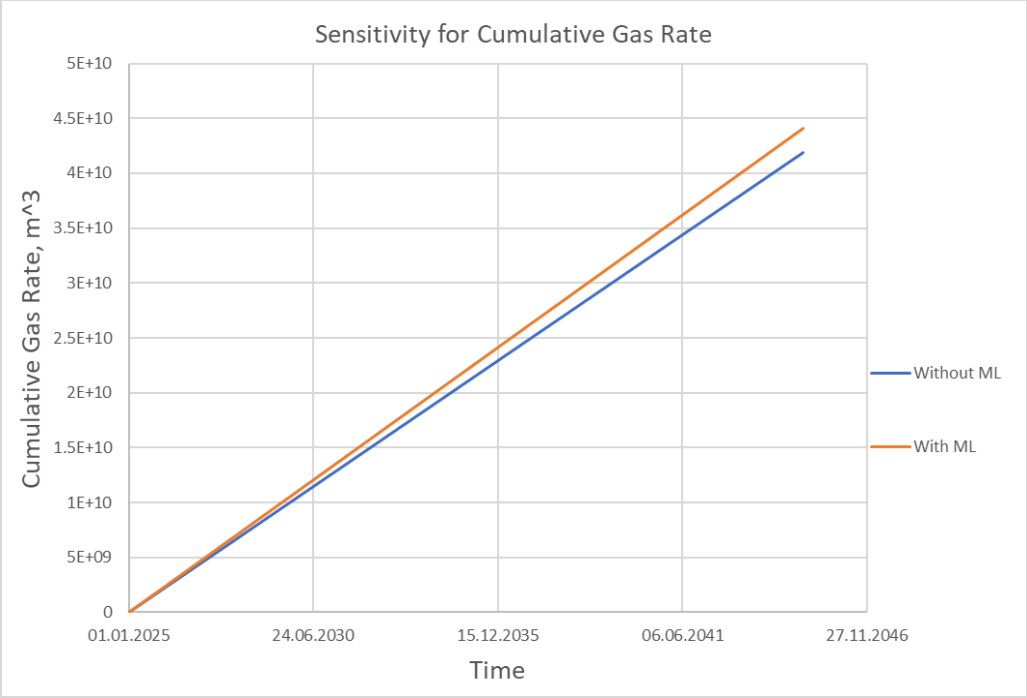

Figure 84. *Sensitivity for Cumulative Gas Rate without ML and with ML.*

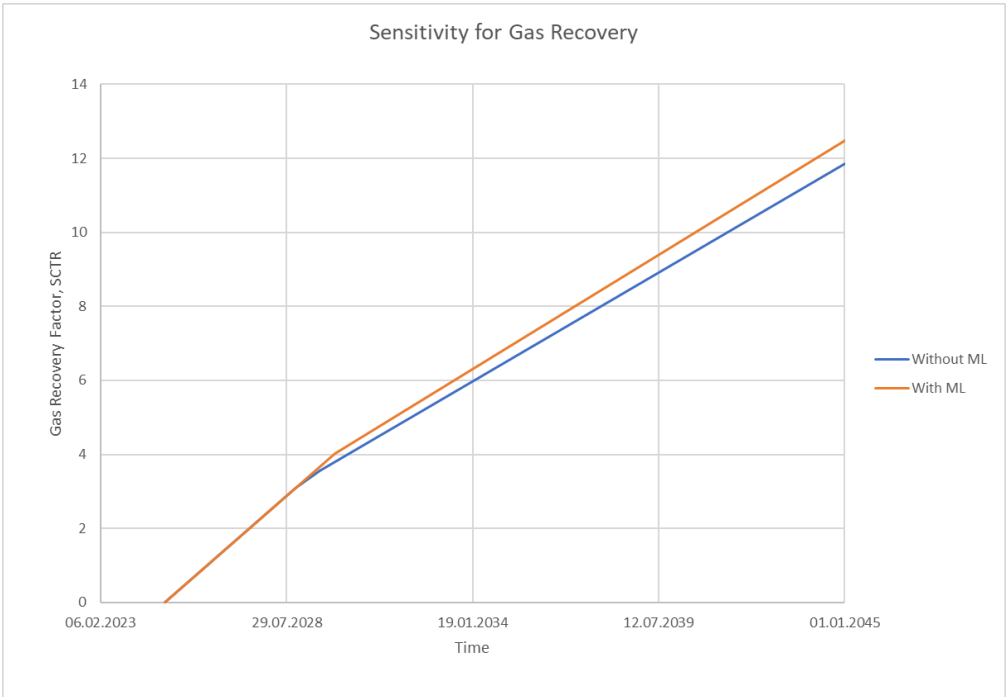

Figure 85. *Sensitivity for Gas Recovery without ML and with ML.*

Part 3: Results and Discussion

3.1 Geology

3.1.1 Tectonic Development

The development of the Browse Basin included six tectonic phases from the Late Carboniferous to the Late Jurassic to the Late Miocene and several events including extension, thermal subsidence and inversion, as shown in the table below (Le Poidevin, 2015).

Table 16. Six tectonic phases of the Browse Basin.

Period	Activity
Late Carboniferous to Early Permian	Extension I
Late Permian to Triassic	Thermal subsidence I
Late Triassic to Early Jurassic	Inversion I
Early to Middle Jurassic	Extension II
Late Jurassic to Early Cenozoic	Thermal subsidence II
Middle to Late Miocene	Inversion II

A detailed interpretation of these six basin phases is shown on **Figure 86.** The formation starts from Late Carboniferous to Early Permian, when extensional rifting and splitting of Sibumasu continental fragment away from Australian plate.The rifting have created intracratonic half-graben structures and large normal faults, that producing distinctive sub-basins separated by basement highs. These structural characteristics have influenced later period reactivation and localised the deposition of sediment successions.

Thermal subsidence of the basin continued during the Late Permian to Triassic, aided by the accelerated rates of sedimentation. Compressional reactivation of the basin during the Late Triassic to early Jurassic resulted in partial inversion of the earlier half-graben. The inversion generated major anticlines (e.g., Brecknock, Brewster and Bassett anticlines) that constitute significant structural traps for hydrocarbon accumulations.

In the Early to Middle Jurassic, renewed extension led to widening of the seaway causing widespread faulting, volcanism and the collapse of the Triassic anticlines. The Heywood Graben was also formed at this time. Thick fluvial-deltaic Plover Formation sediments were deposited which provide good quality reservoirs and mature source rocks. By the Late Jurassic to Early Miocene, the basin passed from being an intracratonic rift system to a passive margin as subsidence of the Scott Plateau and development of the Argo Abyssal Plain took place. A marine transgression culminated in the Late Cretaceous as thick successions of marine claystones were deposited. Large areas of these claystones, including the Echuca Shoals and Jamieson formations, provide regional seals in the basin, and they are regarded as potential source rocks.

Subsidence continued from the Late Cretaceous through the Cenozoic, leading to the north westward migration of the shelf edge and the formation of submarine canyons and turbidite mounds. In the Paleocene, a carbonate wedge prograded northwards. Water depths increased again in the Eocene in response to continued subsidence and a brief regression in the Oligocene associated with a global fall in sea-level only temporarily disrupted these marine conditions. Transgression resumed in the Miocene.

This final tectonic episode occurred in the mid to late Miocene, when renewed convergence between the Australian and Eurasian plates reactivated existing faults and caused north-northeast trending anticlines, along the sub basins of the Leveque Shelf, including the Greater Lombardina structure. This marked the most recent major deformation event in the Browse Basin and created the present-day structural framework.

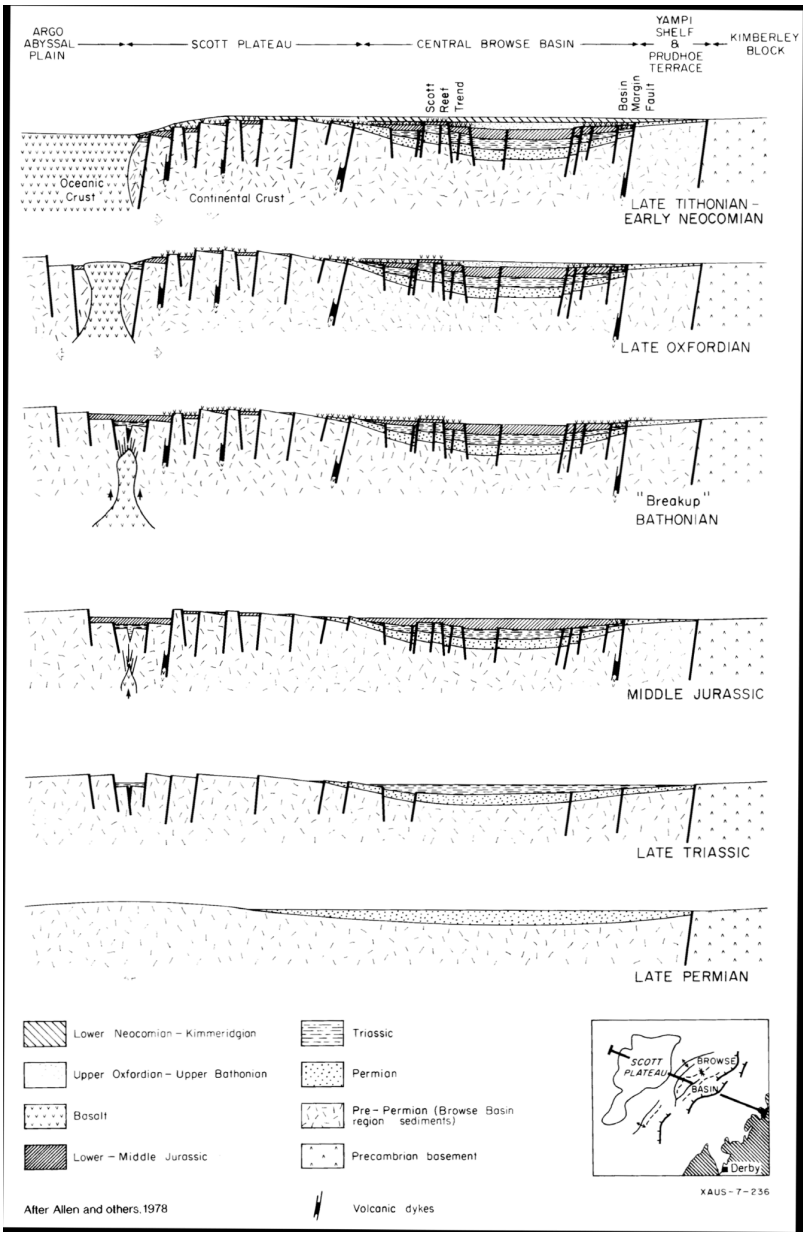

Figure 86. *Structural evolution of the Browse Basin (Le Poidevin, 2015).*

3.1.2 Stratigraphy and Lithology

The lithology of Plover formation is interpreted as being syn-rift succession that has been deposited during a period of active faulting of the Jurassic extension. It is mainly a sequence of sandstones with some conglomerates, interbedded siltstones, carbonaceous claystone, and thin coals with rare limestone (**Figure 87**). Consequently, the lateral continuity and the thickness of the Plover Formation are extremely variable.

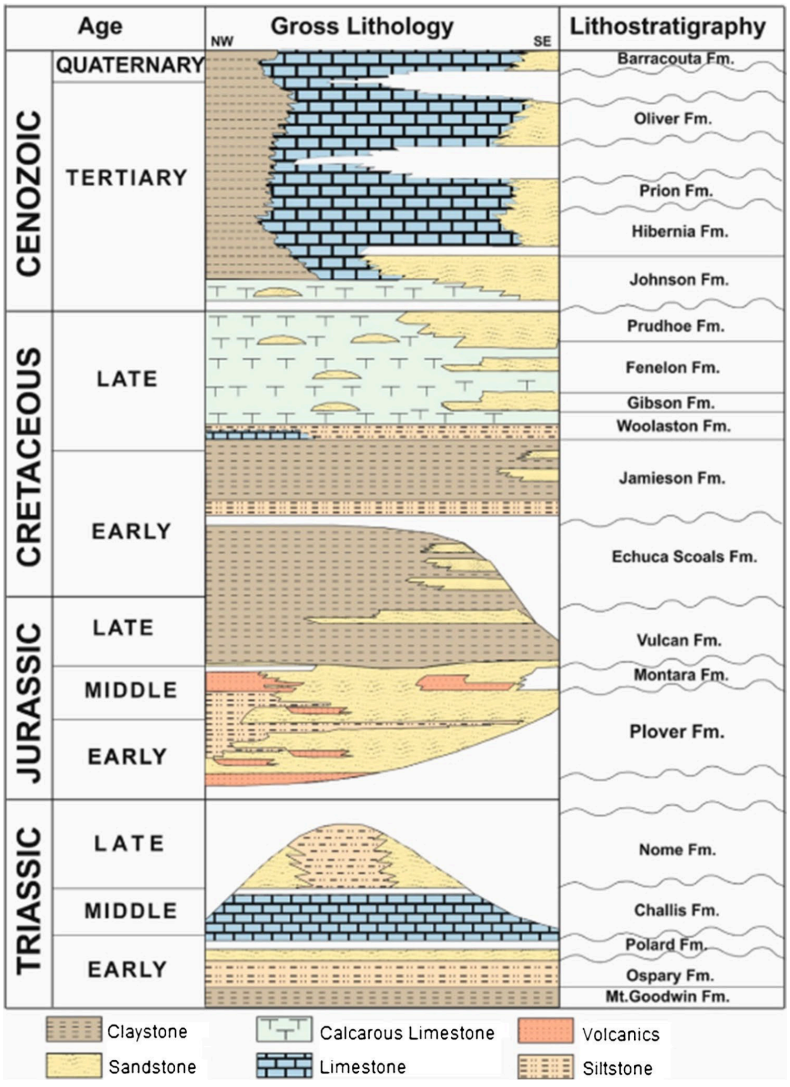

Figure 87. *Lithology (Le Poidevin, 2015).*

3.1.3 Petroleum Systems

Four petroleum systems are known in the Browse Basin; a basin-wide, dry gas-prone petroleum system and three petroleum systems that are presently only recognised within the Caswell Sub-basin. The extent of these petroleum systems, as shown in **Figure 88**, have been confined to well-control where hydrocarbon shows and accumulations from a given petroleum system are known (Edwards et al., 2014).

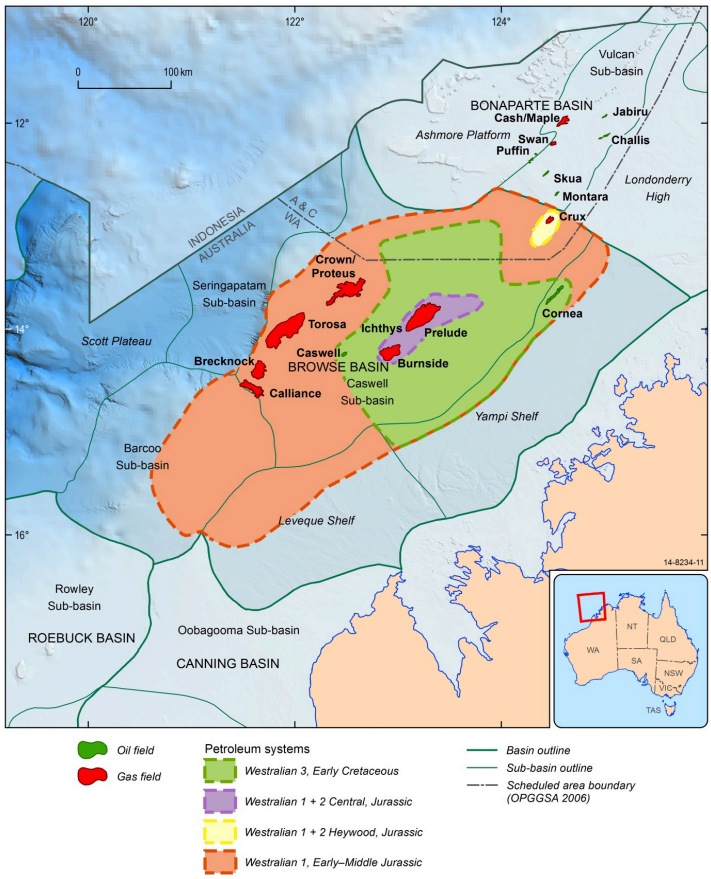

Figure 88. *Distribution of the four petroleum systems of the Browse Basin (Le Poidevin, 2015).*

Poseidon Field is best described by the Westralian 1 Petroleum System (Poivedin et al., 2015). The Westralian 1 Petroleum System consists of a well understood petroleum system Primary exploration targets are Jurassic-aged sequences. The primary source rock is the Lower to Middle Jurassic Plover Formation composed of fluvial-deltaic sediments rich in organic material in

the form of coals and carbonaceous shales. The plover formation is a very rich source rock that is well gas matured. Within the source rocks of the basin, burial and thermal maturity have enabled the generation and expulsion of hydrocarbons that have efficiently charged much of the basin's major gas accumulations.

The reservoir rock in the Poseidon Field is also the Plover Formation, and similarly high-quality and gas-saturated sandstone intervals of the Plover Formation are interbedded with shale and siltstone. The sandstone intervals of the Plover Formation typically have good porosity and permeability that make the sandstones good reservoir rocks for the accumulation of hydrocarbons.

Another key element of the petroleum system is the seal, provided by the Lower Cretaceous Echuca Shoals and Jamieson formations. The marine claystone deposits of these formations represent an effective cap rock, inhibiting the vertical migration of hydrocarbons and resulting in the accumulation of hydrocarbons in underlying Plover Formation reservoirs.

Hydrocarbons in the Poseidon Field are found to be trapped in structural traps as a result of the Triassic-Jurassic extensional tectonics. These structural traps include horsts, tilted fault blocks and roll-over anticlines which allow for structural closures that can accumulate and preserve numerous quantities of gas. These trapping mechanisms have been enhanced by the interaction between extension and inversion phases within the history of the basin, improving the hydrocarbon potential of the field.

In summary, we interpret the Poseidon Field as a relatively unaltered gas-prone petroleum system in the Browse Basin, containing mature source rocks, excellent reservoirs, efficient seals and well defined structural traps to produce large accumulations.

3.1.4 Static Modeling

The study examined the structural features, reservoir characterization, and hydrocarbon potential using seismic interpretation and geological models. The Petrel software platform by

Schlumberger was used for static modeling. The following **Figures** represent the skeleton of the 3D grid with faults and horizons.

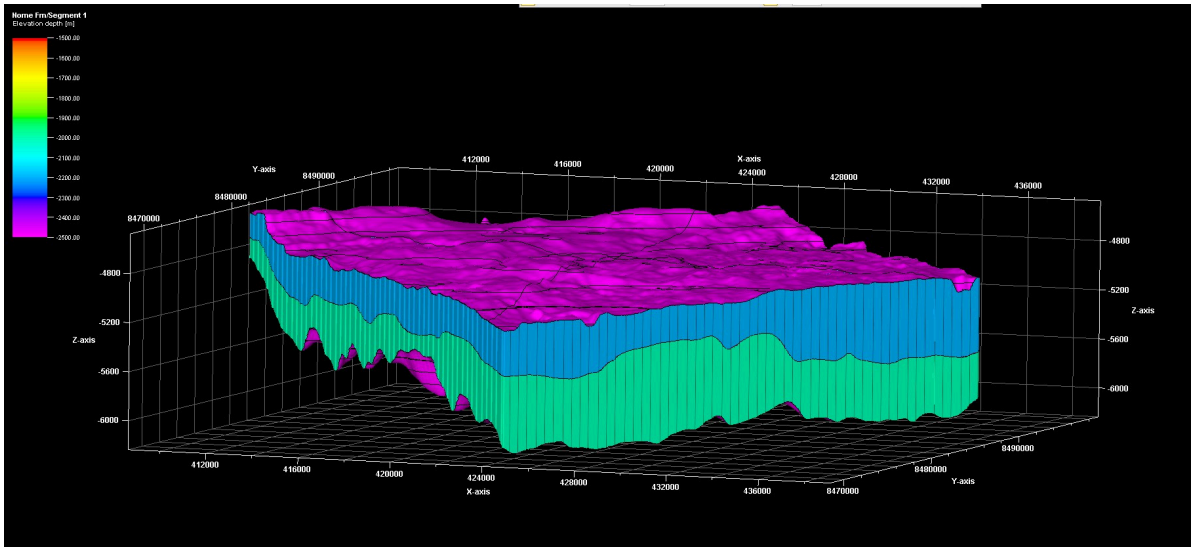

Figure 89. *3D Grid in the Static Model.*

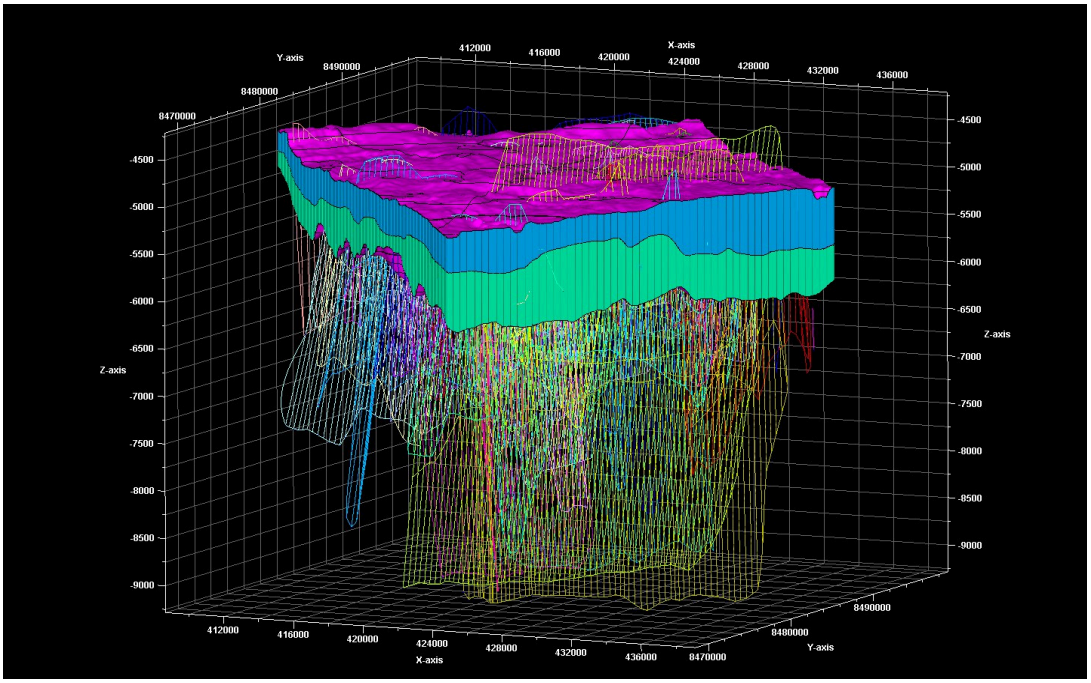

Figure 90. *3D Grid Skeleton with Edges and Faults.*

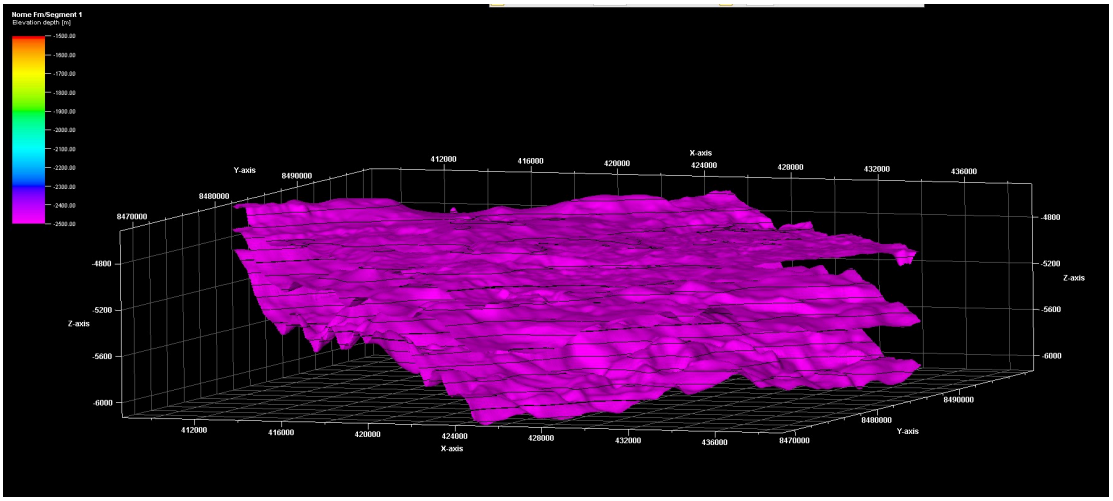

Figure 91. *Horizons in the Static Model.*

Based on the seismic interpretation, the Poseidon field has a structurally complex subsurface with faulted and folded strata. It indicates a dynamic depositional environment. **Figure 92** presents a 2D seismic profile that displays multiple fault systems, with interpreted faults marked in different colors. According to the fault patterns, it can be considered as the normal faulting and anticlines act as structural traps for hydrocarbons. The variation in seismic reflector continuity suggests different lithologies, influencing reservoir quality and distribution.

Additionally, color-coded seismic amplitudes provide insight into lithology changes and potential fluid content variations. The folds appear to be closely related to faults, suggesting they may be fault-propagation folds. Seismological interpretation points to a reservoir with substantial hydrocarbon potential that is divided into several fault-controlled compartments. To verify reservoir quality and connectivity, more research is necessary, including dynamic simulation and well log integration.

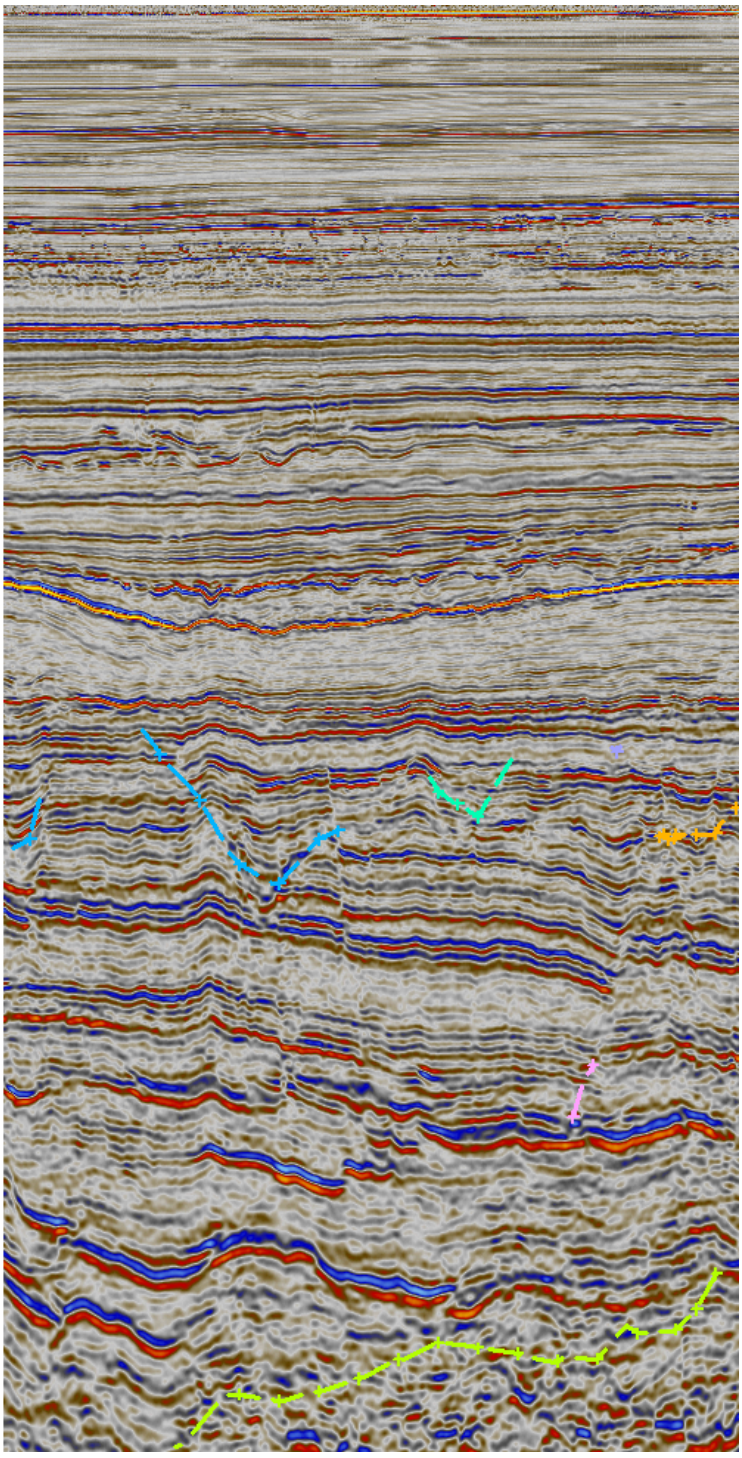

Figure 92. *Horizons and faults on the seismic profile interpretation window*

Figure 93 shows the lithology distribution in the 3D seismic model. The lithology above and below this boundary is interpreted as being variable, with the potential for sandstones and silty sandstones.

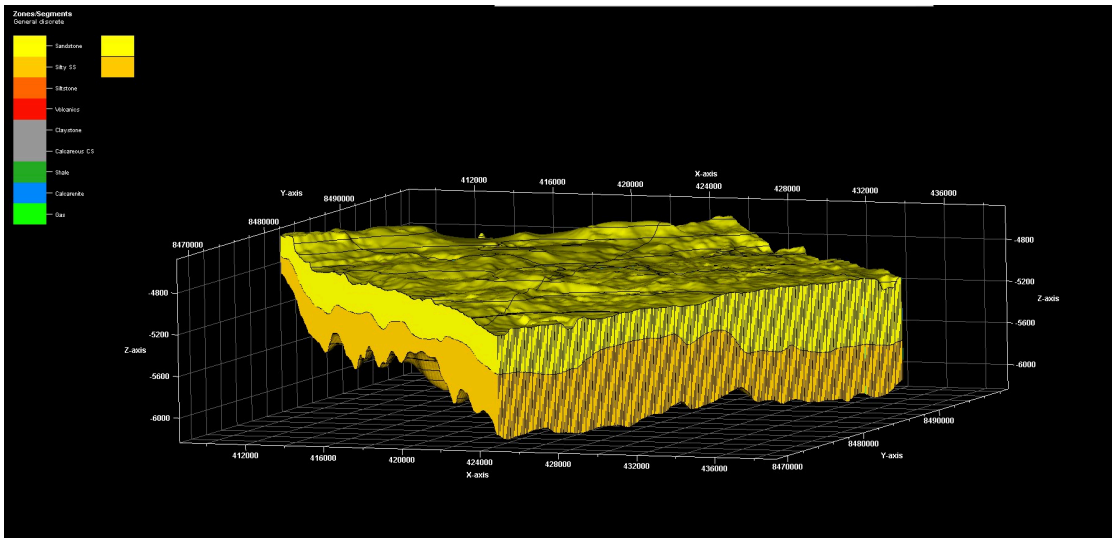

Figure 93. *Lithology of the Zones/Segments in the 3D Seismic Model.*

Moreover, the distribution of the properties including porosity, permeability, water saturation, and gas saturation were created and can be seen in the **Figures 94-97.**

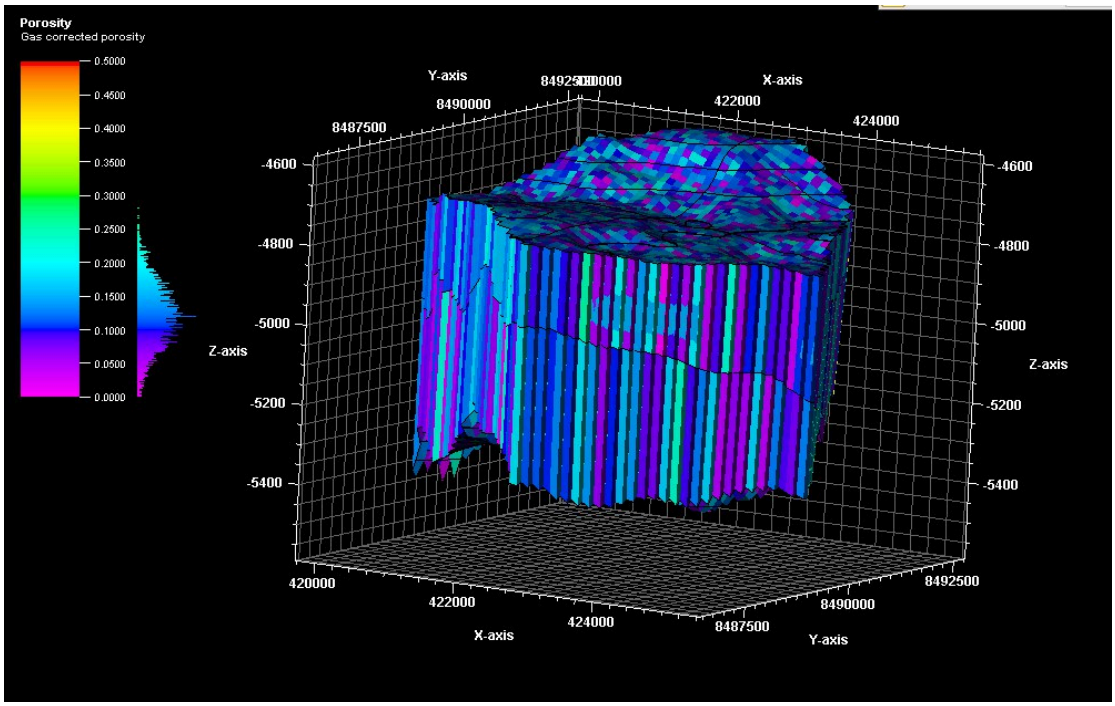

Figure 94. *Porosity Distribution in the Static Model.*

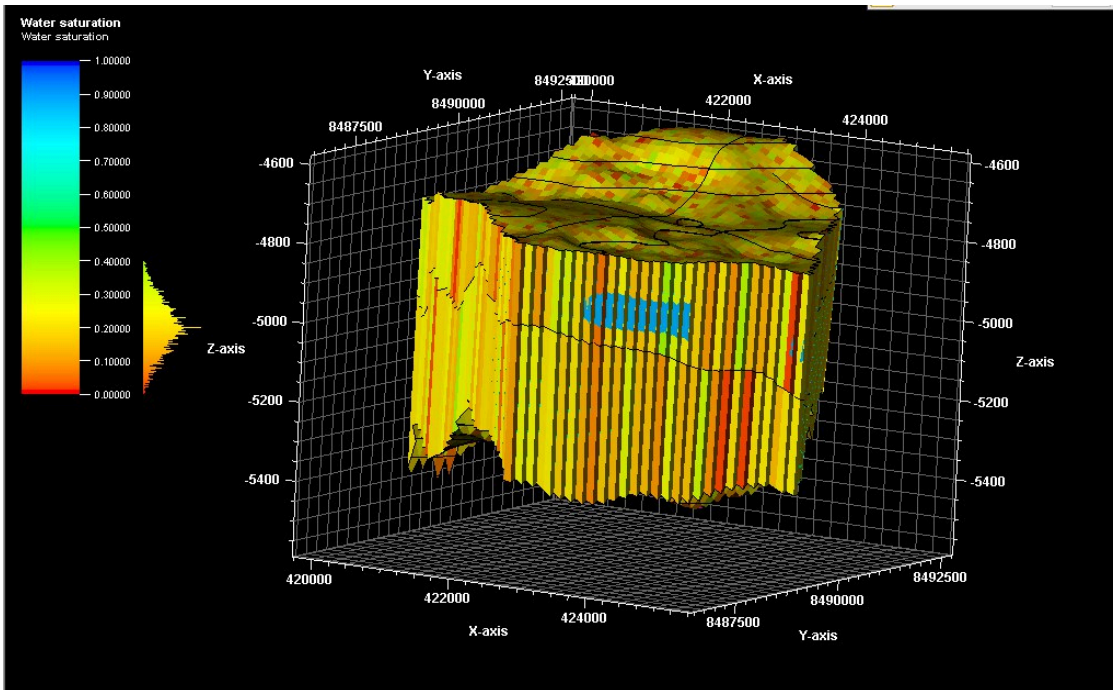

Figure 95. *Water Saturation Distribution in the Static Model.*

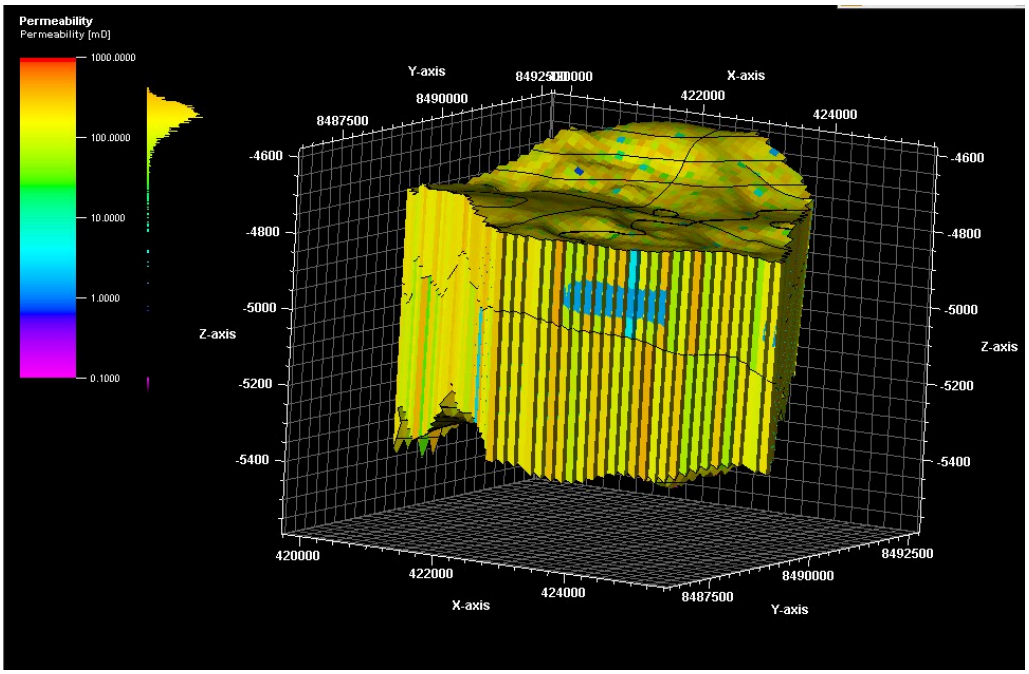

Figure 96. *Permeability Distribution in the Static Model.*

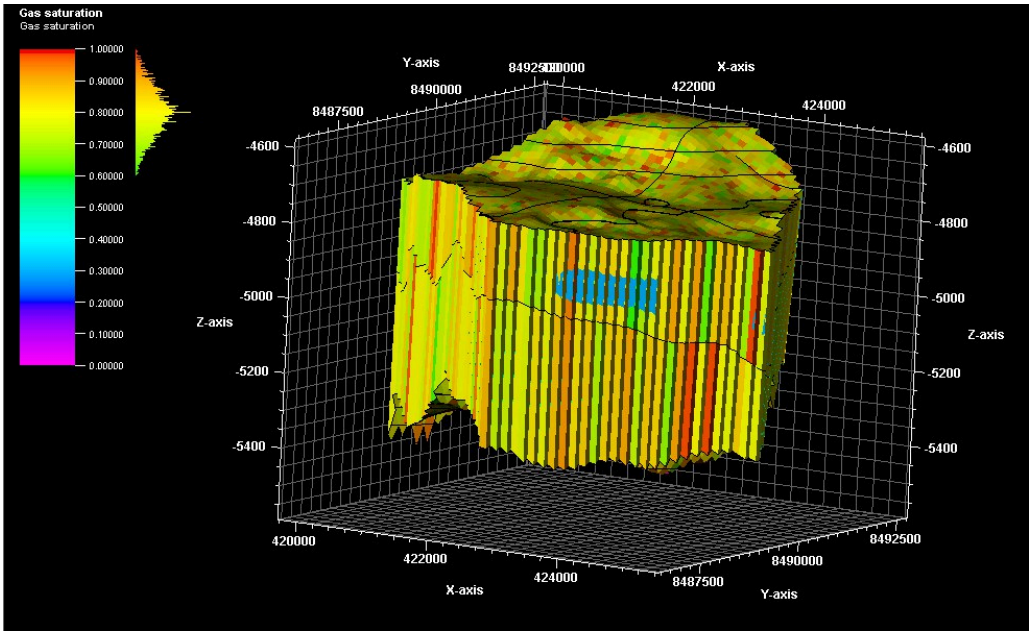

Figure 97. *Gas saturation Distribution in the Static Model.*

3.2 Petrophysics

3.2.1 Well Log Analysis

The available .las files were uploaded to Petrel to analyze and edit well logs. Using various functions, the log tracks were refined and interpreted. The final results of Well Log Analysis for wells Boreas - 1 and Poseidon - 2 can be seen in **Figures 98 and 99** below:

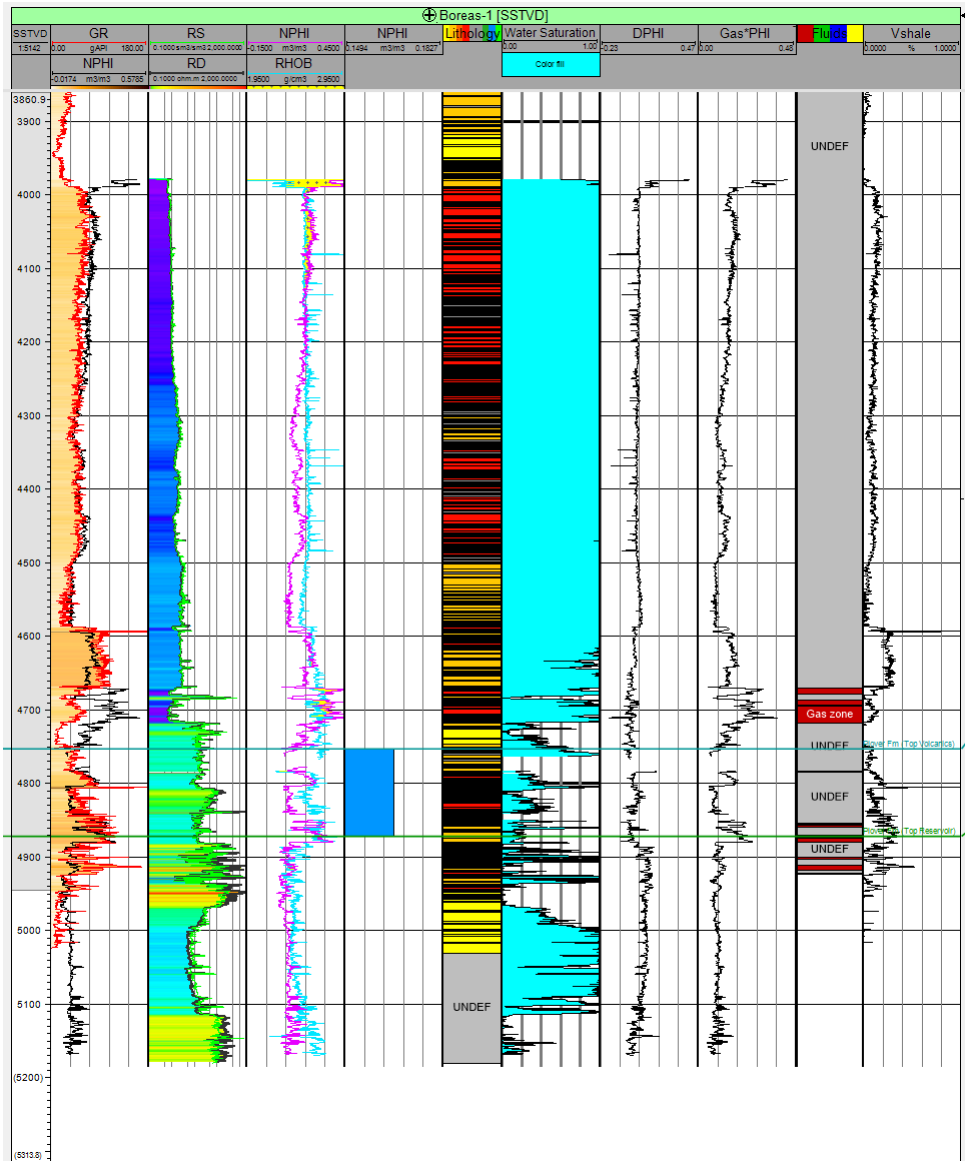

Figure 98. *Well Log interpretation of Boreas - 1.*

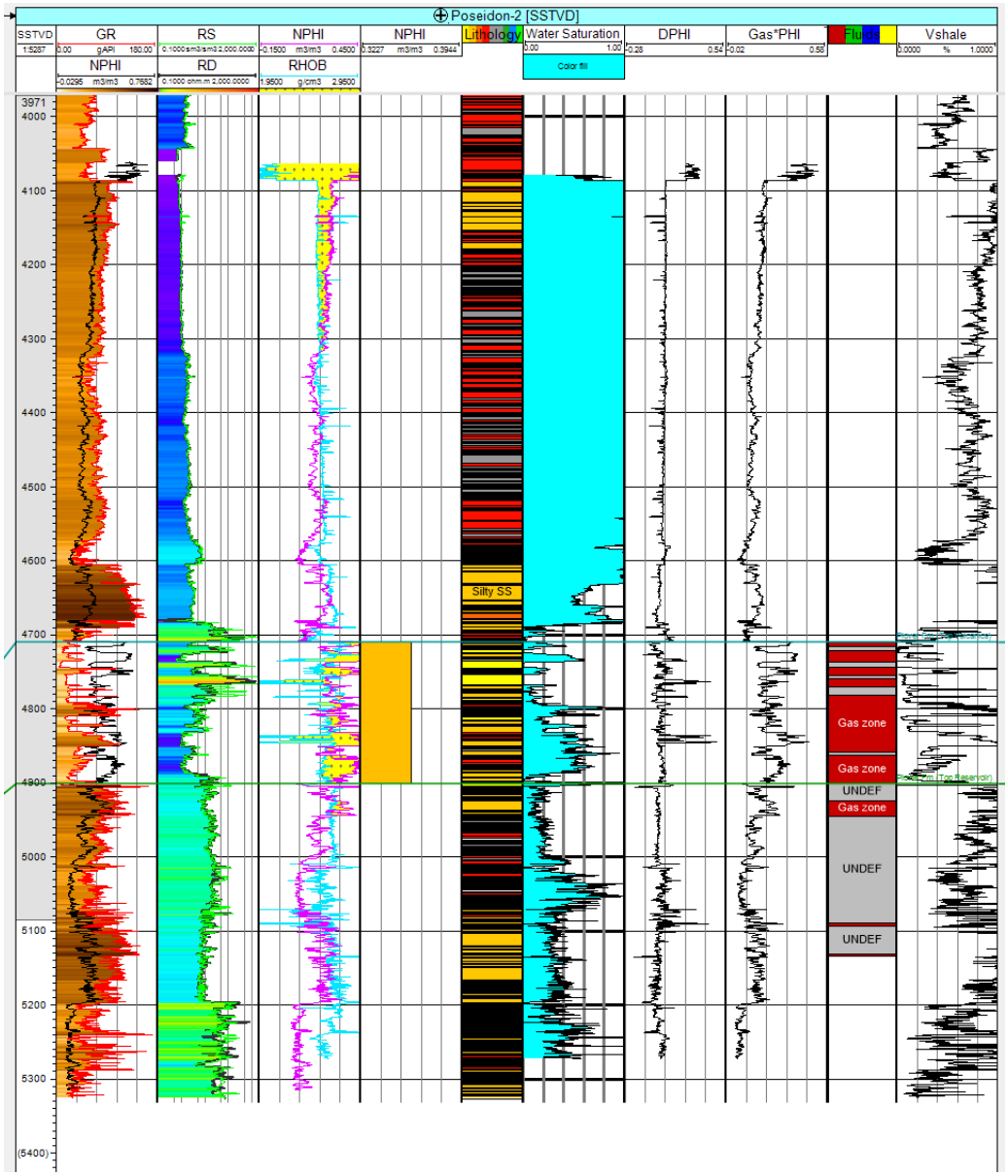

Figure 99. *Well Log interpretation of Poseidon - 2.*

First of all, using the "Calculator" function, the ranges of GR values for different lithologies have been manually entered into Petrel in order to create the discrete track of "Lithology". It can be seen on the portion of the GR and Lithology logs from Boreas - 1 below,

how the function correctly establishes cleaner zones of sandstone interbedded with silty sandstone from higher GR values of volcanics and claystones.

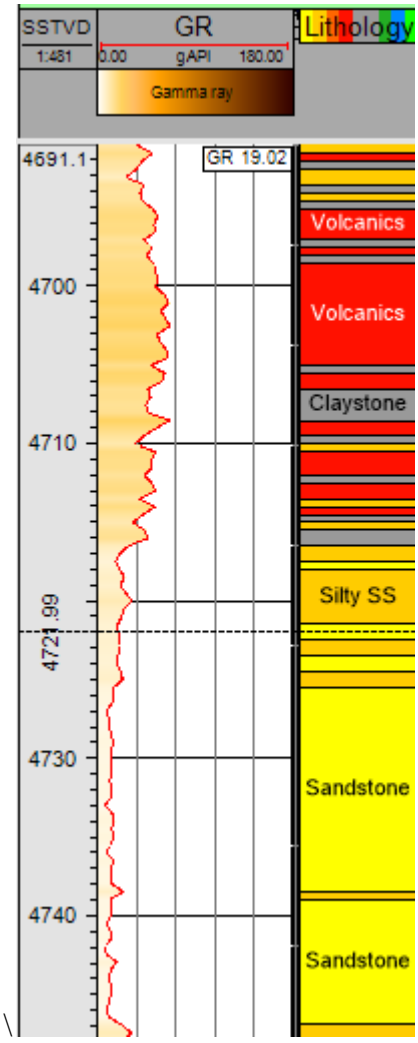

Figure 100. *GR and Lithology logs for Boreas - 1.*

Also using the Calculator, shale volume, Vsh was calculated for the logged interval, and put as a separate log. By taking into account the identified lithologies and calculated shale volume, it is possible to differentiate between porous, clean zones of interest and layers of claystone/shale.

Furthermore, using the equations for DPHI and GasPHI, the density porosity and gas-corrected porosity were determined:

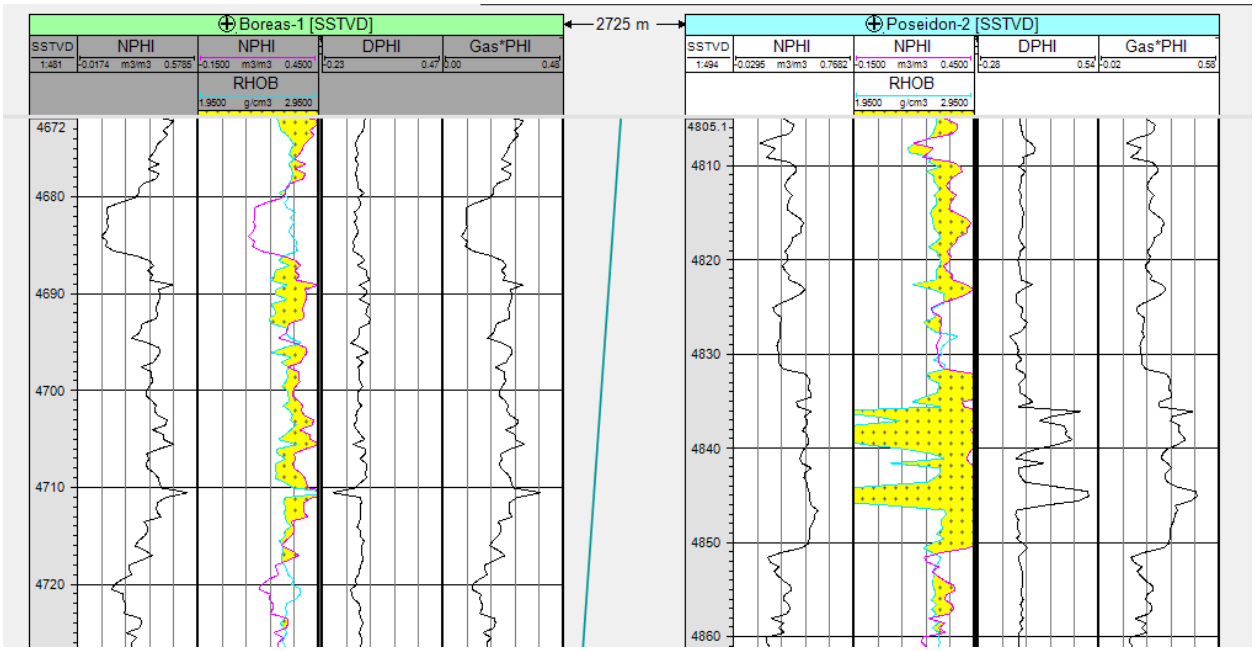

Figure 101. *DPHI and GasPHI logs.*

In the **Figure 101** above, the depth intervals filled in with yellow correspond to the depths where RHOB is considerably smaller than NPHI, which is an indicator of the "fluid effect" taking place, meaning that these layers are likely to contain gas. Expectedly, the DPHI values for these intervals are underestimated, and therefore, it is proven that the gas-corrected porosity value should be calculated by accounting for both density porosity and neutron porosity in these zones.

Following that, using the calculated GasPHI, and the initially given RD logs, the water saturation values were determined for the logged depth via the Archie equation.

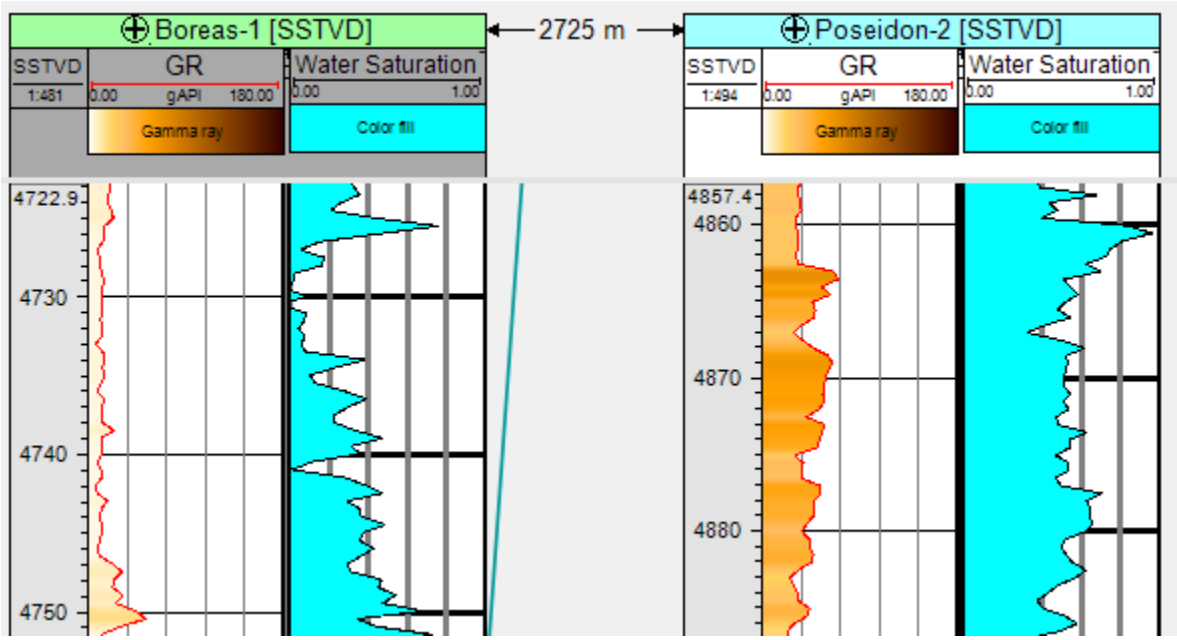

Figure 102. *Calculated Sw for Boreas - 1 and Poseidon -2.*

It is important to note that the equation for DPHI does not account for the heterogeneities of the rock beds, and instead considers the average matrix density (2.65 gcc) for the entire interval. Due to the presence of other lithological units interbedded between the sandstone layers, at certain points the calculation gives erroneous results. In order to clean up the data, the values of GasPHI and Sw were quality-checked by removing outliers using z-scaling. The final average values for GasPHI and Sw calculated via logs and obtained via Conocophillips (2012) results are given in **Table 17** below:

Table 17. Comparison of calculated and reported values of average porosity and water saturation.

	Boreas - 1		Poseidon - 2	
	$\phi_{average}$	$Sw_{average}$	$\phi_{average}$	$Sw_{average}$
Calculated	0.11	0.21	0.09	0.24
Reported	0.13	0.23	0.08	0.22

Lastly, using the fluid effect in the NPHI and RHOB logs, another discrete log with fluid (gas) zones was created. As a result, integrating the interpretations of the Lithology and Fluid zone tracks, as well as the Sw and Vsh, and RD logs, zones of interest for future perforations can be found. For example, in **Figure 103** below, the given interval in Boreas - 1 has relatively low shale volume and water saturation. The deep resistivity in the area is increased, pointing to the presence of hydrocarbons, and the overlap between the porosity logs indicates the possibility of the layer containing gas.

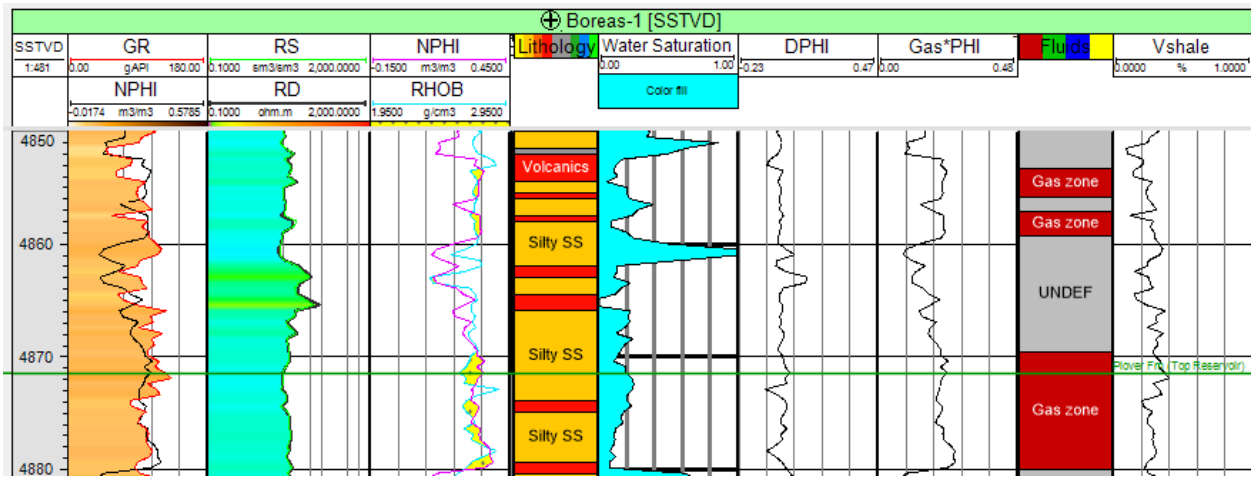

Figure 103. *Possible perforation interval in Boreas - 1.*

Similarly, the following interval in Poseidon - 2 also displays low GR and water saturation, high resistivities, and fluid effect, making it a prospective producing zone.

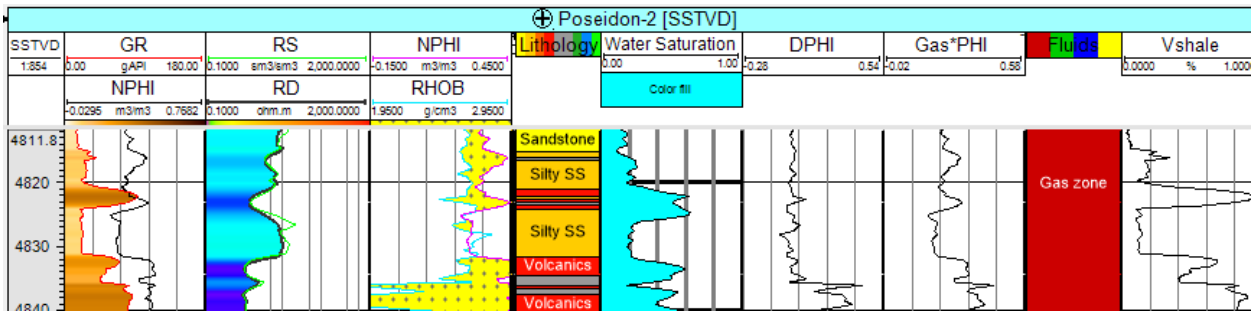

Figure 104. *Possible perforation interval in Poseidon - 2.*

3.2.2 Fluid Analysis

The available chemical composition was averaged between the two wells and the heavier hydrocarbon fractions were lumped together in WinProp:

Component	Primary	Secondary
N2	0.0040581087	0.0
CH4	0.7653098	0.0
CO2	0.16411212	0.0
C2H6	0.033910087	0.0
C3H8_FC6	0.017310097	0.0
BENZ_C9	0.0051582737	0.0
FC10_C19	0.0052907936	0.0
FC20_C29	0.0042606391	0.0
FC30_C36	0.00059008851	0.0

Figure 105. *Chemical composition input into WinProp.*

Figure 106 below demonstrates the change in Relative volume vs Pressure in the CCE test. The modelled test results are represented by the blue curve, and the experimentally reported values

are given in red. As it can be seen, the experimental and simulated results are in satisfactory agreement, pointing to the accuracy of the model. The Relative volume, as a general trend, decreases as pressure increases, changing from 5.9 at roughly 900 psia to 0.7 at 10000 psia.

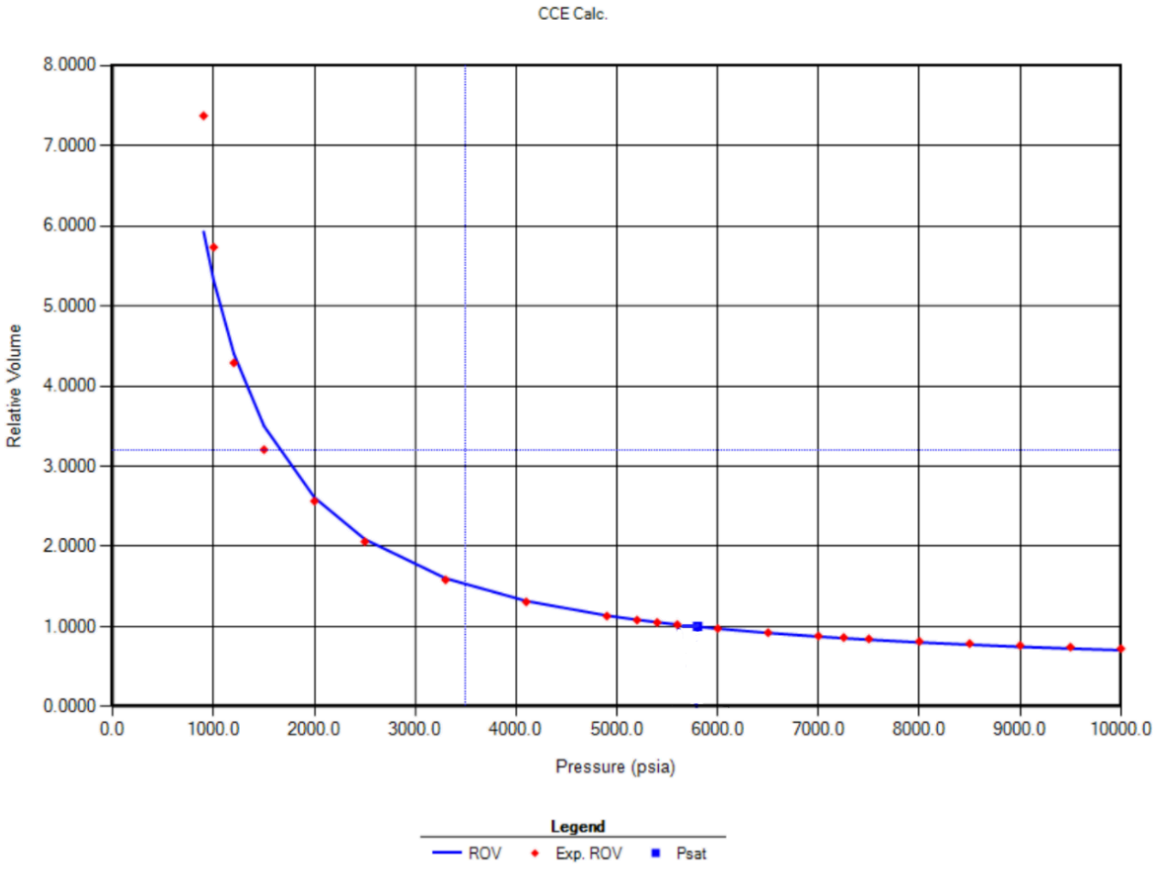

Figure 106. *CCE test results for Relative Volume.*

The graph below shows the changes in oil and gas viscosities with changes in pressure. Oil viscosity, shown on the green curve, decreases with increasing pressure. The maximum value of 0.1755 cp was obtained at approximately 1200 psia, and with a steady decrease, reached 0.1325 cp at 7200 psia. Gas viscosity, on the other hand, experienced an increase from 0.017 cp at 1000 psia to 0.046 at 10000 psia.

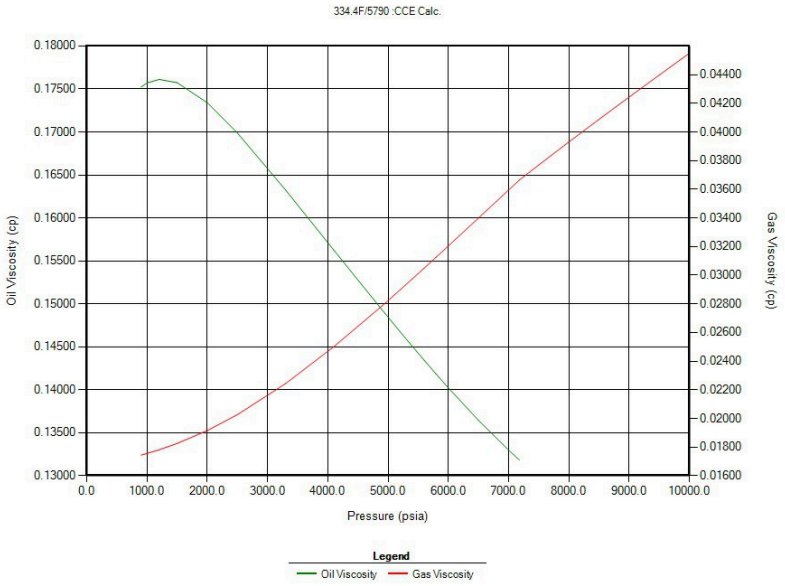

Figure 107. *CCE test results for Oil and Gas Viscosities.*

The CCE test for the Liquid volume % in the cell, shown in the **Figure 108**, demonstrates a rise until the pressure of 4000 psia, where it reaches its peak of 2.2 % of the cell volume. It then falls rapidly, hitting the minimum of 0% at around 7200 psia.

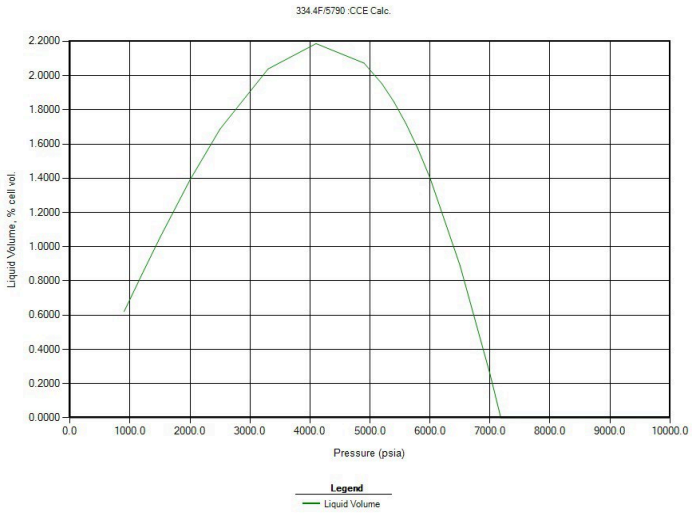

Figure 108. *CCE test results for Liquid Volume.*

When it comes to the Z factors of oil and gas, provided in **Figure 109** below, both curves demonstrate an upward trend, but show different behaviors especially at lower pressures. Oil Z factor increases rapidly between pressures of 1000 to 3000 psia, whereas gas Z factor decreases slightly before slowly rising. The maximum Z factor for oil was established at over 7000 psia with a value of 1.27. Gas Z factor reached the highest point of almost 2.2 at 10000 psia.

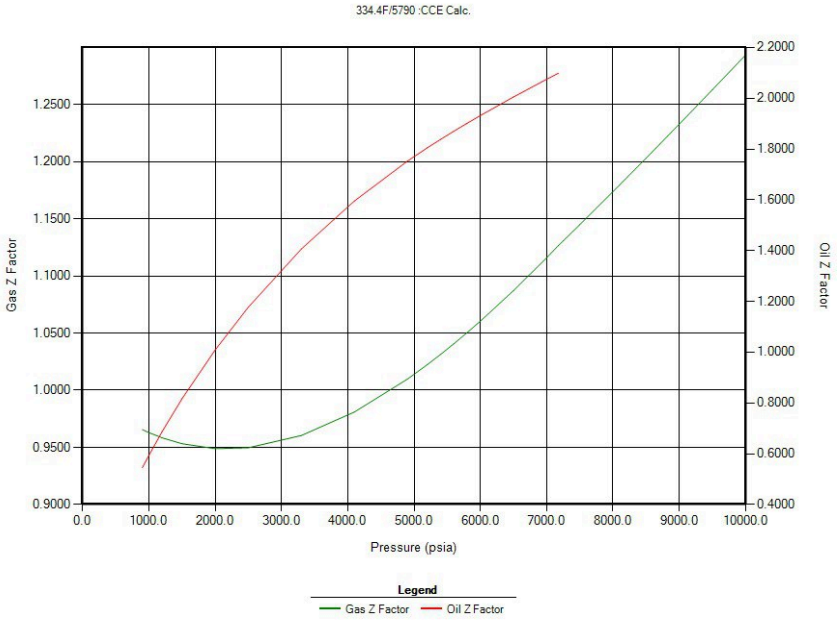

Figure 109. *CCE test results for Oil and Gas Z Factors.*

The tested oil compressibility experiences a moderate climb with lower pressures, gradually increasing to the peak of 1.67E-5 1/psia at 4500 psia. Up until the pressure of 7200 psia, compressibility decreases slowly, and swiftly falls down to the minimum value of 1.07E-5 1/psia after.

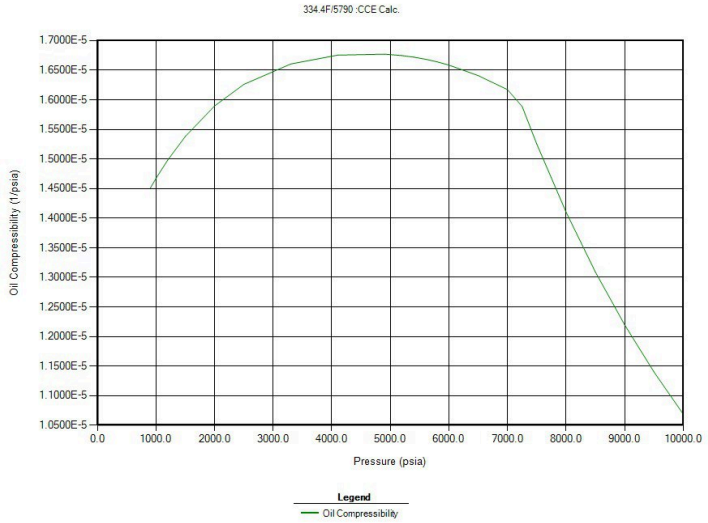

Figure 110. *CCE test results for Oil Compressibility.*

Gas density (in green) experiences an increase with increasing pressure, while oil density (red) decreases. The maximum values for oil and gas densities are 42.2 lbm/ft3 and 23.5 lbm/ft3 respectively. The minimum value for gas density is about 2.5 lbm/ft3, and 38 lbm/ft3 for oil/

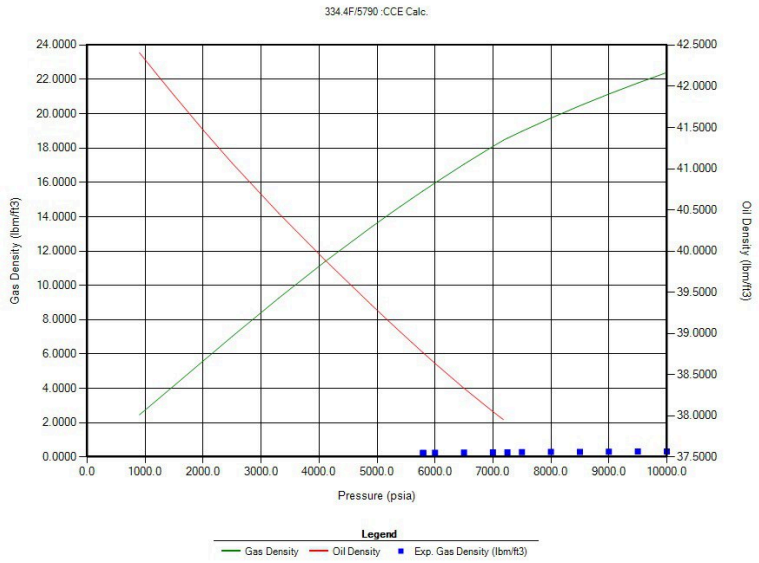

Figure 111. *CCE test results for Oil and Gas Densities.*

Figure 112 presents the compressibility factor (Z-factor) of gas and two-phase fluid along pressure. Overall, the Z-factor first declines with pressure till it reaches a minimum and then rises with reducing pressure. Such behavior is expected since fluids in the reservoir, namely gas and liquid, are non-ideal, and their requisite non-ideality is apparent by the Z-factor correspondingly during the depletion. Hence, the conformity between simulated and experimental results of Z-factors is a manifestation of the accuracy of the EOS model used in the fluid characterization.

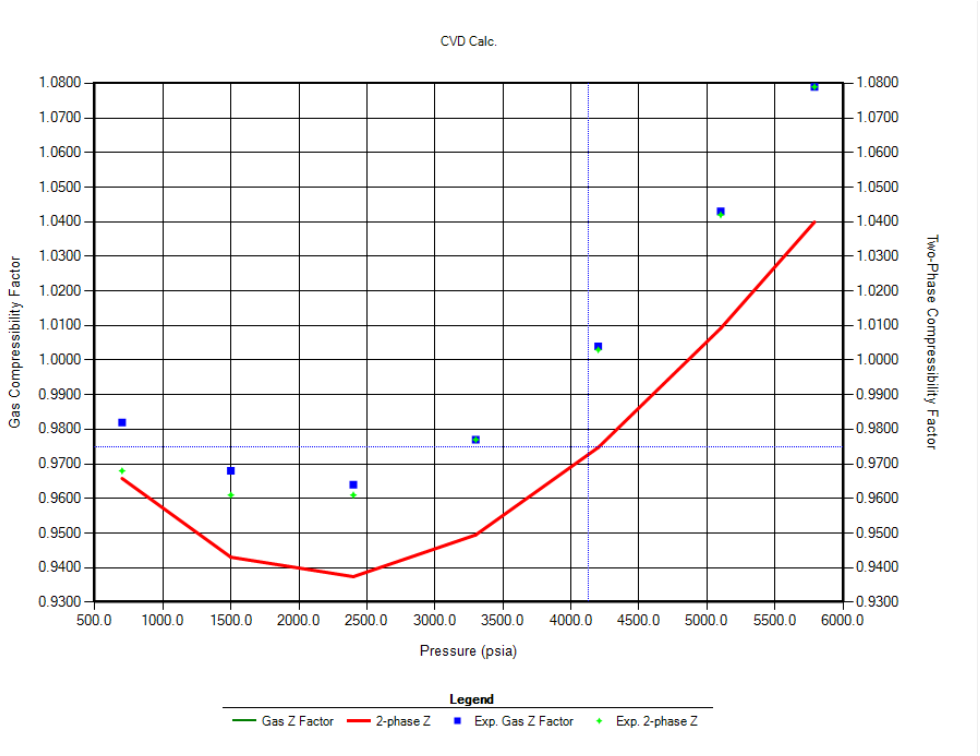

Figure 112. *CVD Results – Liquid Volume and Produced Gas vs Pressure.*

This additional CVD graph (**Figure 113**) essentially highlights the connection between pressure decline and fluid phase behavior. We notice that as the pressure declines, the liquid volume undergoes an almost linear decline, while the fraction of gas generated undergoes an almost linear increase. This confirms the gas liberation phenomenon due to the depressurization process. It proves the presence of a retrograde behavior, which is typical of gas-condensate

systems. This is a key factor in the definition of gas-condensate recovery strategies, specifically pressure maintenance optimization.

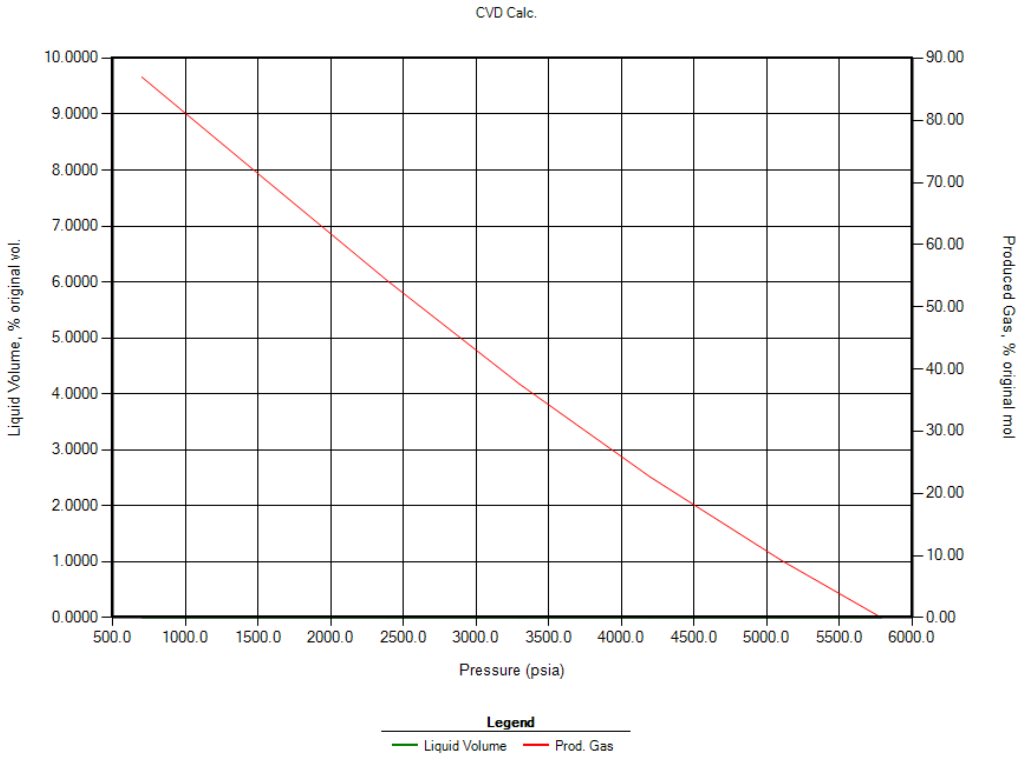

Figure 113. *CVD Results – Liquid Volume and Produced Gas vs Pressure.*

In order to analyze the phase behavior further, Two-Phase Envelope was normalized in CMG WinProp. **Figure 114** shows how phase boundary conditions for coexisting liquid and gas phases are plotted as a function of pressure and temperature on a Two-Phase Boundary Diagram. On the left of the line is the Dew Point, and on the right the Bubble Point, the top of the curve is the Critical Point.

At 320°F and 5790 psia, the reservoir fluid originally exists as a single-phase gas. As pressure decreases during production, the fluid will eventually enter the two-phase region and undergo retrograde condensation. Such a phenomenon indicates the importance of managing

bottomhole pressure so as to keep it away from the region of liquid dropout and high skin factor so that gas can flow efficiently to the wellbore.

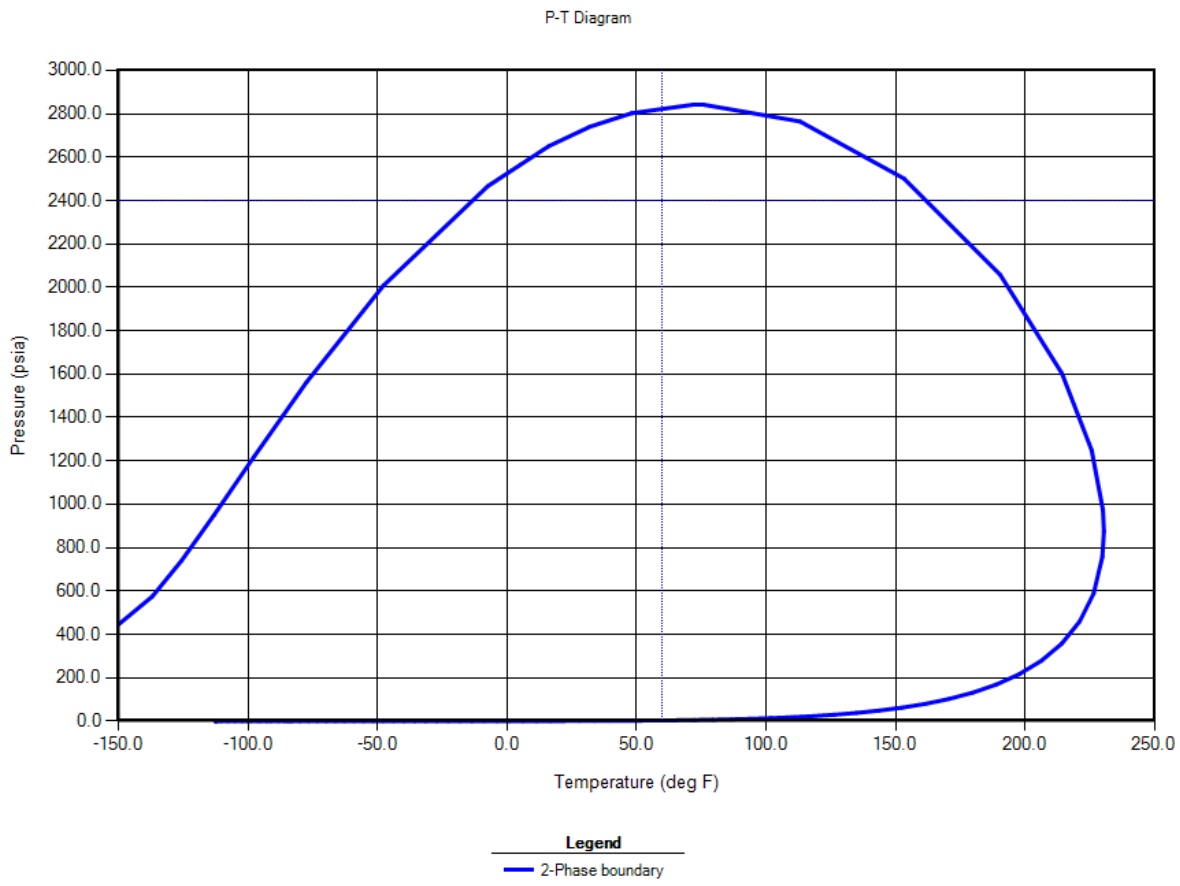

***Figure 114**. 2-Phase Envelope.*

3.3 Reservoir Engineering

3.3.1 Well Test Analysis

The pressure build up behavior, reservoir boundaries and flow characteristics of the Boreas-1 well test analysis form the focus of this work. Reservoir connectivity and fluid flow restrictions are determined using multiple geological scenarios of the build-up data, including closed rectangular fault models, latera composites and parallel fault systems.

Pressure Build-Up & Reservoir Connectivity

A final pressure of 7136.5 psia at 56 hours of shut-in shows the amount of pressure depletion of 5.2 psi indicating a slight pressure depletion of 5.2 psi in the initial reservoir pressure. The log-log derivative plot had an upswing trend implying a limited volume of the reservoir, that might be the result of fault bounded compartments. Data and results were taken from the Boreas-1 well test interpretation report (ConocoPhillips 2012)

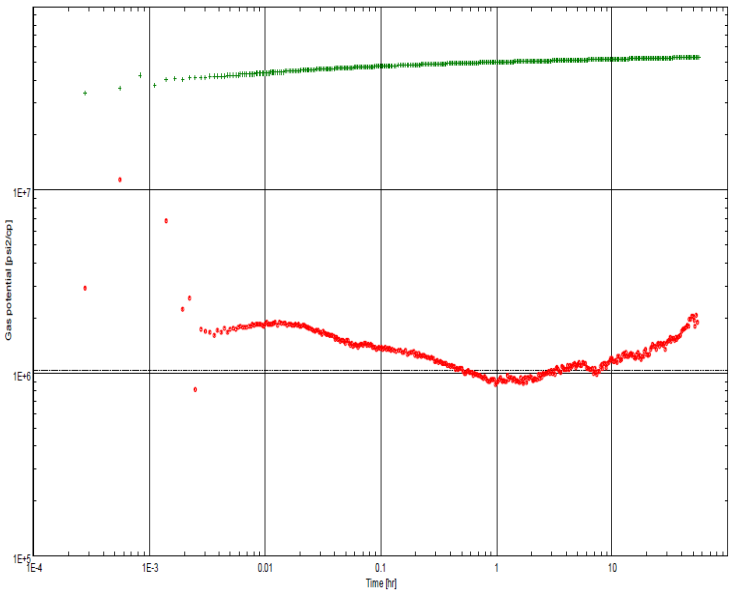

Figure 115. *Final build-up log-log plot.*

The upswing trend on the derivative curve indicated that there was limited reservoir volume because of faulting or compartmentalization. The radial flow regime was seen in the early time response indicating that the wellbore was draining a circular area in the reservoir. Mid time response is transient flow with moderate skin effects, most probably due to slight formation damage or slight partial perforation. An upswing trend in the late time response pointed to the existence of a reservoir boundary restricting the coefficients of fluid flow.

Permeability and Skin Factor Interpretation

Permeability (k) Estimate: 60.2 – 71.8 mD, derived from the build-up slope.

Transmissibility (kh) Estimate: 14,200 – 17,000 mD-ft, confirming good reservoir quality.

Skin Factor (S) Value: 6.9 – 12, indicating some near-wellbore damage or completion inefficiency.

Mobility Ratio (k/μ) indicated moderate gas mobility, suggesting an effective drainage area.

Reservoir Boundaries and Flow Regimes

The build-up test provided critical insights into reservoir boundary conditions and fluid flow behavior, helping to define the effective drainage area and potential barriers to flow. The build-up curve deviates sharply, indicating a no-flow boundary. Suggests reservoir compartmentalization, potentially affecting pressure support and depletion strategy.

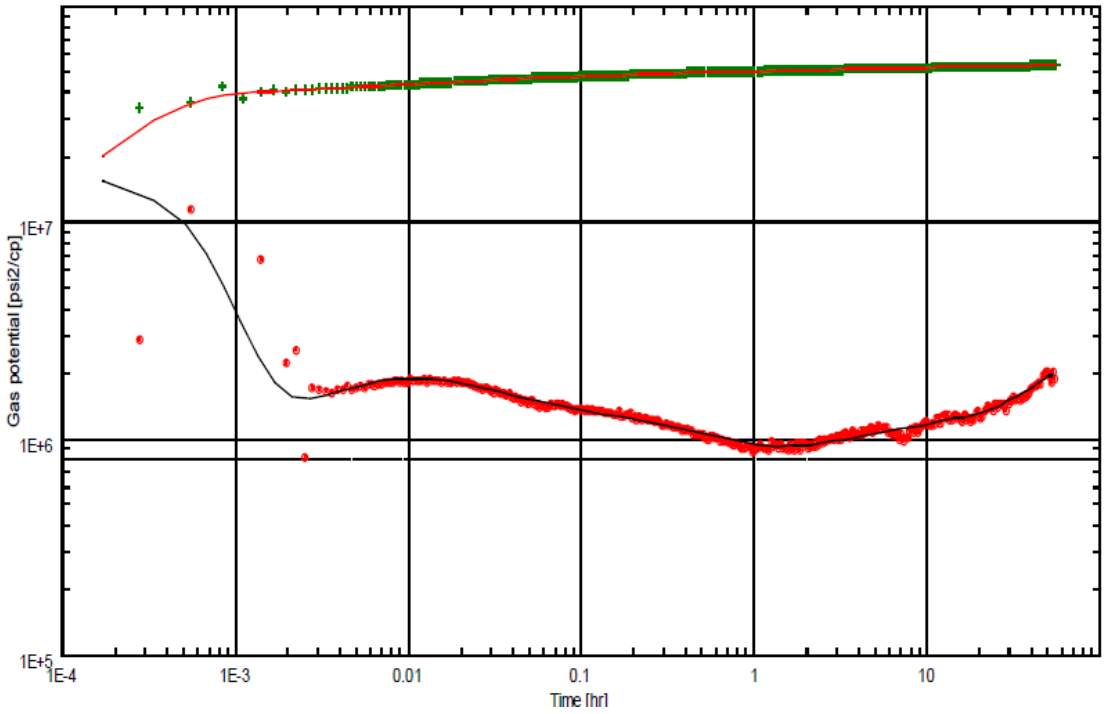

Figure 116. *Build-up matching with a closed rectangular fault boundary model, confirming flow restrictions.*

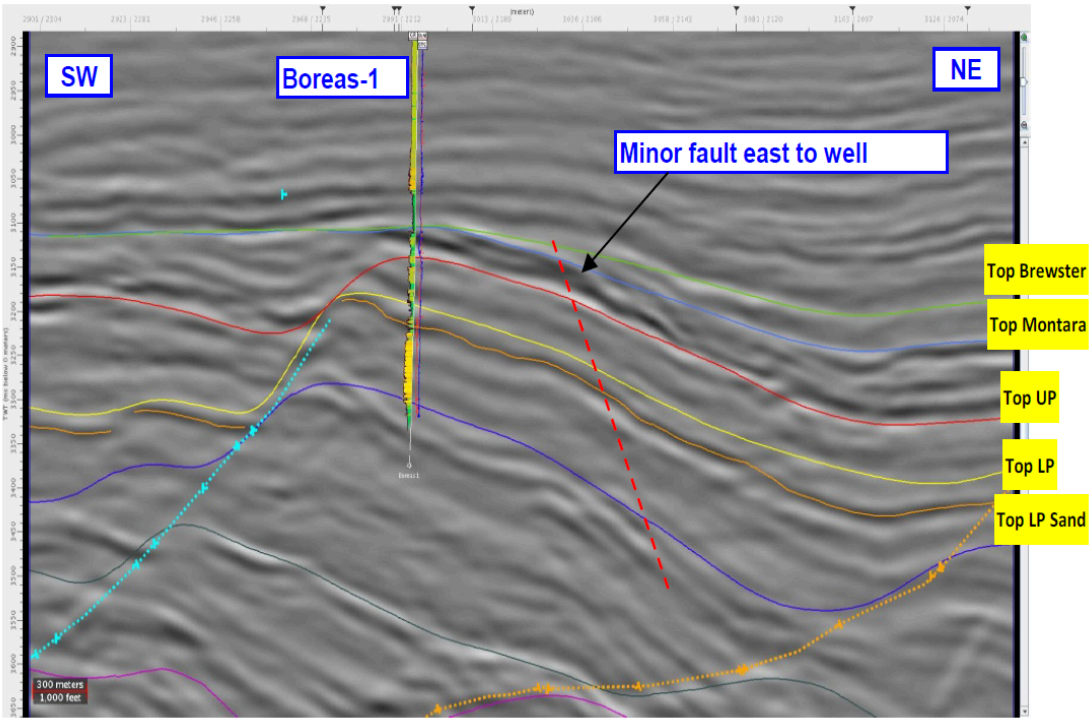

Figure 117. *Seismic Line Across Boreas-1.*

The well test analysis for Boreas-1 provided valuable insights into reservoir pressure behavior, permeability, and boundary effects, confirming the presence of fault-controlled flow restrictions. The pressure build-up test revealed a low depletion rate (5.2 psi), suggesting a moderate pressure support system, while the permeability range (60.2 – 71.8 mD) indicates favorable reservoir quality for production. However, the presence of a sealing fault to the east and a potential aquifer boundary to the south suggests reservoir compartmentalization, which may limit long-term drainage efficiency.

3.3.2 Reserves Estimation

The reserves estimation for Gas Initially In Place (GIIP) was conducted using the Monte Carlo simulation technique implemented in Python. This method accounts for uncertainties in reservoir parameters by generating 10,000 random realizations to estimate P90, P50, and P10 values. In this context, P90 represents a conservative estimate with a 90% probability of at least

this volume being present, P50 is the most likely (median) estimate, and P10 is an optimistic case where there is a 10% probability of exceeding this volume. These values provide a probabilistic assessment of gas volumes, aiding in better reservoir management decisions.

To estimate the Gas Initially In Place (GIIP), the volumetric method is used, which calculates the total gas volume in the reservoir based on key geological and petrophysical parameters. This method accounts for reservoir area, net pay thickness, porosity, water saturation, and gas formation volume factor. The general equation for GIIP is expressed as follows:

The GIIP estimation is based on key reservoir parameters from Petrel modeling, well logs, and PVT analysis. The reservoir area (42.3 km²) was derived from Petrel structural maps, while net pay thickness (60 – 100 m) was obtained from well correlations and Petrel model outputs. Porosity (0.08 – 0.25) and water saturation (0.10 – 0.60) were determined from well log calculations, ensuring accurate reservoir characterization. The gas formation volume factor Bg (0.00339 – 0.00513 ft³/SCF) was sourced from PVT analysis and reservoir simulation results. These parameters were incorporated into a Monte Carlo simulation to generate probabilistic GIIP estimates (P90, P50, P10) for a more reliable reserves assessment

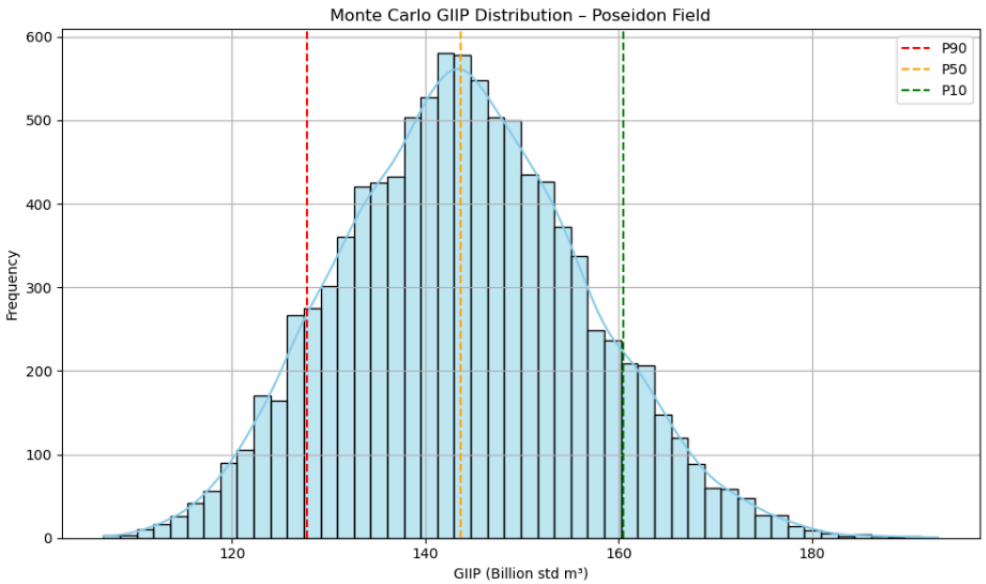

Figure 118. *GIIP distribution calculated by Monte-Carlo technique.*

P90 (Conservative GIIP Estimate): 1.28e+11 STD M^3

P50 (Median GIIP Estimate): 1.43e+11 STD M^3

P10 (Optimistic GIIP Estimate): 1.61e+11 STD M^3

#	Item	Units	Value
1	Total Bulk Reservoir ...	RES M3	1.00831E+10
2	Total Pore Volume,	RES M3	1.24051E+09
3	Total Hydrocarbon Po...	RES M3	9.81429E+08
4	Original Oil in Place, ...	STD M3	1.27766E+07
5	Original Gas in Place, ...	STD M3	1.93826E+11

Figure 119. *GIIP data from Petrel modeling.*

The GIIP estimates of around 1.28 × 10^{11} std m^3 (P90), 1.43 × 10^{11} std m^3 (P50) and 1.60 × 10^{11} std m^3 (P10) were generated by Monte Carlo simulation. Although slightly lower than the deterministic estimate of 1.938 × 10^{11} std m^3 of the petrel model, these values do reveal a large gas volume in place. With respect to this context, a conservative estimate is P90, which means that there is a 90 percent chance that the true GIIP will be greater than P90. P50 is the median value (most likely estimate) and P10 is an optimistic case with only a 10% probability the GIIP is greater. The values that were spread between these two values were more tight than earlier simulations which make it possible for the model to be more reliable. It is likely that the variance from Petrel's result comes from assumption of different reservoir area, average net pay, and how parameter uncertainties are treated. A more probabilistic, risk aware assessment is performed using Monte Carlo, which includes uncertainty and reservoir heterogeneity yet uses fixed inputs – maybe based on optimistic or ideal conditions as in Petrel.

3.3.3 Field Development Strategy

The field's development strategy includes both primary recovery and enhanced oil recovery (EOR) techniques. Initially, the field was developed with vertical wells targeting the most productive zones, particularly those with favorable permeability-porosity relationships. With the maturation of the field, more advanced techniques such as gas injection and waterflooding were introduced to improve the recovery factor.

Drive Mechanism

On the basis of geological and dynamic indicators, the gas expansion drive is interpreted as the main reservoir drive mechanism in the Poseidon Field. The stacked fluvial-deltaic sandstones with variable reservoir quality (Dong et al., 2020) form the reservoir, which is in the Plover Formation. Such formations are typically attributed to minimum aquifer support and hence, a water drive mechanism is not possible.

Amplitude Versus Offset (AVO) analysis and seismic interpretation indicate that Poseidon gas sands have AVO Classes II responses which are expected from gas satured zones (Adebayo et al., 2021). This suggests that most of the production energy is from expanding the gas as the reservoir pressure declines.

Pressure build up testing at the Boreas-1 appraisal well also showed little pressure depletion and little or no strong aquifer activity despite the large gas flow volumes seen during testing (ConocoPhillips, 2024). This behavior is expected when production drive is mainly gas expansion and pressure maintenance from adjacent formations is negligible.

Despite the lack of available direct long term production data, a strong case for gas expansion as the dominant drive mechanism for the Poseidon Field is made through the integration of petrophysical, seismic, and well test analysis. Overall, this result is consistent with other high-pressure gas reservoir research in Australia, which has reported gas expansion and limited influence of the aquifer (Singh et al., 2020).

Boundary Selection

The selected reservoir boundary is defined based on structural and petrophysical analysis, ensuring optimal well placement. The two white lines represent faults, which influence fluid flow and compartmentalization. Wells are strategically placed to maximize production while avoiding pressure depletion issues or water breakthrough risks. The polygon outlines the high-quality reservoir zone, ensuring that drilling targets areas with good porosity and permeability while maintaining distance from sealing faults that could limit connectivity.

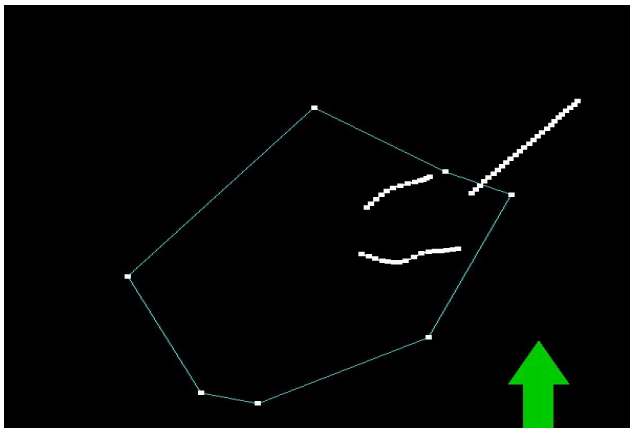

Figure 120. *Reservoir Boundary and Fault Map.*

The Neutron Porosity Map

The Neutron Porosity Map shows varying porosity across the Poseidon Field, with higher Neutron Porosity values (0.20–0.25 m^3/m^3) indicating better reservoir quality. These high-porosity zones are ideal for well placement, as they suggest higher fluid storage potential. Poseidon-2 is strategically placed in the central high-porosity area, maximizing hydrocarbon storage. Boreas-1 and Kronos-1 are located in areas with slightly lower porosity, likely to assess reservoir continuity and access multiple reservoir layers. This placement strategy optimizes reservoir evaluation and production potential.

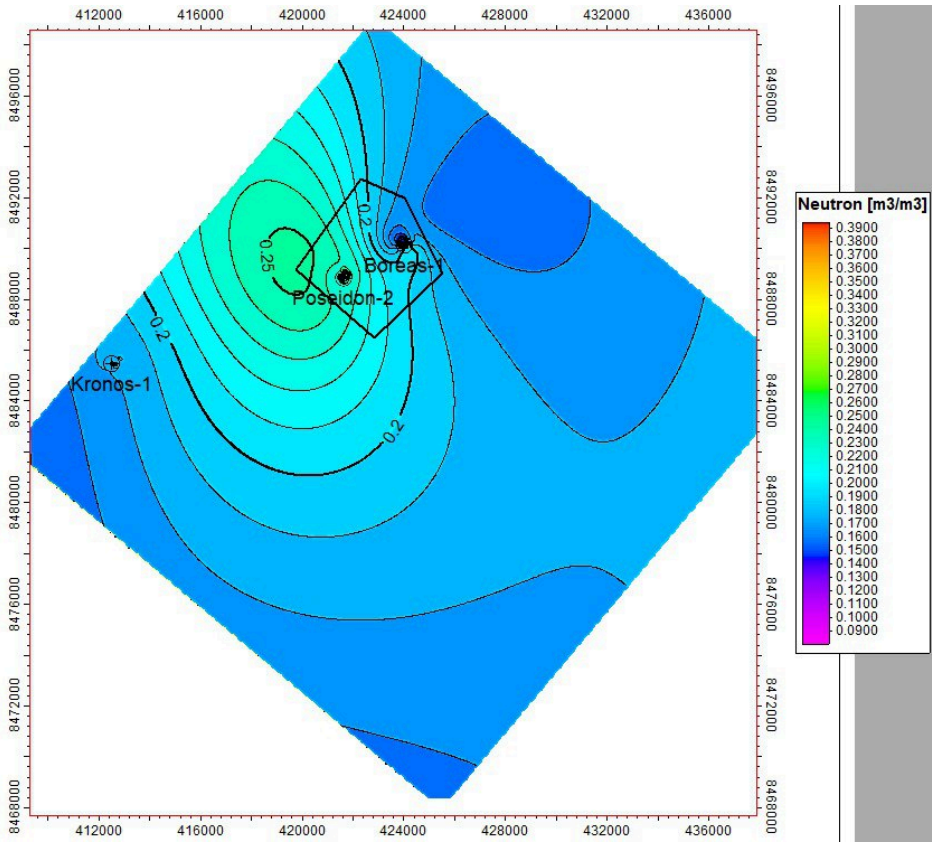

Figure 121. *Neutron Porosity Map for Reservoir Characterization and Well Placement.*

The Resistivity Map

The Resistivity Map shows the distribution of resistivity across the Poseidon Field. High resistivity zones (red and purple) near Poseidon-2 and Boreas-1 indicate hydrocarbon-bearing formations or low-water saturation, making them ideal locations for well placement. In contrast, Kronos-1 is located in a moderate resistivity zone (blue and green), suggesting a more water-saturated or clay-rich formation with lower hydrocarbon potential. The well placements target high resistivity areas to optimize hydrocarbon recovery, while the moderate resistivity zones require further evaluation to assess their viability for production.

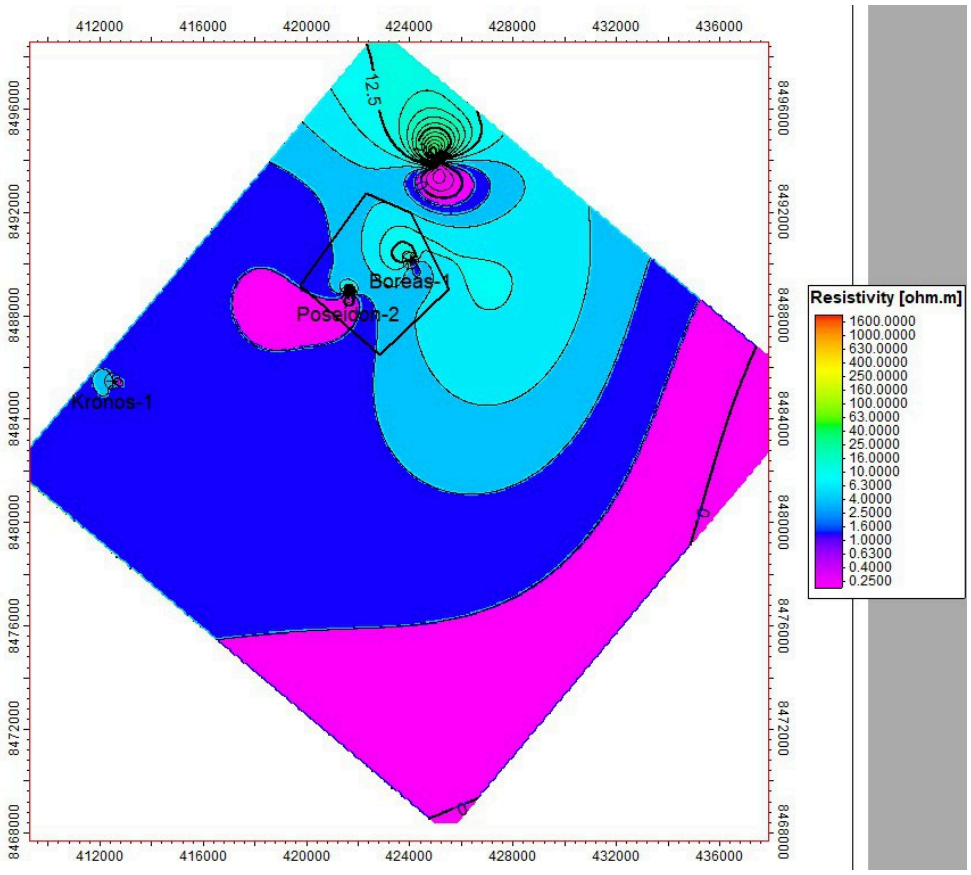

Figure 122. *Resistivity Map for Hydrocarbon Identification and Well Placement.*

Well Placement Strategy

Implementing a five-spot well pattern, with a central gas injection well surrounded by four production wells at the corners, is a well-established strategy in enhanced oil recovery (EOR). This configuration facilitates efficient displacement of hydrocarbons toward production wells, optimizing reservoir sweep efficiency and maximizing oil recovery. Studies have demonstrated that the five-spot pattern can achieve incremental oil recovery of approximately 10.3%, making it an attractive option for reservoir development (Wang et al., 2009).

In reservoirs characterized by high water cut, traditional water injection methods often become less effective due to excessive water production, leading to operational challenges and diminished oil recovery. In such scenarios, gas injection, particularly with carbon dioxide (CO_2), offers a more suitable alternative. CO_2 injection not only aids in maintaining reservoir pressure but also enhances oil recovery through mechanisms such as oil swelling and viscosity reduction. Research indicates that increasing CO_2 pressure recovery from 60% to 100% can raise oil recovery from 9.56% to 35.42% and improve water reduction, effectively delaying water invasion (Zhang et al., 2024).

Furthermore, CO_2 injection into depleted gas reservoirs serves the dual purpose of enhancing hydrocarbon recovery and sequestering CO_2, thereby contributing to greenhouse gas mitigation efforts. Depleted gas reservoirs are considered promising candidates for CO_2 storage due to their substantial capacity and proven sealing capabilities. Studies have highlighted that among the available CO_2 capturing sinks, depleted gas reservoirs have high potential to sequester CO_2 effectively (Singh et al., 2020).

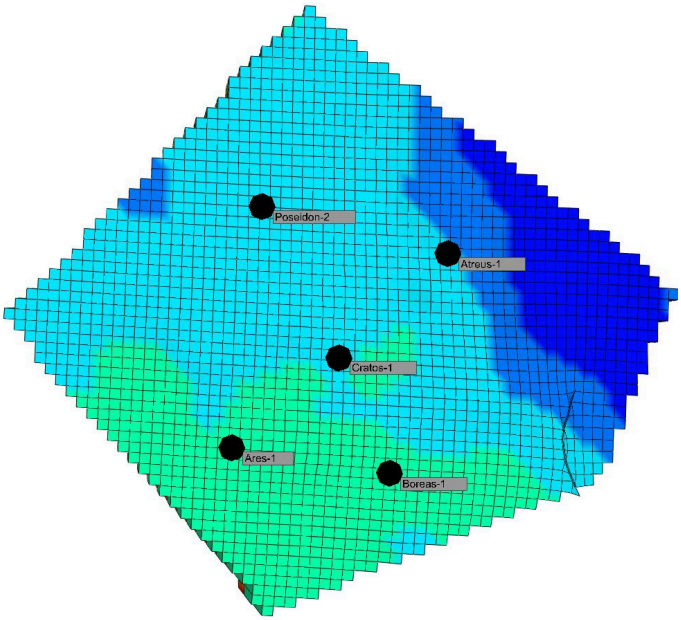

Figure 123 . *Five-Spot Gas Injection Well Pattern.*

3.4 Drilling and Completion Engineering

3.4.1 Well completions

The schematic of the two exploratory wells that were exhibited in the reservoir was sketched by using PIPESIM and Eclipse simulation softwares. Specifically, it was the Poseidon-2 and Boreas wells. The figures below show that the every well consists of 3 casings (conductor, surface, and intermediate), 1-2 liners (depending on the depths of each production well), permanent packer (for better well integrity and pressure control, also involved for injection control in injection well), and tubing. In both of the wells that were displayed, perforations were also constructed for production and injection purposes.

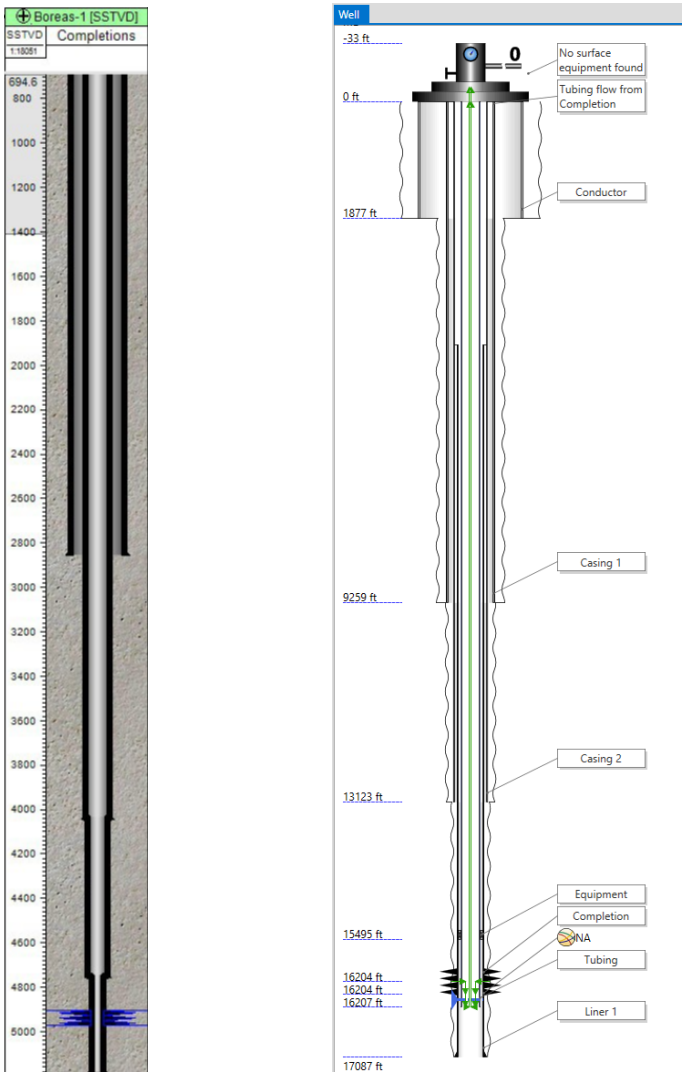

Figure 124. *Well Scheme of Boreas-1 (Petrel vs PipeSim).*

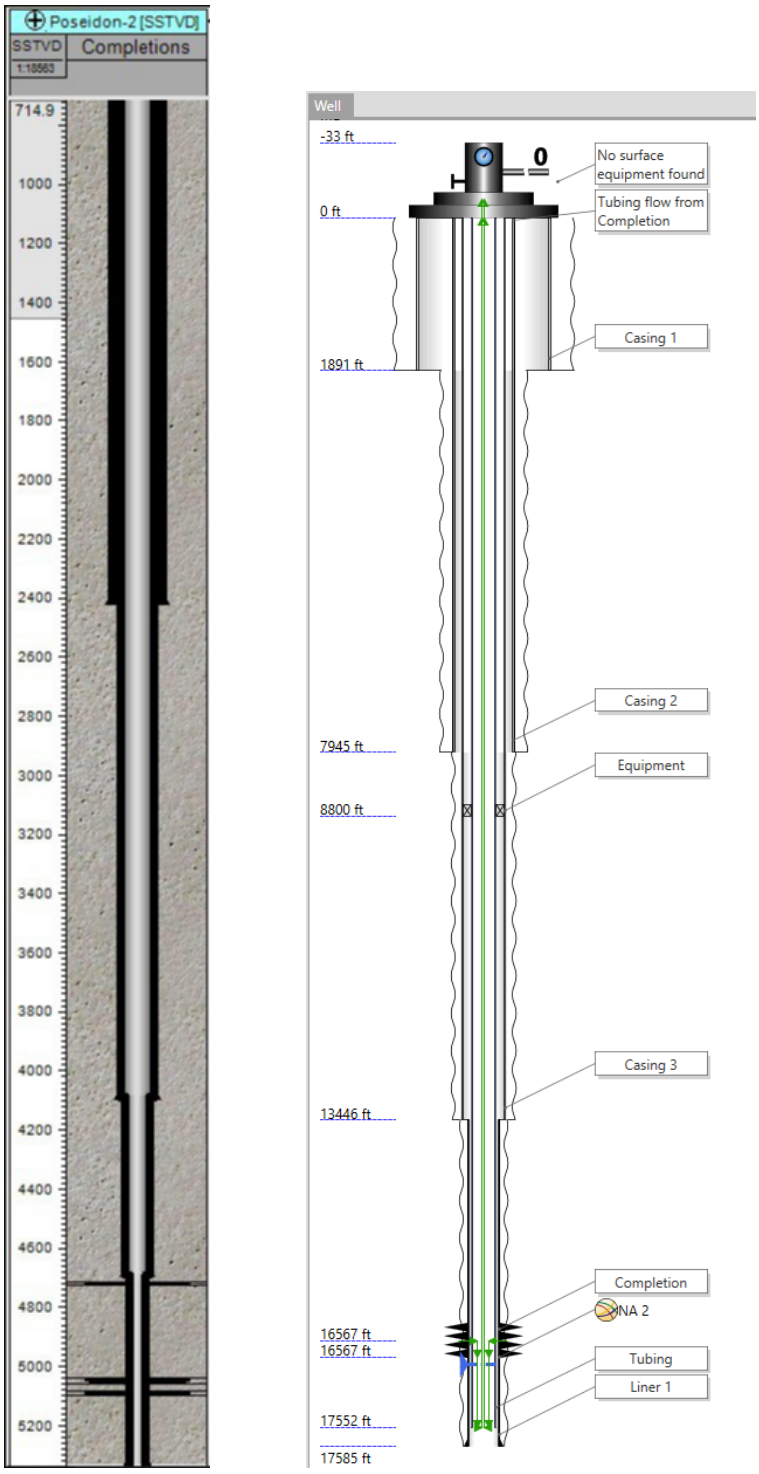

Figure 125. *Well Scheme of Poseidon-2 (Petrel vs PipeSim).*

Based on the diagrams shown above, it was decided that the completion of the new production well would be similar, and the injection well would lack a liner.

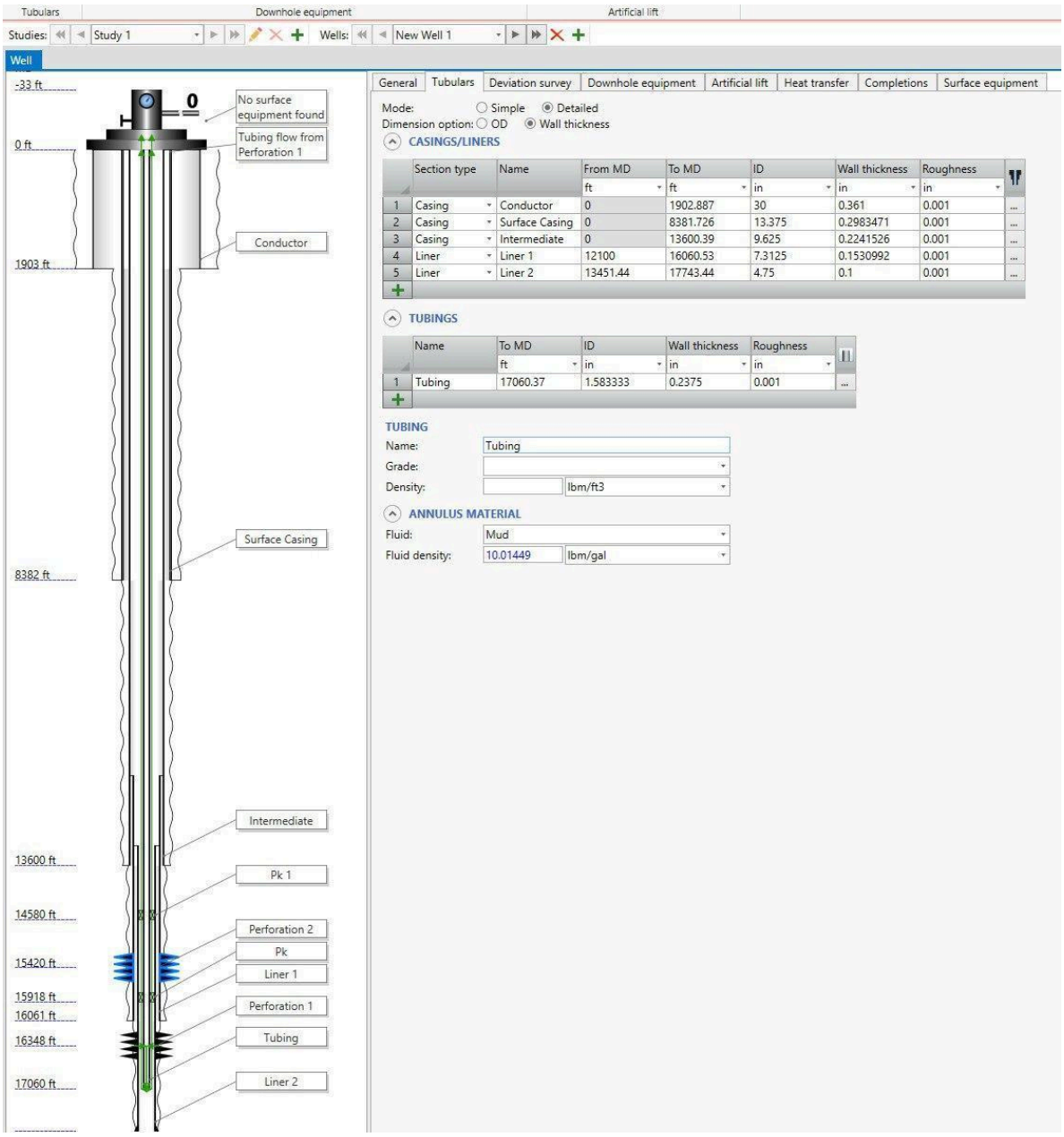

Figure 126a*. Completion of new production well.*

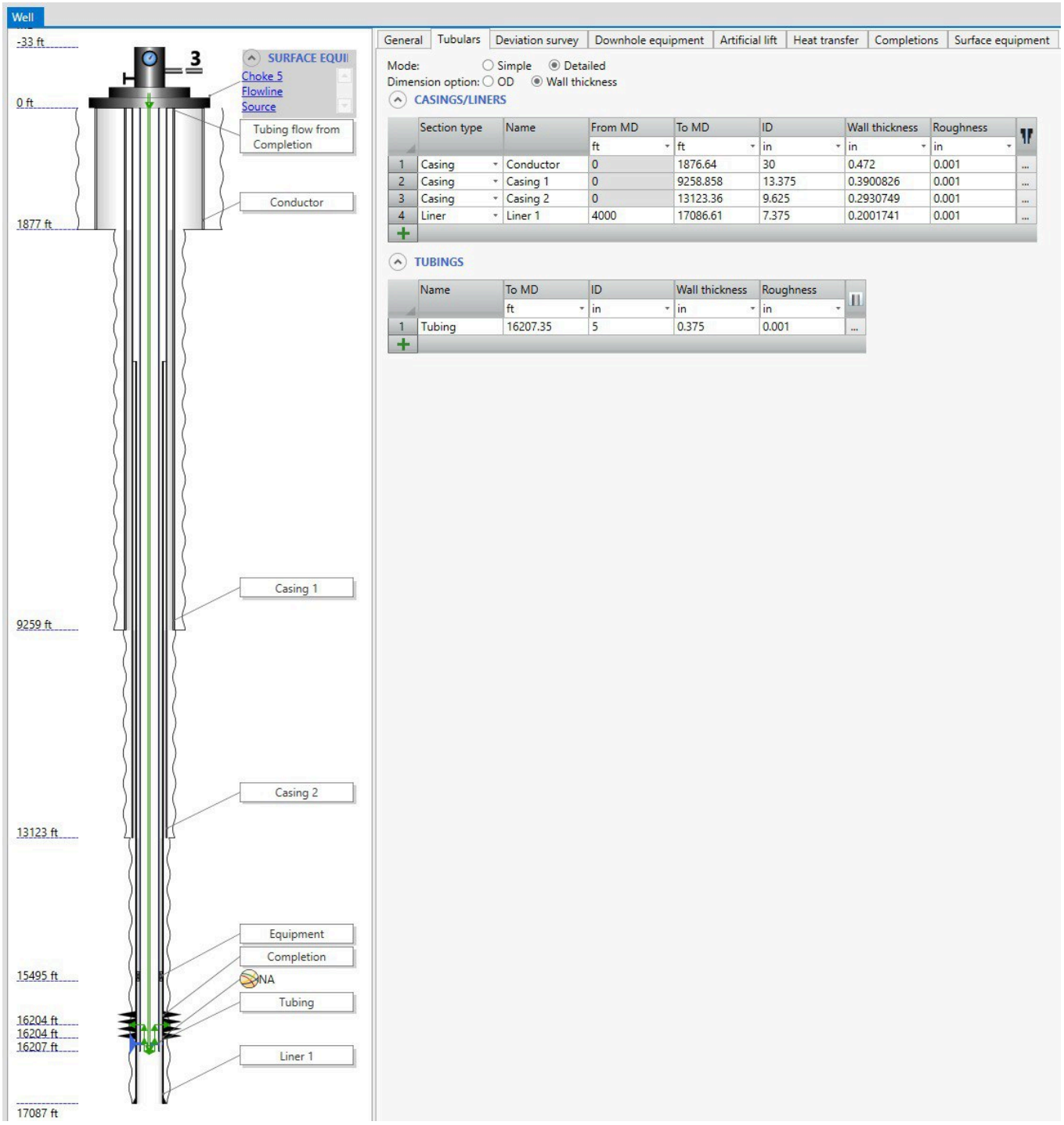

***Figure 126b**. Completion of new injection well.*

3.4.2 Surface facilities

Also, in the PIPESIM a design of a surface facilities network was created and shown below. The surface production network for the Poseidon field is designed to manage multiphase flow from four production wells and support one injector well. All the wells are connected to the choke valves which are used to regulate pressure and control slugging. Production well fluids will travel to a central subsea manifold via dedicated subsea flowlines. The length of each flowline will be varied from two to five kilometers. The manifold consolidates production fluids and manages distribution to the processing facility. Approximately 400-meter-long steel catenary risers link the subsea manifold and flowlines to the floating production unit (semi-submersible unit), where treatment and separation take place. These risers are made to resist mechanical fatigue, corrosion, and thermal expansion in dynamic offshore environments. A three-phase separator onboard the platform divides the wellstream into gas, condensate, and water. The gas stream is compressed using a gas compressor, with a working power from 3000 – 5000 hp, and then transferred to a gas tank. The compression step guarantees that the gas pressure is enough for transportation in the event of an export or re-injection. Oil is directed through an oil export pump, which has a 1000 – 1500 hp operating power and is needed to boost pressure for transport, to storage or export modules. Water is transferred from the separator into a water tank where further treatment takes place. Injector well is connected via flowline to the outside CO2 source.

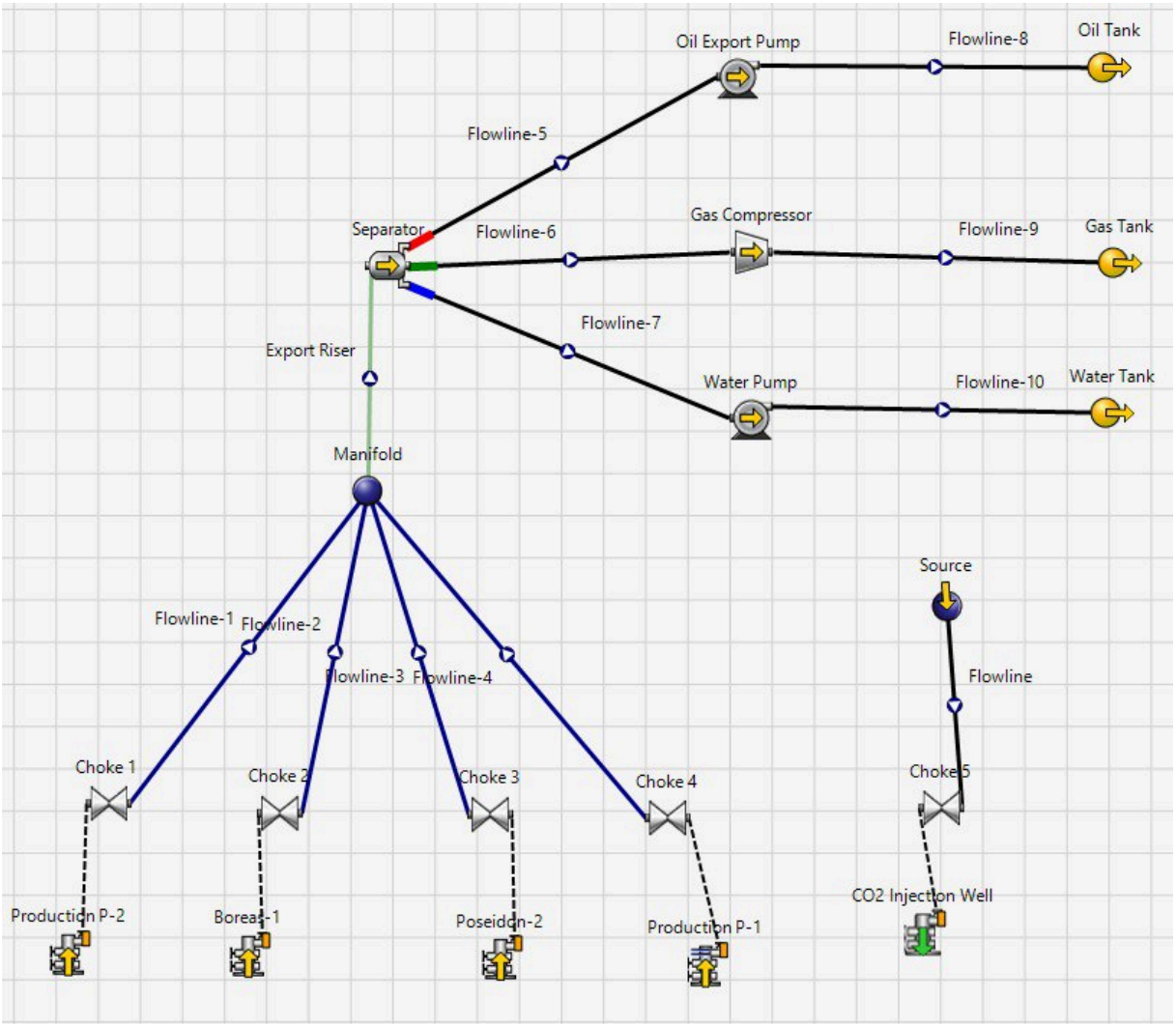

Figure 127. *Surface Network Design.*

3.5 Production Engineering

3.5.1 Nodal Analysis

The Pipesim simulator by SLB was used to carry out nodal analysis on the bottom hole node. The inflow performance curves for wells Boreas-1 and Poseidon-2 are shown in **Figures 128 and 129** below:

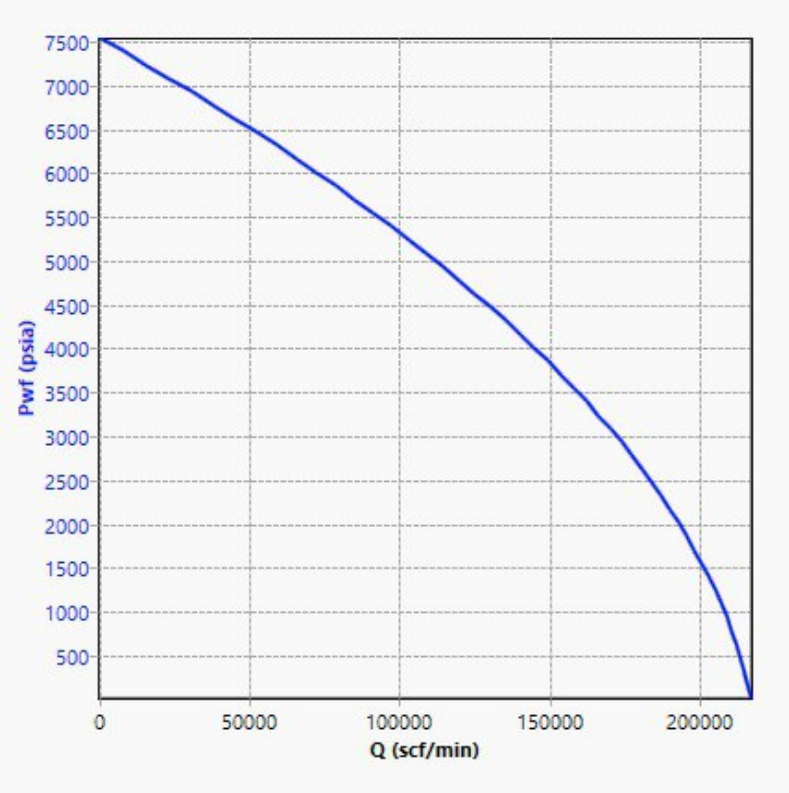

Figure 128. *IPR curve for Boreas-1.*

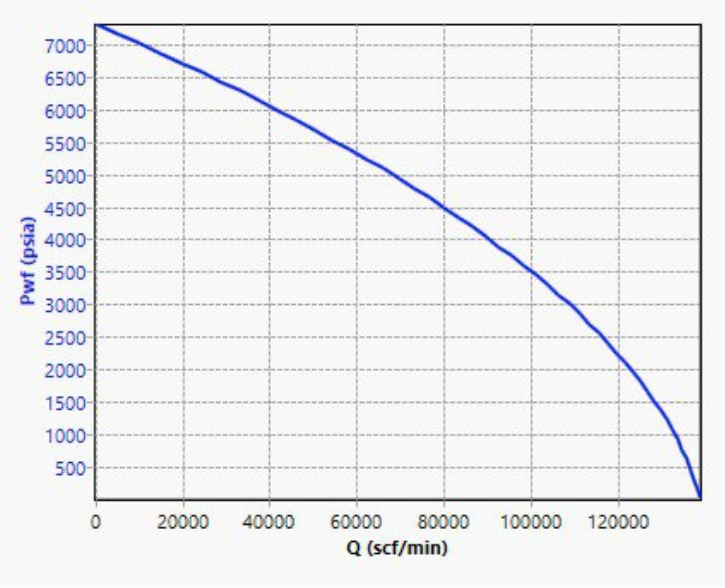

Figure 129. *IPR curve for Poseidon-2.*

As it can be seen from the **figures**, the Absolute Open Flow value for the wells are 217 Mscf/min (312 MMscf/d) and 139 Mscf/min (200 MMscf/d) for Boreas-1 and Poseidon-2, respectively.

Using the Nodal Analysis module in Pipesim, Tubing performance and Inflow performance relationship curves were built for the bottomhole node:

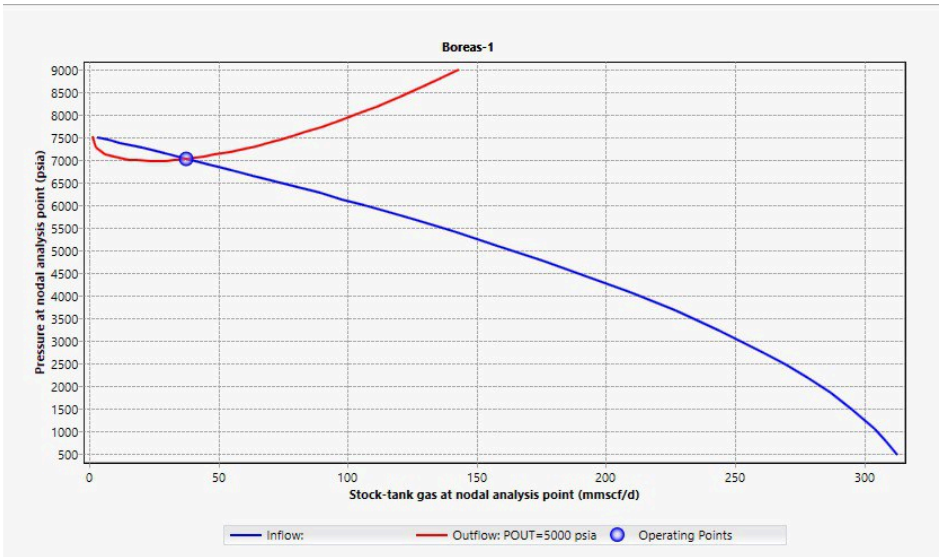

Figure 130. *IPR and TPR curves for Boreas-1.*

The **figure** above shows the optimal operating pressure and flow rate for the original conditions with 5 inch tubing and 5000 psi outlet pressure. The optimal performance conditions were established as 7029.7 psia pressure, and 37.6 MMscf/day flow rate for Boreas-1.

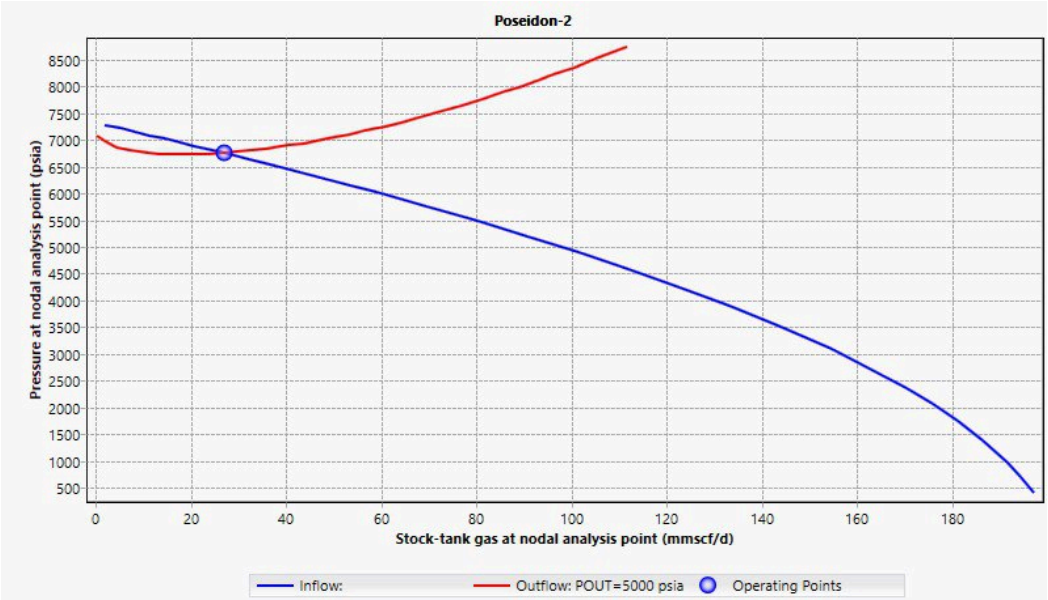

Figure 131. *IPR and TPR curves for Poseidon-2.*

When it comes to Poseidon-2, by the same method, the optimal production pressure and flow rate were established as 6750.6 psia, and 27 MMscf/day.

Both operating pressure values are considerably above the dew point pressure of the reservoir fluid, which ensures that the gas is produced without the formation of the condensate, which would otherwise decrease the efficiency of the production process.

When it comes to the injection well, Cratos - 1, the Nodal Analysis shows the optimal conditions for CO_2 injection to maintain the reservoir pressure. The constructed IPR curve can be seen in the **figure** below:

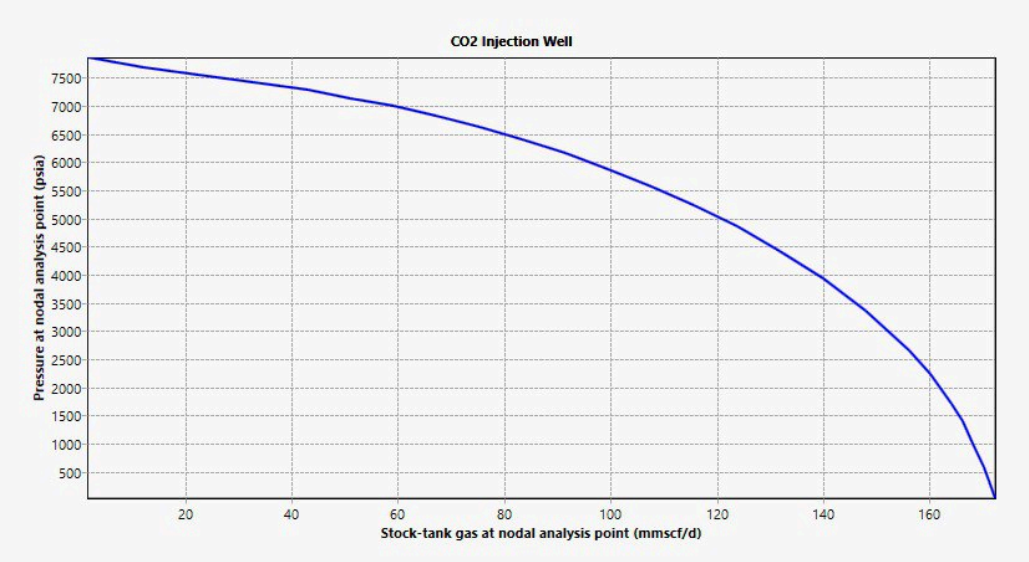

Figure 132. IPR curve for Cratos - 1.

As it can be seen, for the base case (Inflow pressure = 2500 psi), the maximum possible injection rate is just above 170 MMscf/day when the pressure at the bottomhole node is equal to 0 psi.

Judging from the intersection of the IPR and TPR curves, at the defined reservoir conditions, the optimum injection operating point is maintaining the rate of 42.9 MMscf/day at the bottomhole pressure of 7278.2 psi.

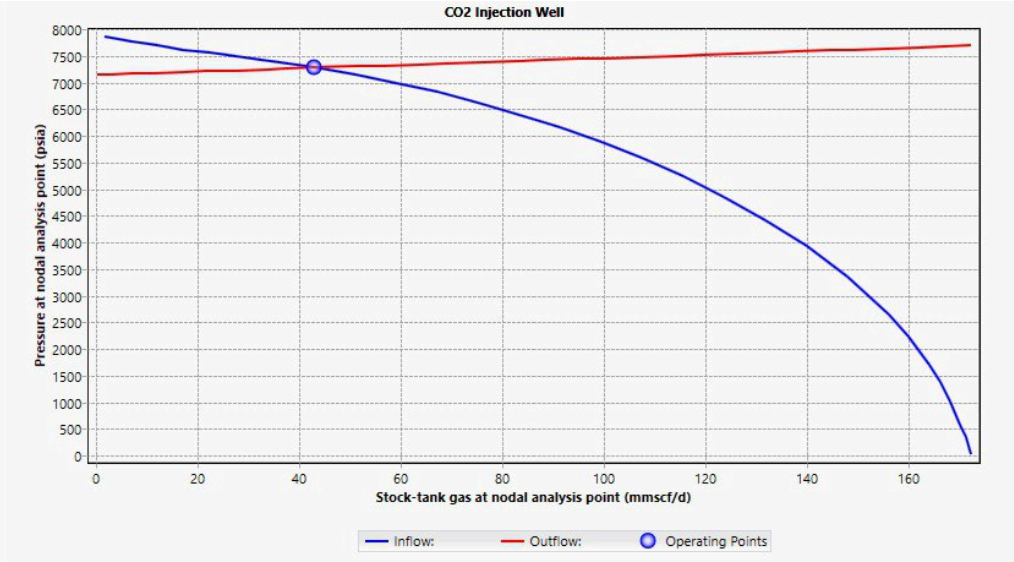

Figure 133. IPR and TPR curves for Cratos - 1.

Since the injected CO_2 is actually derived from the contents of the produced gas, this is a sensible rate, which is roughly equal to the amount of carbon dioxide that can be extracted from the production wells daily. It allows for effective reinjection of the unwanted mixtures in the produced fluid and ensures that the carbon footprint of the operation is minimized by sequestration of the CO_2.

3.5.2 Sensitivity Tests

To further analyze the influence of the outlet pressure on production conditions, a series of sensitivity analyses were performed by applying different values of outflow pressure in the range of 1500 psia to 5000 psia. The results for each well can be observed from **Figures 134 to 135** below:

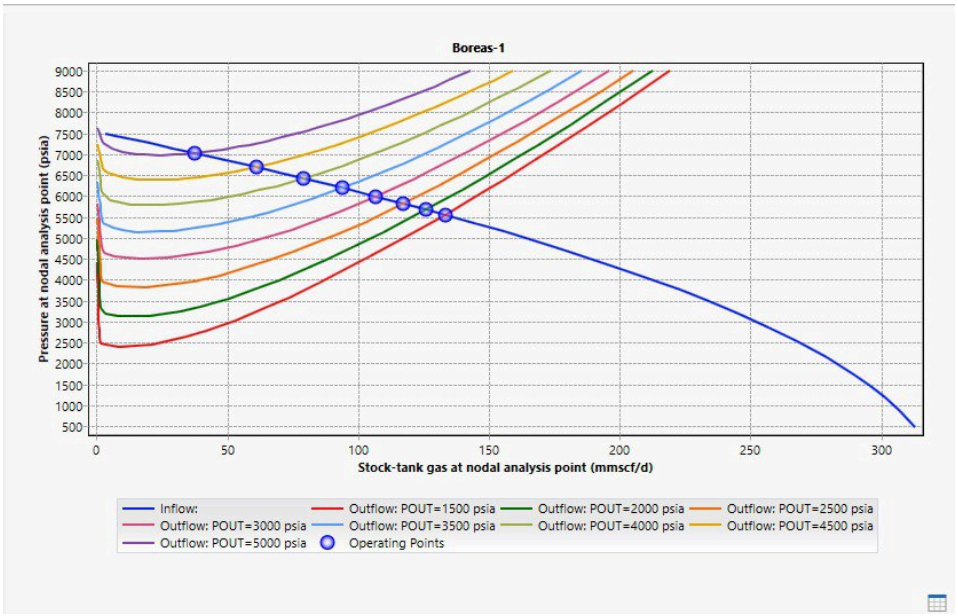

Figure 134. *Boreas-1 Sensitivity analysis for outflow pressure.*

	Operating point	P at NA	ST Gas at NA
		psia	mmscf/d
1	POUT=1500 ps...	5551.62	133.21
2	POUT=2000 ps...	5673.868	126.0449
3	POUT=2500 ps...	5820.527	117.2727
4	POUT=3000 ps...	5992.715	106.728
5	POUT=3500 ps...	6193.188	94.11712
6	POUT=4000 ps...	6425.071	79.08208
7	POUT=4500 ps...	6695.464	60.94284
8	POUT=5000 ps...	7029.298	37.64569

Figure 135. *Boreas-1 operating points at different outflow pressures.*

With the application of higher outflow pressures, the operating pressure increases, and the gas flow rate decreases. The maximum flow rate can be achieved at the outflow pressure of 1500 psia, when the production rate equals 133 MMscf/day.

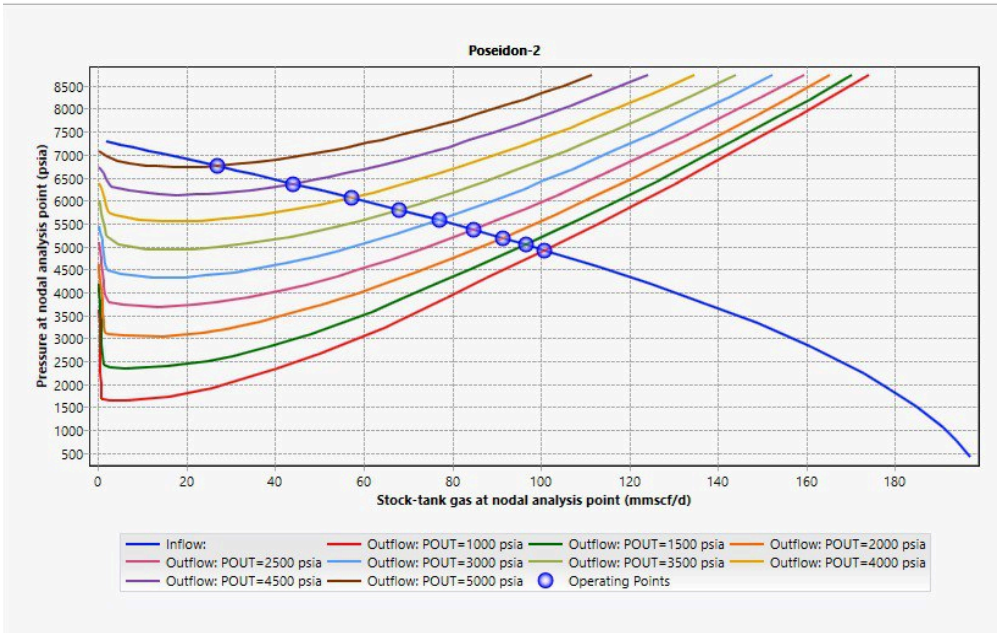

Figure 136. *Poseidon - 2 Sensitivity analysis for outflow pressure.*

	Operating point	P at NA	ST Gas at NA
		psia	mmscf/d
1	POUT=1000 ps...	4915.991	100.8953
2	POUT=1500 ps...	5036.053	96.67489
3	POUT=2000 ps...	5185.623	91.29683
4	POUT=2500 ps...	5363.012	84.74534
5	POUT=3000 ps...	5567.646	76.95433
6	POUT=3500 ps...	5797.392	67.90936
7	POUT=4000 ps...	6061.219	57.134
8	POUT=4500 ps...	6367.413	44.10729
9	POUT=5000 ps...	6750.694	27.0122

Figure 137. *Poseidon - 2 operating points at different outflow pressures.*

For the Poseidon - 2 well, the maximum flow rate is slightly lower than that in Boreas - 1: 100.9 MMscf/day at Pout = 1000 psia.

Expectedly, at the greater values of the outflow pressure, the flow rate at the optimal operating point is smaller, because the fluid needs to overcome a higher resistance to reach the surface facilities. However, for the functioning field, an outflow pressure of 5000 psia is selected, because smaller values will result in temporary increase in flow rate, but in the long run might

shorten the life of the reservoir, or cause issues with water coning and sand production. Moreover, at the smaller values of the outflow pressure, the optimal production pressure also decreases. Considering the fact that the reservoir will naturally be depleted and have a declining pressure with time, producing extremely high rates leads to the reservoir pressure reaching the dew point pressure faster. In that case, the production is cut short due to the formation of the undesirable condensate.

The results of the inflow pressure sensitivity analysis for the Cratos - 1 injection well can also be seen below. Inflow pressures from 2000 psi up to 5000 psi were studied for their influence on the optimal operating point.

Generally, decreasing the inflow pressure leads to lower rates of injection of CO_2, so the minimum value of rate (1.72 MMscf/day) was obtained at the inflow pressure of 2000 psi. However, this amount of gas injection most likely would not be enough to support pressure maintenance across the whole reservoir. Subsequently, the highest rate of injection - 179.7 MMscf/day - can be achieved with the inflow pressure of 5000 psia. Although injecting CO_2 at this rate could help support the reservoir pressure for a much longer time, this scenario is not feasible in terms of the supply of the available injection fluid. Attempting to keep the injection rate this high would require additional supply of CO_2, which needs further economic considerations. Therefore, the inflow pressure of 2500 psi should be chosen as the base case.

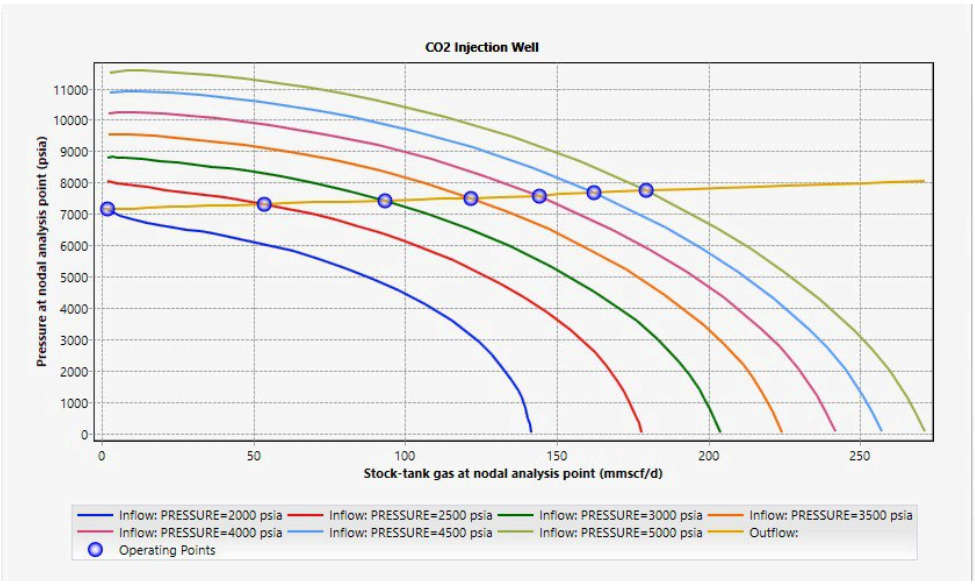

Figure 138. *Cratos - 1 Sensitivity analysis for inflow pressure.*

	Operating point	P at NA	ST Gas at NA
		psia	mmscf/d
1	PRESSURE=20...	7146.289	1.717536
2	PRESSURE=25...	7312.083	53.58656
3	PRESSURE=30...	7427.531	93.4167
4	PRESSURE=35...	7503.737	121.494
5	PRESSURE=40...	7566.004	144.1351
6	PRESSURE=45...	7675.761	162.3476
7	PRESSURE=50...	7734.952	179.6583

Figure 139. *Cratos - 1 operating points at different inflow pressures.*

3.6 Dynamic Reservoir Simulation

Defining New Well Configuration

Dynamic reservoir simulation was performed to assess the production performance of different development strategies, which is implemented via CMG GEM. This compositional model accounted for the geological complexity, fluid behavior, and operational constraints to predict the reservoir response at specific particular times.

The first simulation case considered two production wells (Boreas-1 and Poseidon-2) to be placed in structurally high parts of the reservoir system (**Figure 140**). Structurally high locations of both wells corresponded to locations of high production potential that had been defined based on the results of static modelling and petrophysical analysis.

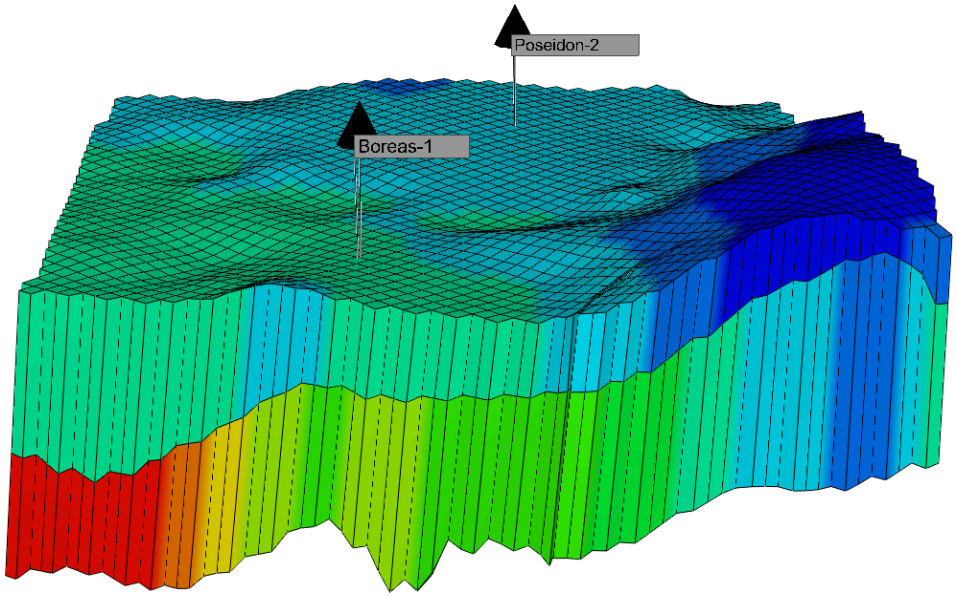

Figure 140. *Initial Well Configuration with Two Producers (Boreas-1 and Poseidon-2).*

To optimize reservoir drainage and elevate recovery efficiency, the well arrangement was redesigned to a five-spot pattern. One target injector, in this case Cratos-1 was placed in the center and four producers placed in each corner: Boreas-1, Poseidon-2, Ares-1 and Atreus-1. Compared with the previous well pattern, the updated well configuration targets improved pressure maintenance and sweep efficiency across the target zone. **Figure 141** illustrated the updated well configuration.

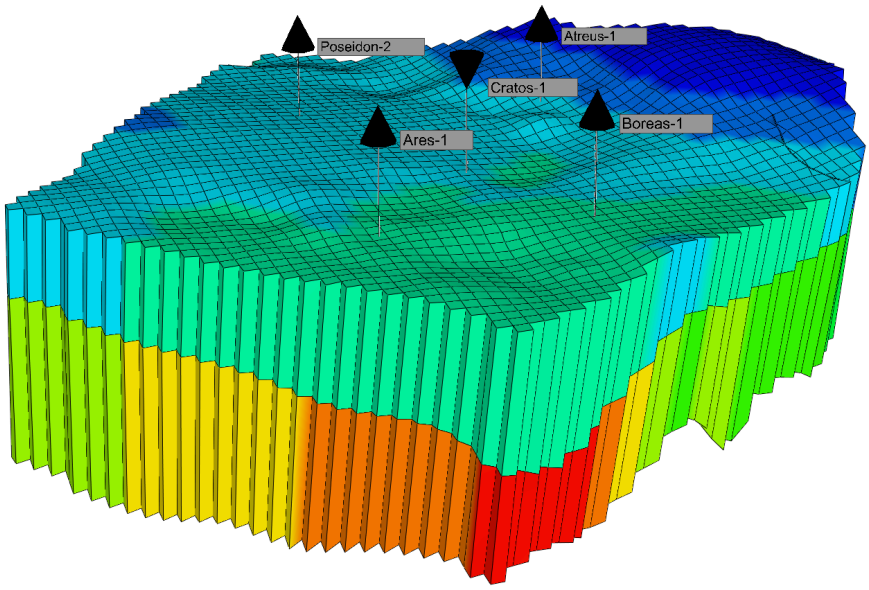

Figure 141. *Optimized Five-Spot Pattern with One Injector and Four Producers.*

Defining New Well Perforations

Following the development of the five-spot well pattern, perforation intervals in each of the new production wells were defined to determine the ideal connectivity to high-permeability zones in the reservoir. Potential perforated grid blocks were selected based on the reservoir quality, grid block location, and geometric well index values to achieve maximum inflow performance and effective drainage. Hence, the completion defined for Ares-1 includes two perforated intervals in high-quality reservoir layers (**Figure 142**). In the same way, Atreus-1 was perforated in zones of high flow potential according to the same selection criteria (**Figure 143**). Completions were added to the simulation model using the Well Completion Data (PERF) tab in CMG Builder. This allows input of perforation depths from true vertical depths as well as well conditions such as flow potential and geometric index.

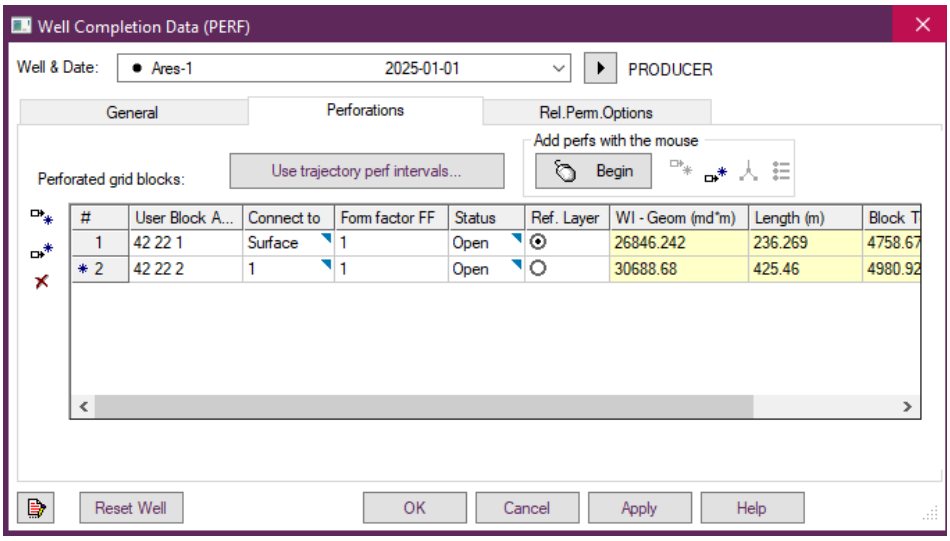

Figure 142. *Well Completion Setup for Ares-1.*

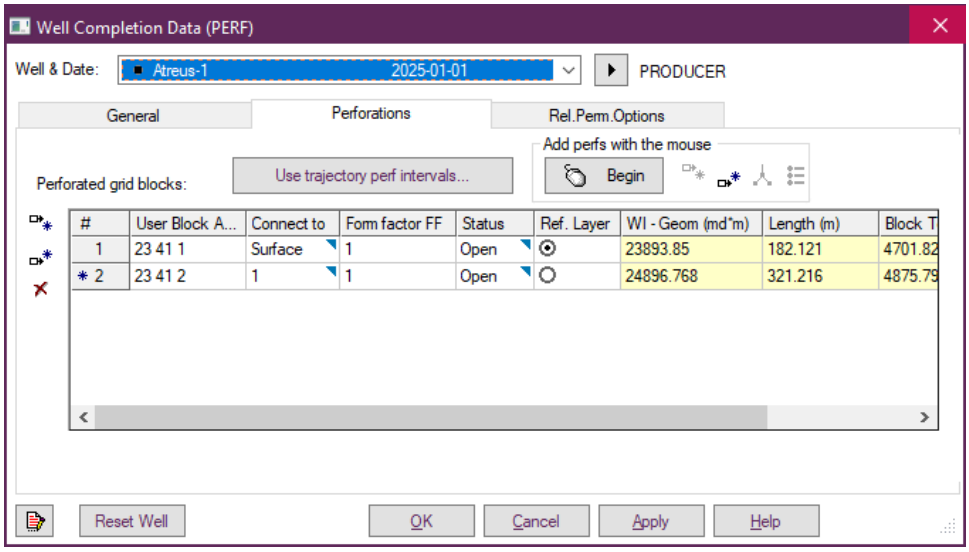

Figure 143. *Well Completion Setup for Atreus-1.*

Complementing the producers is the central injector well, Cratos-1. The well was designed for pressure support and enhanced sweep efficiency in the pattern. It was perforated in a deeper grid block of good transmissibility, such that it maintained a strong communication with surrounding producers. As illustrated in **Figure 144**, the surface connection of Cratos-1 is closed

and injection occurs in the lower zone, to facilitate fluid entry in the reservoir and to effect an even hydrocarbon displacement from the centre of the pattern to the producer wells.

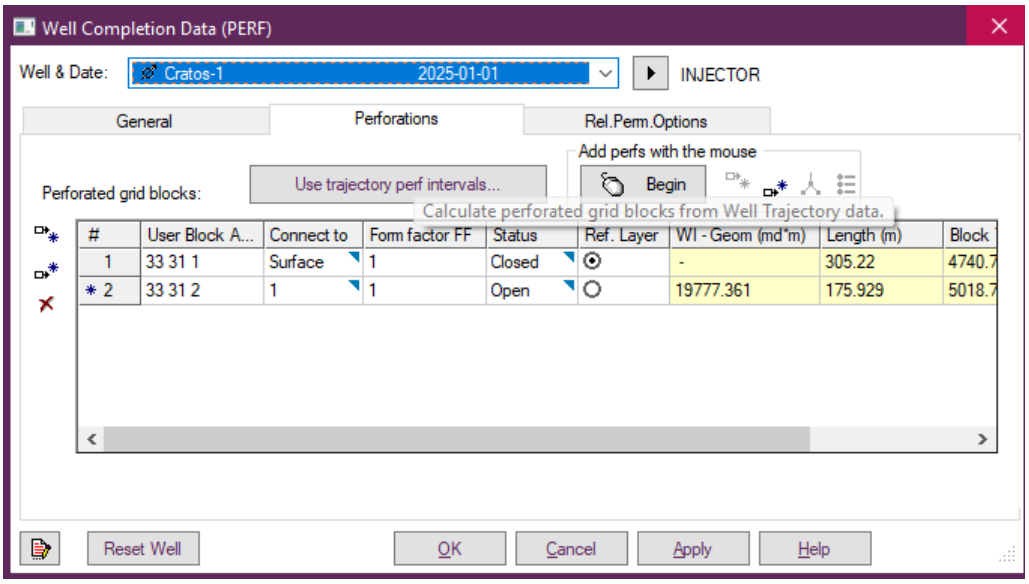

Figure 144. *Well Completion Setup for Cratos-1 (Injector).*

Simulation Timeframe

The dynamic simulations are performed over a duration of 20 years (from 1st January 2025 to 1st January 2045) with monthly time steps results writing. This large simulation period allows to determine the field production lifecycle under several development scenarios. (see **Figure 145**).

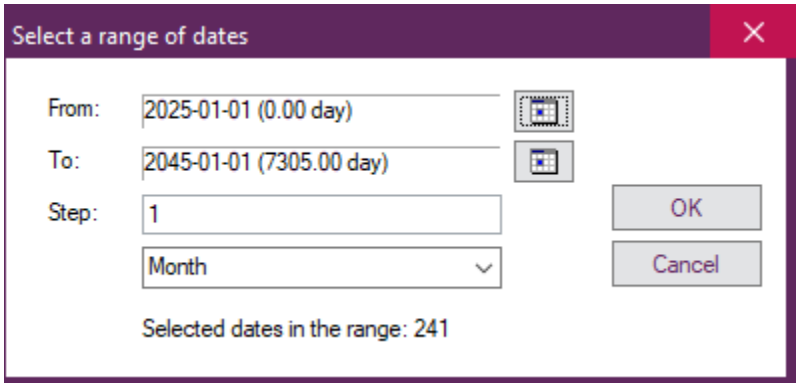

Figure 145. *Simulation Timeframe Setup – 20-Year Period with Monthly Time Steps.*

In order to evaluate efficiency of proposed infill wells five-spot pattern with respect to the base dual-producer case, sensitivity analysis was carried out based on major KPIs which include the following:

- Gas production rate
- Cumulative gas production
- gas recovery factor
- Oil production rate
- Cumulative Oil Production
- Water cut
- Reservoir Pressure

Dynamic Sensitivity Analysis

Cumulative Gas Production

Figure 146 shows the comparison of **cumulative gas production** over the 20-year simulation period between the original dual-well setup and the optimized five-spot pattern. The five-spot configuration demonstrates a significantly higher gas recovery, nearly tripling the cumulative output by the end of the simulation.

This improvement is attributed to better pressure maintenance and enhanced areal sweep efficiency enabled by the central injector and strategically positioned producers. The original Setup shows a steady but limited increase, indicating poor drainage and early pressure decline. The five-spot pattern clearly outperforms the original, emphasizing the effectiveness of the updated development strategy.

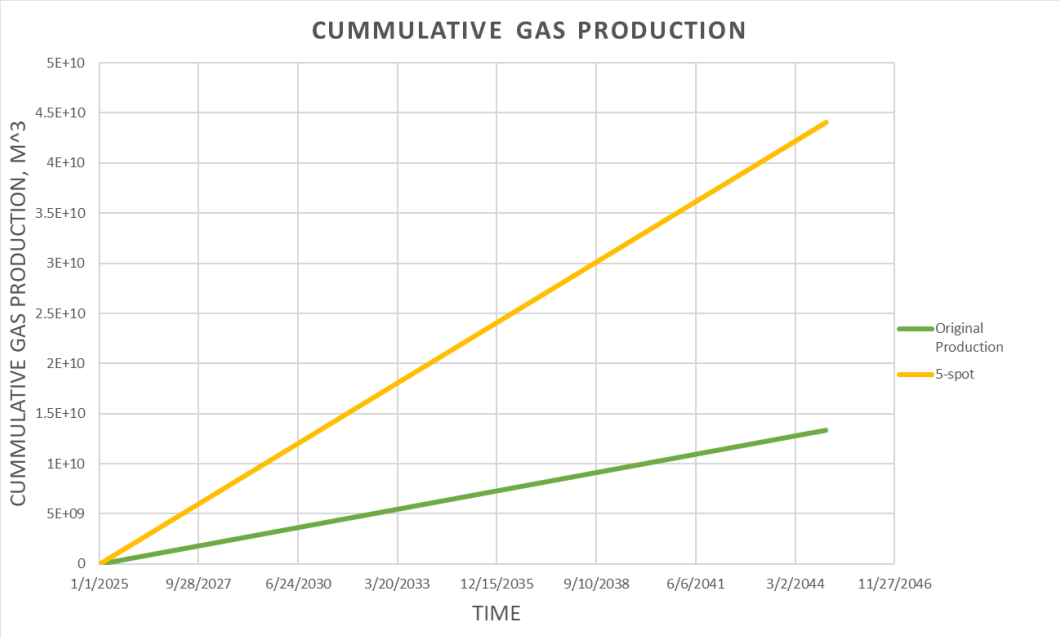

Figure 146. *Cumulative Gas Production – Five-Spot vs Original Configuration.*

Gas Production Rate

In **Figure 147**, the gas production rate under the original dual-well mode and the optimized five-spot development mode are compared. The production rate of five-spot pattern is basically maintained at 600000 m³/month, that is, the production rate of five-spot pattern is maintained at about 600,000 m³/month, which is about twice that of the original scheme, which is maintained at about 300,000 m

This flat and stable production profile indicates the benefit of the improved reservoir management enabled by the five-spot pattern, such as better pressure support through center injection and more efficient use of the drainage area. The stable and constant production profile in the five-spot case suggests robust epidemic and balanced reservoir drawdown in contrast to the original case, where drawbacks in well placement and pressure maintenance lead to poor long-term performance. This development confirms both the technical and operational advantages of the five-spot models by providing enhanced recovery and consistent production over the reservoir's life.

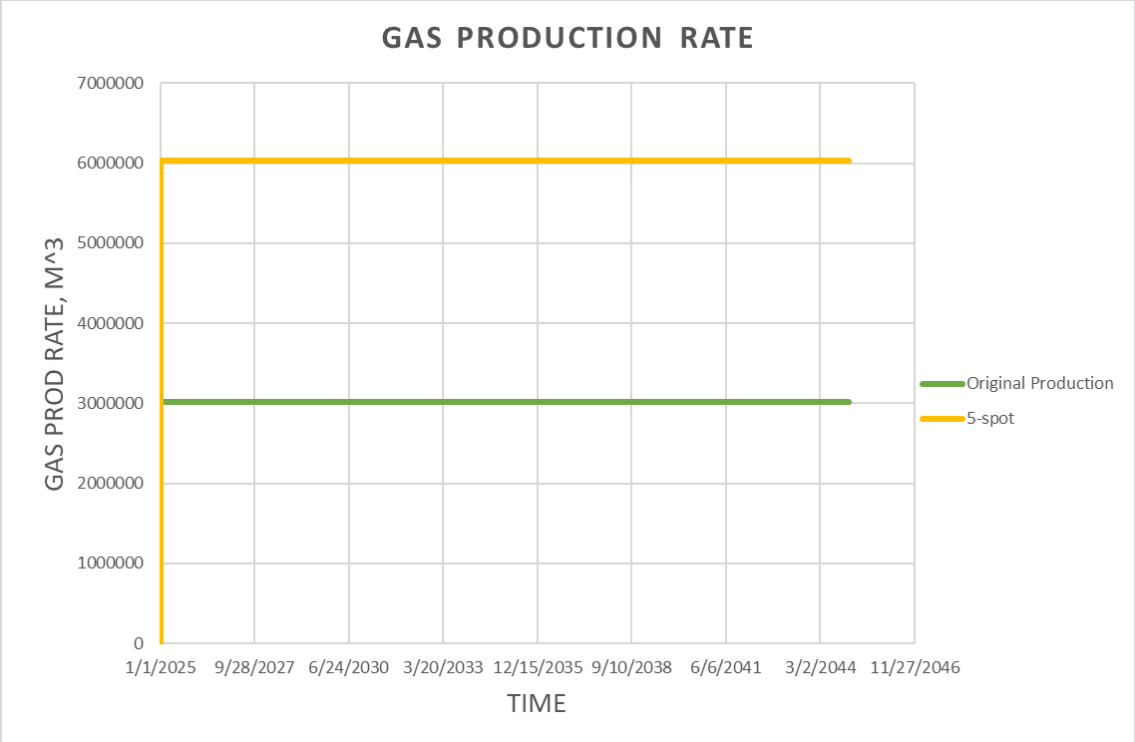

Figure 147. *Gas Production Rate – Five-Spot vs Original Configuration.*

Gas Production for 5-spot Pattern

The annual gas production rate from each of the producers in the five-spot pattern is represented in **Figure 148** for the 20 years of simulation. The analysis indicates that each of the producers is a stable long-term gas producer. As evident from **Figure below**, the production rates of all the wells accommodate a discernible brine influx while leveling out immediately after the well ramp-up.

Atreus-1 is the highest-output of the producers, with production rates consistently above 80 million meters cubed per year of gas. Next highest is Ares-1 with similar production rates, while Boreas-1 and Poseidon-2 have lower but constant production rates of ~39 million meters cubed per year and ~29 million meters cubed per year, respectively.

The productivity distribution is a consequence of the spatial heterogeneity in reservoir quality and the spatial configuration of each well inside the drainage area. Overall, wells closer to

the central injector, or situated in richer portions, benefit from better sweep and sustained pressure support. The plot, overall, demonstrates the efficacy of the five-spot arrangement in spreading the load as evenly as possible among the different producers, helping attain an evened out gas recovery among the field.

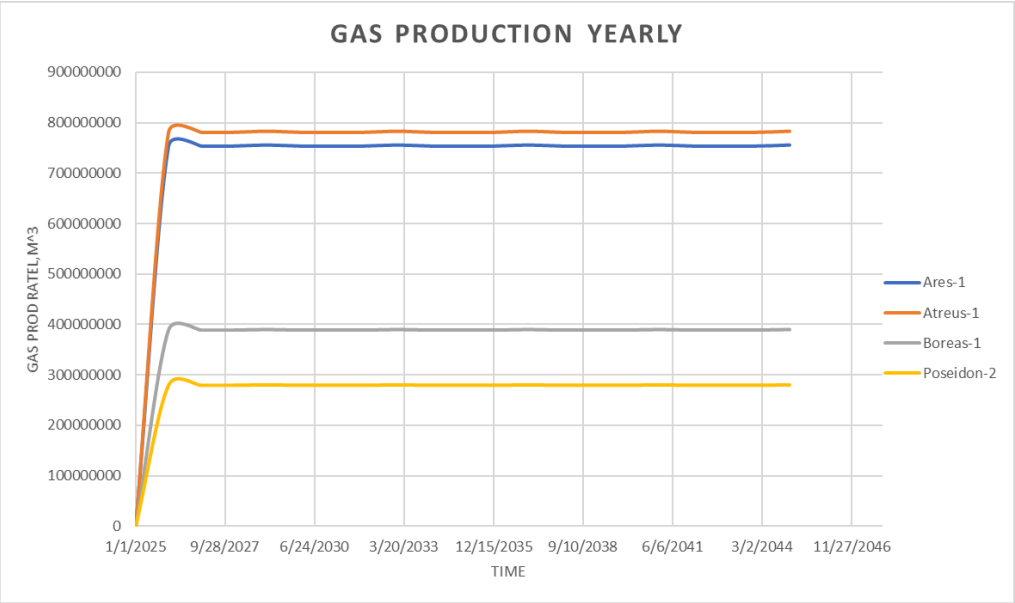

Figure 148. *Annual Gas Production Rate per Well – Five-Spot Pattern Configuration.*

Gas Injection for 5-Spot Pattern

In **Figure 149** we plot the cumulative water injection volume through Cratos-1 for the 20 years of simulation. Water injection was initiated in the early stages of the development. The volume injected rapidly reached a plateau of about 1.3 million m3 and remained constant from then on, throughout the project life.

This steady rate of injection indicates the controlled and sustainable pressure maintenance work, which is needed to maintain the production performance of the offset wells in the five-spot well pattern. The early commencement of injection ensures that the reservoir pressure exceeds the critical pressures e.g. the dew point of a complex process to help improve project economics, enhance ultimate gas recovery and reduce the condensate dropout.

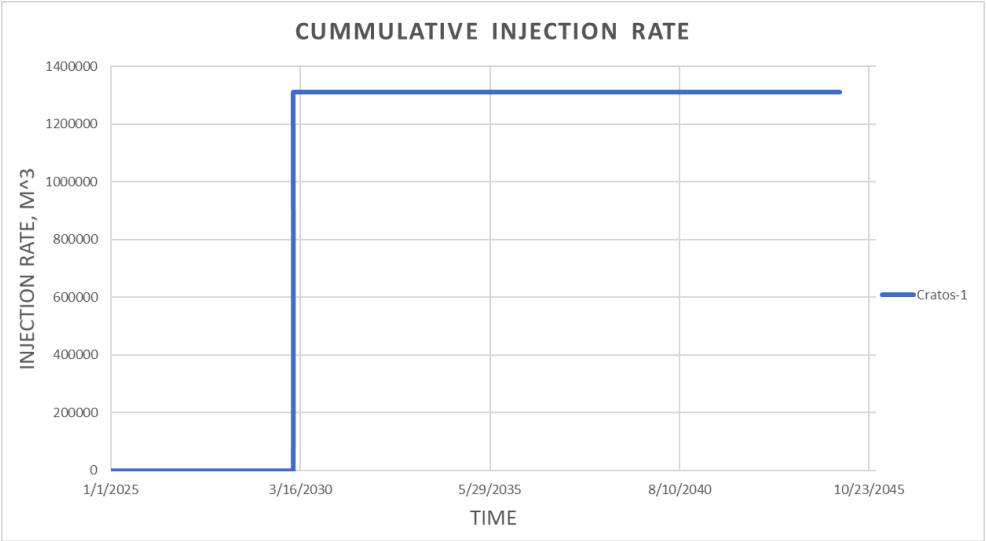

Figure 149. *Annual Gas Production Rate per Well – Five-Spot Pattern Configuration.*

Gas Recovery Rate

Figure 150 shows the recovery factor of gas as a function of time for the original development scenario and the optimised five-spot pattern. The five-spot pattern exhibits a much greater recovery performance, reaching a final recovery by the end of the simulation period of about 16%, compared to 11% for the original case.

This increase is directly due to improved reservoir contact and pressure support provided by the injector in the center of the five-spot pattern. This improved areal and vertical sweep efficiency allows more reservoir to be drained, resulting in improved recovery of original gas in place. The linear, consistently higher trend of the five-spot curve highlights this well pattern as strategically maximizing gas recovery.

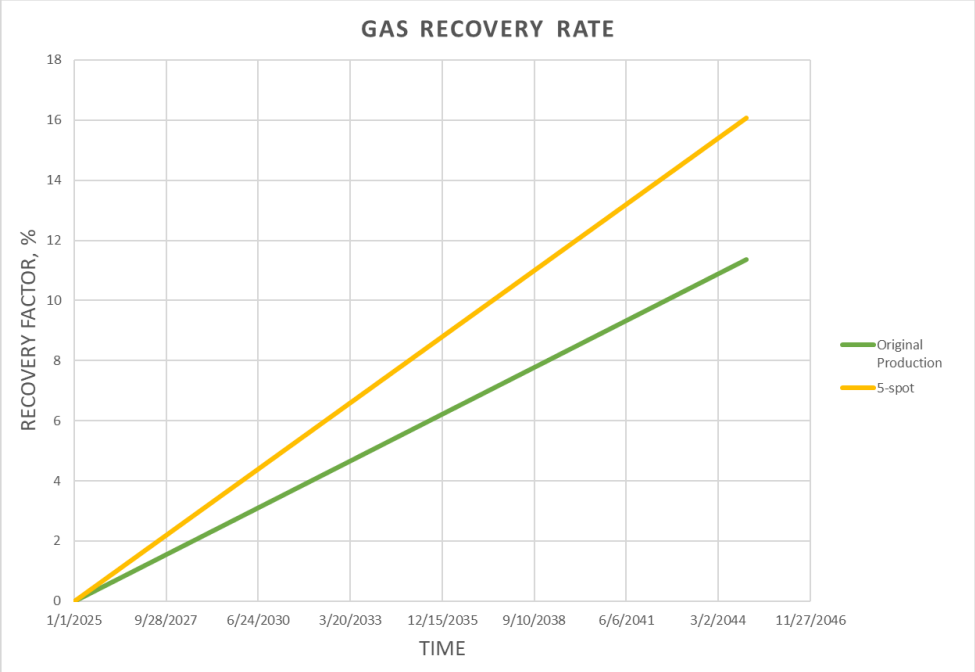

Figure 150. *Gas Recovery Factor – Five-Spot vs Original Configuration.*

Cumulative Oil Production

Figure 151 presents cumulative oil production for the base case and the five-spot development strategy over the twenty years of simulation. The five-spot development pattern leads to much more cumulative oil recovery, close to 3MM m^3, die original well layout, less than 1.2M m^3.

The improvement is due to both better pressure support from the injector as well as better sweep efficiency from the geometry of the four producers. The five spot pattern maintains continued production because the pattern allows for more uniform drainage of the reservoir and less region of bypassed oil. Overall, these results demonstrate that the five-spot geometry is superior in terms of liquid hydrocarbon production over a prolonged production time.

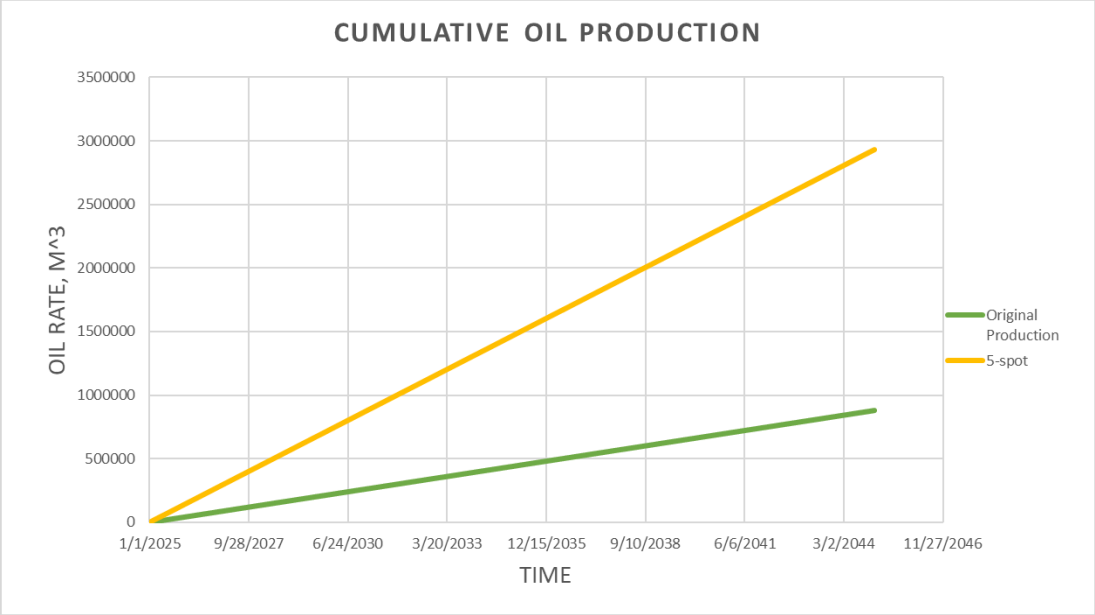

Figure 151. *Cumulative Oil Production – Five-Spot vs Original Configuration.*

Oil Production Rate

Figure 152 shows the oil production rate over the seasons for the two development strategies. The five-spot configuration steadily produces 400 m^3/month throughout the seasons which is twice that of the original scenario, which plateaus at 200 m^3/month.

This higher and stable production behavior in the five-spot scenario highlights the advantages of increased reservoir pressure support and optimal placement of wells. This design allows for better fluid displacement, minimizes pressure drop around producers, and ensures continual oil deliverability. The original design is limited by poor reservoir connectivity and inefficient drainage, leading to lower productivity over the project lifetime.

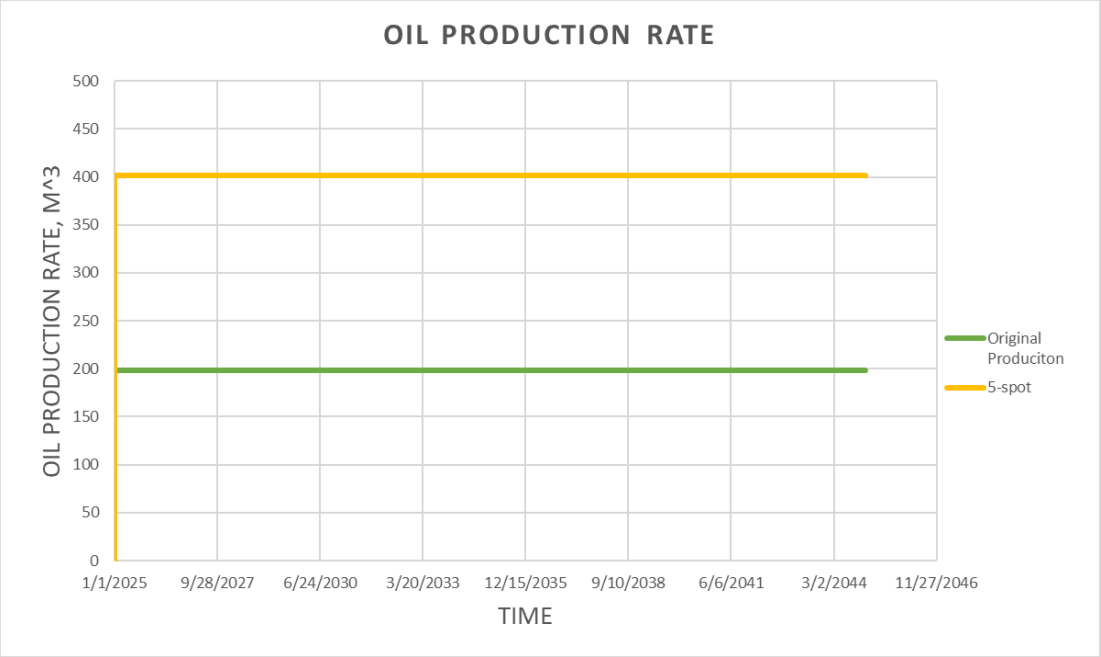

Figure 152. *Oil Production Rate – Five-Spot vs Original Configuration.*

Oil Recovery

Figure 153 shows the oil recovery factor for the original and five-spot configurations during the simulation time of 20 years. The recovery performance of the five-spot pattern is clearly much better than the original configuration achieving about 23% while the base case ends with less than 12% recovery.

This main increment comes from improved pressure maintenance and displacement efficiency realized by proper well spacing and injection assistance. Five-spot pattern can drain the reservoir more efficiently and reduce the bypassed oil to maximize the production of original oil in place, and the calculated results show the technical benefit of five-spot strategy in enhancing recovery efficiency over conventional mode of development patterns.

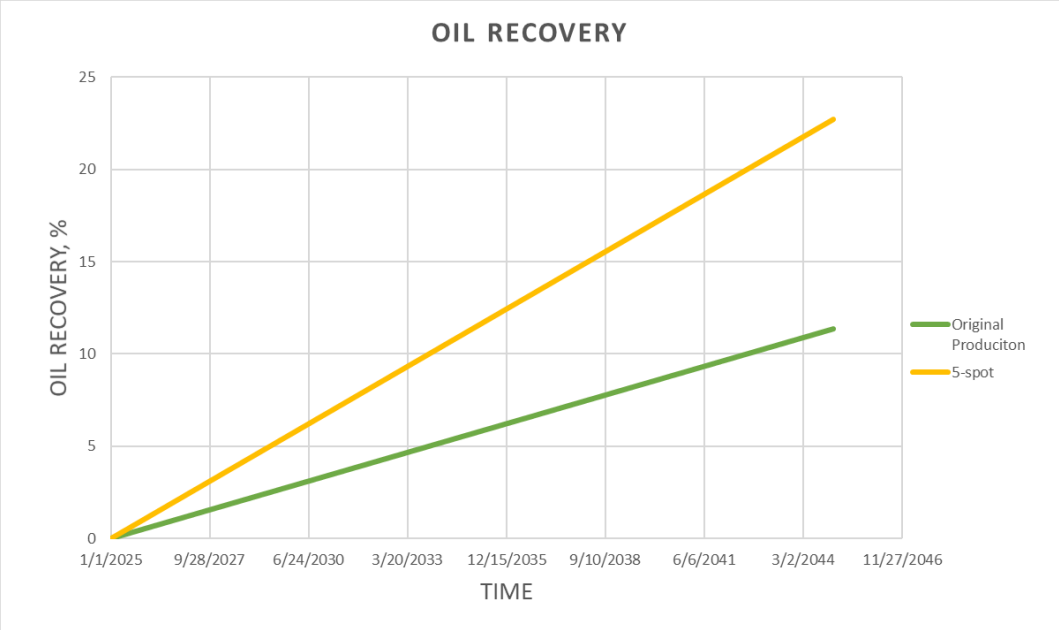

Figure 153. Oil Recovery Factor – Five-Spot vs Original Configuration.

Water Cut

Figure 154 shows the water cut development over the simulation period for the five-spot and base development scenarios. The five-spot case has a low initial water cut of about 3.5 %, before declining and establishing in the sub 1.5 % range for the most part of the reservoir's productive life. There is a small rise at the end, probably due to moving water fronts after long periods of injection.

On the other hand, the initial configuration retains almost 0 water cut; this is mainly from the small recovery and the low amount of pressure disturbance. Water production in the five-spot scenario is more obvious yet minor and well-controlled, given the amount of recovery achieved compared to the initial configuration. Therefore, the five-spot scenario showcases more efficient control of water production in light of the greater oil displacement achieved and the improved reservoir performance.

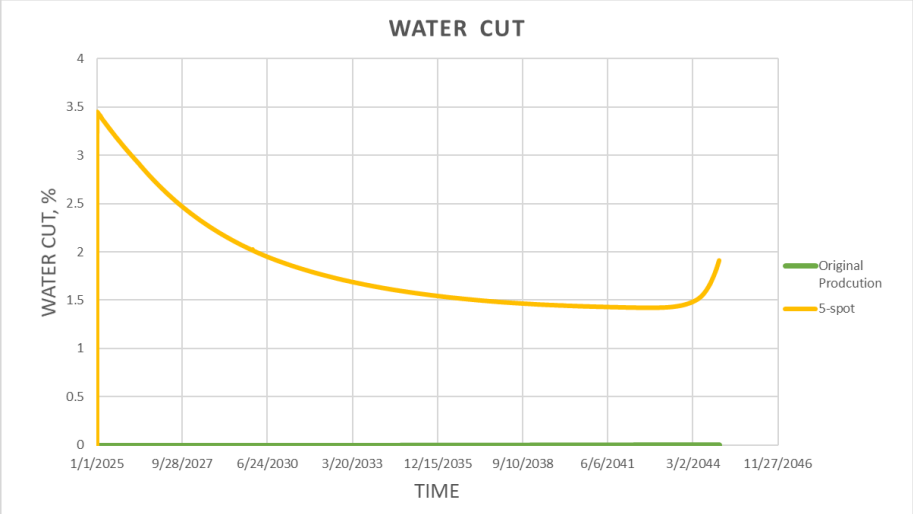

Figure 154. *Water Cut – Five-Spot vs Original Configuration.*

Pressure Drop

The reservoir pressure depletion behaviour over time for both original well configuration and five-spot completion configuration are shown in **Figure 155**. A reference line of the dew point pressure is shown as marks. The reservoir pressure during the entire simulation period is much higher in the five-spot completion case in comparison to original well configuration. This is attributed to the higher energy support from the central injector.

For the five-spot case, pressure is above dew point for a long time, which is critical to avoid retrograde condensation and preserve gas deliverability. While in the original configuration, pressure is below dew point earlier which leads to liquid drop out and decrease gas mobility.

The results demonstrate the positive impact of the five-spot strategy in terms of delaying the dew point crossing and maintaining reservoir pressure as well as more stable conditions for multiphase flow.

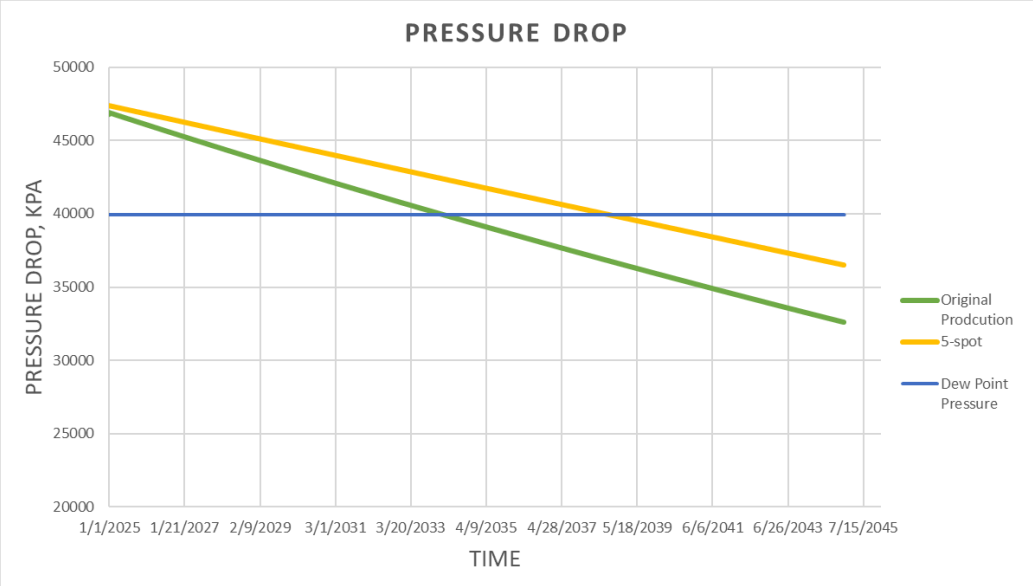

Figure 155. *Reservoir Pressure Decline with Dew Point Reference – Five-Spot vs Original Configuration.*

3.7 Economics

3.7.1 Prediction of Economic Factors

Annual Oil and Natural Gas Production

The CMG Results simulation was implemented in the economic forecast. The annual cumulative oil and gas production values are the technical input for the evaluation forecast. Their profiles are presented in **Figures 156 and 157.**

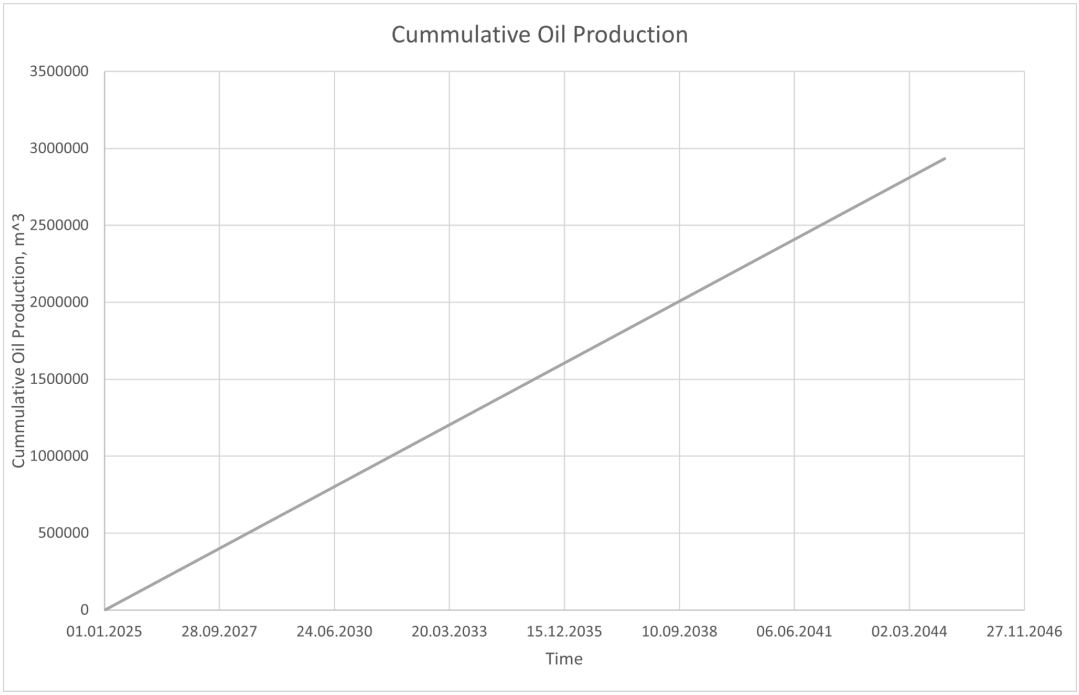

Figure 156. *The cumulative oil production profile.*

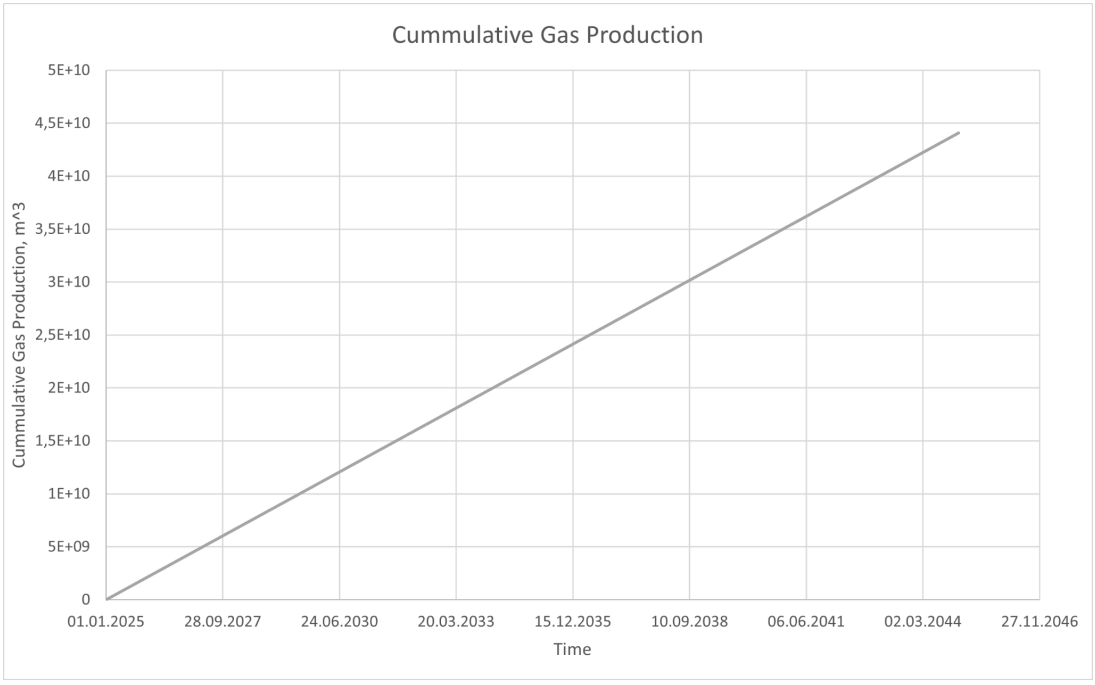

Figure 157. *The cumulative gas production profile.*

Oil and Natural Gas Prices Forecast

As times goes by, the prices for natural gas and oil change. Therefore, using one constant value for a 20 year period is not valid in the real-world. For prediction of oil and natural gas prices, the knowledge in machine learning and historical data from Investing.com was implemented.

ARIMA Models were used for the forecast, because it is widely used for price prediction. Since the ARIMA model was used to estimate the prices under the fundamental premise that it would follow a completely linear pattern, non-linear forecasting methods utilizing soft computing techniques might be taken into consideration in the future with a lower white noise term(Guha & Bandyopadhyay, 2016). However, in the scope of this study, the assumption will ignore government policy and economic instability. **Table 18** illustrates the ultimate run of the model provided the following data for oil and natural gas prices.

Table 18. The forecasted oil and gas prices.

Year	Oil Price USD/Barrel	Natural Gas Price USD/MMBtu
2025	66.908	2.189
2026	67.292	2.986
2027	66.013	2.933
2028	65.604	2.528
2029	65.106	2.991
2030	64.617	2.736
2031	64.219	2.539
2032	63.808	2.605
2033	63.411	2.603
2034	63.006	2.469
2035	62.611	2.317
2036	62.267	2.467
2037	61.864	2.612
2038	61.504	2.757
2039	61.155	2.87
2040	60.805	2.944
2041	60.479	2.836
2042	60.163	2.733
2043	59.86	2.667

2044	59.567	2.721
2045	59.294	2.746
2046	59.43	2.734

The Anticipated Capital Expenditures (CAPEX)

All the costs associated with drilling wells, surface platform facilities expenditures are the investments that are made in advance, and called capital expenditures (CAPEX) (Ganat, 2020). These expenses are usually incurred in the early stages of a project and are necessary to determine the project's operational capacity (Akpe et al., 2024).

Drilling and Completion Costs

Parameters like depth of drilling, water depth, distance from the shore and the daily rig rate are significant in determining the expenditures related to the drilling operations (Ganat, 2020). In the case of the Poseidon field, the deepwater offshore drilling costs may vary between 600 000$/day to 800 000$/day (Ganat, 2020). According to the drilling section estimation the approximate depth of drilling is 17000 ft. Therefore, the approximate time period that is required is 70-80 days (Ganat, 2020). Additionally, there are completion costs, which are nearly 180% of the drilling cost. For the estimation of drilling and completion of 3 wells, the Monte Carlo simulation was produced, as the values are variable (**Table 19**).

Table 19. The Drilling Cost, Completion Cost, and Total Cost for 3 new wells.

	Average Cost Estimate
Drilling, M$	157.36
Completion, M$	283.25
Total, M$	440.61

Upstream Facilities and Production Unit Costs

Floating production systems, floating production storage offloading vessels (FPSO), semi submersible platforms like tension leg platforms (TLP), compliant platforms, gravity concrete platforms, spar platforms, etc. are typically used as standalone hosts by production systems and hydrocarbon storage units in offshore deep water or ultra-deep water (Ganat, 2020). In our case, a new semi-submersible will be used, the cost of it varies between 300-600MM$ (*Offshore Drilling Rigs Market Demand and Future Scope Including Top Key Players – Oil & Gas 360*, 2020). According to the plan, the additional facilities are required:

Table 20. The final upstream facilities and production costs

	Cost per Unit	Quantity	Total Cost, MM$	Reference
Flowline, 3.1 miles	0.23 MM$/miles	4	2.852	Ganat, 2020
Flowline, 0.62 miles	0.23 MM$/miles	3	0.4278	Ganat, 2020
Flowline, 0.31 miles	0.23 MM$/miles	2	0.2139	Ganat, 2020
Riser, 1312 ft	0.35 MM$/(1000 ft)	2	0.9184	Ganat, 2020
Semi-submersible	300-600MM$	1	450	*Offshore Drilling Rigs Market Demand and Future Scope Including Top Key Players – Oil & Gas 360*, 2020

The Anticipated Operating Expenditure (OPEX)

Operating expenditure (OPEX), the other term frequently used in cash flow, refers to the company's recurring expenses. According to the Oil & Gas Authority (2020), the UKCS unit operating costs in 2020 were reported in their annual summary, and the change in operating cost from 2017 to 2025. According to the dataset provided in their report, the forecast for 20 years was determined using the Linear Regression. This model was chosen as the trend in data is linearly increasing throughout the given time period, and the relatively small dataset was used. Additionally, the following assumptions were made in order not to underestimate the operating expenses, and in order to make them realistic. For example, some sources report a low operating cost of 8$ per oil equivalent for deepwater fields, when compared to the report that was used in estimation, which has nearly twice the value for the same year (Smyth et al., 2024). Additionally, the injection of CO_2 was added to the operating expenditures. The work of Neal, Hou, Allinson, and Cinar (2010) provides a detailed analysis of the economic factors influencing CO_2 transport and injection costs in Australia, and through analogue method, the average cost of the carbon dioxide was estimated to 45 A$ per tonne of CO_2, which is approximately 28.8 US$ per tonne of CO_2. Therefore, the quantity of 2217.6 tonnes will be used in the evaluation.

3.7.2 Fiscal System Modeling

In Australia, for primary production license, the royalty rate is typically fixed at 10% of the wellhead value, and for a secondary production license, it is 12.5% of the wellhead value (*Petroleum Royalties*, 2025). In the case of the Poseidon field, the royalty of 10% will be used. In order to guarantee that Australians profit from oil and gas, the Petroleum Resource Rent Tax was implemented in 1988. Originally intended for oil production, it is now mostly used in offshore gas fields.It imposes a 40% tax on rents associated with the extraction of natural resources, such as condensate, gas, and petroleum, called a "resource rent tax" (Gittins, 2024).

3.7.3 Economic Indicator Calculation

The crucial parameters that determine the project profitability are NPV, IRR, and Payback. To perform the calculations, the CashFlow model is presented in Appendix 1. The NPV of a project, assuming the discount rate of 10% (Glossary | Practical Law - Legal Resources & Know-How for Professionals, n.d.), was calculated to be approximately 516.6 MM$, the IRR is 12%, and the payback period is roughly 2 years. The field development project's aim is to maintain pressure stability, increase the oil and gas recovery, and increase the project's profitability. The technical solution was to choose a 5-spot pattern, which implies drilling 2 new production wells and 1 new injector well to existing 2 production wells. The oil and gas production rates stabilized and increased significantly. The additional economical assessment highlighted the benefits of the chosen development plan, the original NPV is nearly 355.7 MM$. As a result, not only the NPV rises, but also the field's life is extended. Moreover, oil and gas firms use IRR as a valuable tool to evaluate a project's financial viability, because it helps to assess risk and compare various investment options. As the IRR is nearly 12%, the project's risk can be classified as moderate-risk because it is in a range of 10-15% (*What Is a Good IRR in Real Estate?*, n.d.). The payback period is two years, and an investment gets more appealing the shorter the payback period (Kagan, 2025).

Sensitivity Analysis

To determine the factors affecting the NPV, the sensitivity analysis was conducted (**Table 21**). The parameters that were tested are the oil and gas prices, capital and operating expenditures. From the analysis, it was found that the most crucial element in the case of the Poseidon field is the gas price changes (**Figure158**). That is because the major product is natural gas, and the price under which the gas will be sold is a factor that determines the profitability of the project. Although, it is clear that the decrease of expenses would positively affect the project.

Table 21. Sensitivity Analysis for NPV

Variation,%	Oil Price	Gas Price	CAPEX	OPEX
-30	515.38	416.81	516.74	518.27
-20	515.77	450.06	516.68	517.7
-10	516.16	483.31	516.62	517.13
0	516.74	516.74	516.74	516.74
+10	517.35	549.81	516.5	515.99
+20	516.95	583.05	516.44	515.42
+30	517.74	616.3	516.38	514.85

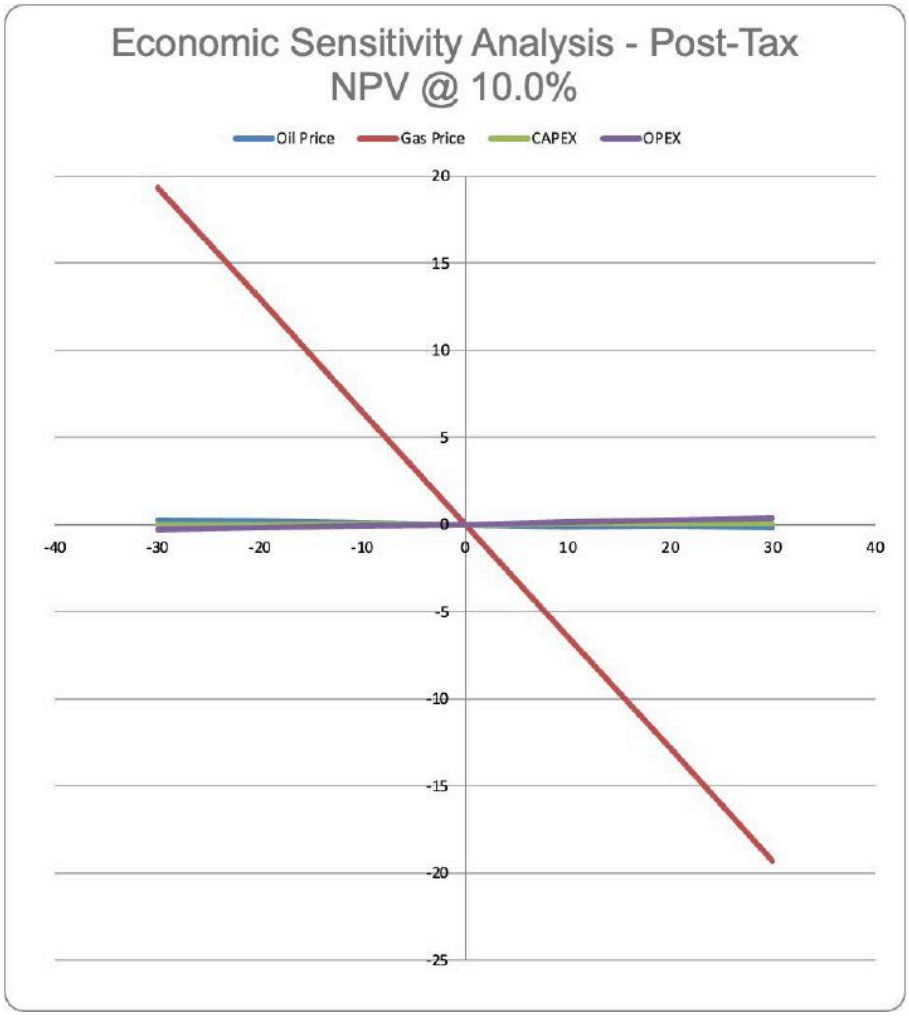

Figure 157. *The NPV sensitivity chart.*

3.8 Health, Safety, and Environment (HSE)

3.8.1 Australian Commonwealth

Australia Offshore Petroleum and Greenhouse Gas Storage Act 2006 Titleholders are responsible for the upkeep and disposal of buildings, machinery, and other property purchased onto their title under Section 572 of the OPGGS Act (*Legislation and Regulation | NOPSEMA*, n.d.). According to Section 572 (3): All buildings, equipment, and other property that are not being used or intended for use in connection with the operations that the titleholder is or will be involved in, as well as those that are permitted by the permit, lease, license, or authority, must be removed from the title area by the titleholder.

Established under the OPGGS Act, NOPSEMA is the independent legislative entity that oversees environmental management, structural well integrity, and health and safety for offshore petroleum.

Environment Plans (EPs) must be submitted by titleholders to NOPSEMA. Before they can begin any operation, including exploration, production, and decommissioning, they must have that EP approved by NOPSEMA. Every five years, these strategies must be updated and altered.

Titleholders may request an exception from the property removal requirement. NOPSEMA evaluates this on an individual basis. In certain situations, where equal or advantageous environmental outcomes can be obtained while satisfying safety and all other relevant requirements under the OPGGS Act and regulations, as well as other applicable laws, titleholders may be permitted to leave property in-situ rather than remove it.In these situations, an environment plan must demonstrate that the suggested arrangement complies with the concepts of ecologically sustainable development and lowers environmental impacts and risks to the lowest level that is both acceptable and reasonably achievable.

3.8.2 Sea Dumping

The following are governed by the Environment Protection (Sea Dumping) Act of 1981(*Sea Dumping - DCCEEW*, 2024):

- the loading and disposal of rubbish at sea
- any artificial reef construction in Australian waters.

The Environment Protection (Sea Dumping) Act of 1981 governs the disposal of carbon dioxide (CO 2) at sea through carbon capture and sequestration (CCS). Emissions from industrial sectors that are difficult to mitigate could be decreased by offshore CCS. In industrial processes, CO_2 is compressed and isolated from other gases. Submerged geological formations may then be able to hold an appropriate CO_2 stream.

Australia's waters are protected from pollution and garbage that is deposited at sea under the Sea Dumping Act. A sea dumping permission can also be required if a titleholder wants to dump or abandon oil and gas infrastructure in-situ. The Minister of Environment and Water has the last say over whether to approve or deny a request to dump or abandon assets and infrastructure in accordance with the Sea Dumping Act.

3.8.3 Preservation of the Environment and Biodiversity

The primary environmental law of the Australian Government is the Environment Protection and Biodiversity Conservation Act 1999 (*Environment Protection and Biodiversity Conservation Act 1999 (EPBC Act) - DCCEEW*, 2025). NOPSEMA's procedure was approved by the Environment and Water Minister as a program that satisfies part 10 of the EPBC Act.

Additionally, the minister approved all measures that adhere to the program that NOPSEMA has adopted, avoiding the requirement for these acts to be evaluated individually under the EPBC Act.With a few exceptions, all petroleum and greenhouse gas operations are covered by the class approval.Decommissioning operations in Commonwealth waters are one of the actions discussed. If there is a chance that an issue of national environmental significance will

be impacted, the EPBC Act is applicable. Activities that take place outside the title area can still need a referral if they are not covered by NOPSEMA's program or expected to significantly affect an issue of national environmental significance.

3.8.4 International Regulations

London Convention and Protocol: The 1972 Convention on the Prevention of Marine Pollution by Dumping of Wastes and Other Matters has been updated as the London Protocol. This treaty was ratified by Australia in 1981 with the Sea Dumping and Environmental Protection Act of 1981. The London Protocol seeks to prevent, lessen, and eradicate pollution brought on by the disposal of garbage or other materials at sea, as well as to safeguard and maintain the maritime environment from all sources of pollution.

The Basel Convention: An international agreement known as the Basel Convention on the Control of Transboundary Movements of Hazardous Waste guarantees that hazardous waste is handled properly. In 1992, Australia ratified the treaty. Through the Hazardous Waste (Regulation of Exports and Imports) Act 1989 ((*Hazardous Waste (Regulation of Exports and Imports) Act 1989 - DCCEEW*, 2021), it was included into domestic law. In order to export from, import into, and transport garbage through Australia, organizations must acquire a permission.

The Minamata Convention: An international agreement known as the Minamata Convention on Mercury aims to safeguard the environment and public health from anthropogenic (produced by humans) discharges and emissions of mercury and mercury compounds. The Minamata Convention was ratified by Australia in 2021.

Convention of Hong Kong: Effective June 26, 2025, the Hong Kong Convention for the Safe and Environmentally Sound Recycling of Ships will come into effect. The Convention has not yet been ratified by Australia.

Additional treaties and conventions: The United Nations Convention on the Law of the Sea and Australia's bilateral treaties with nations like Indonesia and Timor-Leste are two other conventions and treaties that will have an impact on decommissioning.

3.8.5 Safety of Workers During Offshore Decommissioning

With a solid track record, NOPSEMA is Australia's independent expert safety regulator for offshore resources operations(*Decommissioning | NOPSEMA*, n.d.). However, in a high-risk sector, offshore decommissioning is a relatively new business. The first and most crucial step in creating a sustainable decommissioning sector in Australia is ensuring the safety of our employees along the value chain is our top responsibility.

By strengthening worker rights against discrimination and coercion and broadening the meaning of health in Australia's offshore legislation to encompass both physical and psychological health, the Australian Government is putting improvements into our offshore safety frameworks.

Additionally, the government will enhance reporting requirements for sexual harassment by amending current safety regulations. The Australian Government will make sure that our current offshore safety measures continue to be functional as part of its dedication to continuously enhancing them. In order to achieve comparable or better safety outcomes, especially for people working on decommissioning, this entails seeking out additional possibilities to harmonize the offshore petroleum safety regime with our national Work Health and Safety legislation.

3.8.6 Activities

The Australian Government will keep examining the country's offshore safety frameworks to find ways to harmonize with national work health and safety regulations, where applicable, in order to support the development of a competent, secure, and diversified decommissioning workforce. Furthermore, the creation of a decommissioning workforce by offering counsel and direction on skills, workforce opportunities, and barriers. To guarantee that skills needs are met when necessary, assist the decommissioning sector and workforce in connecting to already-existing employment and skills initiatives, like employment and Skills Councils (Department of Industry, Science and Resources, 2024).

Part 4: Conclusion

This capstone project provided an integrated Field Development Plan (FDP) for the Poseidon offshore gas-condensate field in the Browse Basin, Western Australia. The multidisciplinary FDP encompasses geological, petrophysics, reservoir, production, drilling, economic and environmental analyses to obtain an integrated and technically valid development strategy while being economically feasible.

Geological and petrophysical characterisation, plus interpretation of 3D seismic and well log data defined the Plover Formation as the main reservoir "objective". The reservoir is characterised by its moderate porosity (8–18%) and heterogeneous permeability (10–200 mD). Reservoir "compartmentalisation" by faulting has been a big issue that had to be tackled using detailed static and dynamic modelling.

A fullfield static model of the gas reservoir was created in Petrel by integrating well data with the seismic attribute and stratigraphic model. The static model was upscaled and exported to CMG GEM simulator for dynamic simulation. Several production scenarios were considered to evaluate the field performance, including natural depletion and separate injection of CO_2. The results demonstrate that the five-spot well configuration provides substantial pressure support and substantially increases gas recovery. Dynamic simulation results provided insights into reservoir performance with varying operating constraints. These results enabled better decision-making for field development.

Drilling and completion plans were developed based on operational experience from previous wells. Casing program was developed to counter wellbore instability and high-pressure gradients. The use of synthetic-based muds and pressurized drilling systems was suggested to eliminate subsurface uncertainties.

Production rate Performance was evaluated using nodal analysis from PIPESIM. Production performance evaluation allows Production performance evaluation step to consider optimization of inflow/outflow parameters and surface facility design before Oil economic point. Profitability of a project is considered to be one of the main concerns of a prospect development.

With forecast models and fiscal system simulation, economic analysis could be evaluated. Based on the economic results, the commerciality of development projects can therefore be determined. Furthermore, Index of

Health, Safety and Environmental (HSE) considerations were aligned to meet Australian offshore regulatory requirements to ensure safe and sustainable development.

In conclusion, this project has shown that with technical analysis integrated alongside digital modelling tools and strategic planning, the development of the Poseidon gas field is possible despite a geologically challenging environment. The results of the work undertaken in this project are meaningful to future field development endeavours by providing a transferrable methodology that can be applied to offshore gas assets in a broad range of analogous settings.

References

AAPG Wiki. (n.d.). *Quick-look lithology from logs*. https://wiki.aapg.org/Quick-look_lithology_from_logs

Adebayo, B., Abdullah, W. H., & Abubakar, A. (2021). Seismic attributes for hydrocarbon detection and reservoir characterization: A case study from Poseidon Field, Northwestern Australia. Retrieved from https://www.researchgate.net/publication/356892170

Akpe, N. a. T., Nuan, N. S. I., Solanke, N. B., & Iriogbe, N. H. O. (2024). Development and implementation of cost control strategies in oil and gas engineering projects. *Global Journal of Advanced Research and Reviews*, *2*(1), 001–022. https://doi.org/10.58175/gjarr.2024.2.1.0028

Baker, R. (2004). Well logging. In C. J. Cleveland (Ed.), *Encyclopedia of Energy.*

Baker, R. O., Yarranton, H. W. & Jensen, J. L. (2015). Openhole well logs—Log interpretation basics. In *Practical Reservoir Engineering and Characterization* (Section 9.2.7, Resistivity Log). Gulf Professional Publishing.

Blevin, J.E., Boreham, C.J., Summons, R.E., Struckmeyer, H.I.M. and Loutit, T.S. (1998). An effective Early Cretaceous petroleum system on the North West Shelf: evidence from the Browse Basin. In: Purcell, P.G. and R.R. (eds) The Sedimentary Basins of Western Australia 2. Proceedings of Petroleum Exploration Society of Australia Symposium, Perth, WA, 397-420.

Brent oil futures historical prices - Investing.com. (n.d.). Investing.com. https://www.investing.com/commodities/brent-oil-historical-data

Cheng, F., & Zhao, J. (2019). 29th European Symposium on Computer Aided Process Engineering. *Computer Aided Chemical Engineering, 46*, 2473–2478.

ConocoPhillips. (2024). Boreas-1 Well Test Interpretation, Browse Basin, WA-315-P Permit. Internal FDP report.

Decommissioning NOPSEMA. (n.d.). https://www.nopsema.gov.au/offshore-industry/decommissioning

Department of Industry, Science and Resources. (2024). *Australia's offshore resources decommissioning roadmap*. Commonwealth of Australia. https://www.industry.gov.au/sites/default/files/2024-12/australias-offshore-resources-decommissioning-roadmap.pdf

Dixit, A., & Mandal, A. (2020). Detection of gas chimney and its linkage with deep-seated reservoir in Poseidon, NW Shelf, Australia from 3D seismic data using multi-attribute analysis and artificial neural network approach. *Journal of Natural Gas Science and Engineering, 83*, 103586. https://doi.org/10.1016/j.jngse.2020.103586

Dixit, A., Mandal, A., & Ganguli, S. S. (2024). Reservoir heterogeneity analysis using multi-directional textural attributes from deep learning-based enhanced acoustic impedance inversion: A study from Poseidon, NW shelf Australia. *Energy Geoscience*, 5(2), 100235. https://doi.org/10.1016/j.engeos.2023.100235

Dong, X., He, Z., & Tang, H. (2020). Detection of hydrocarbon-saturated reservoirs in a challenging geological setting. Elsevier Pure. Retrieved from https://squ.elsevierpure.com/ar/publications/detection-of-hydrocarbon-saturated-reservoirs-in-a-challenging-ge

Environment Protection and Biodiversity Conservation Act 1999 (EPBC Act) - DCCEEW. (2025, February 5). https://www.dcceew.gov.au/environment/epbc

Fanchi, J. R. (2010). Density logs. In *Integrated Reservoir Asset Management*. Elsevier.

Farfour, M., & Foster, D. (2022). Detection of hydrocarbon-saturated reservoirs in a challenging geological setting using AVO attributes: A case study from Poseidon field, offshore northwest region of Australia. *Journal of Applied Geophysics, 203*, 104687. https://doi.org/10.1016/j.jappgeo.2022.104687

Farfour, M., & Foster, D. (2022). Machine learning and seismic attributes for prospect identification and risking: An example from offshore Australia. *Paper presented at the SEG/AAPG International Meeting for Applied Geoscience & Energy*, Houston, Texas, USA, August 2022. https://doi.org/10.1190/image2022-3752064.1

Farfour, M., El-Ghali, M. A. K., Gaci, S., Moustafa, M. S. H., & Siddiqui, N. A. (2021). Seismic attributes for hydrocarbon detection and reservoir characterization: A case study from Poseidon field, Northwestern Australia. Arabian Journal of Geosciences, 14, 2814. https://doi.org/10.1007/s12517-021-06557-x

Gambella, C., Ghaddar, B., & Naoum-Sawaya, J. (2021). Optimization problems for machine learning: A survey. *European Journal of Operational Research, 290*(3), 807–828.

Ganat, T. a. O. (2020). Technical guidance for petroleum exploration and production plans. In *SpringerBriefs in applied sciences and technology*. https://doi.org/10.1007/978-3-030-45250-6

Gitman, L. J. 2003. Principles of Managerial Finance: Brief. 3rd ed. Pearson Education Inc., Boston, MA.

Gittins, Y. W. (2024, April 30). *What is the PRRT?* The Australia Institute. https://australiainstitute.org.au/post/what-is-the-prrt/

Glossary | Practical Law - Legal Resources & Know-How for Professionals. (n.d.). https://content.next.westlaw.com/Glossary/PracticalLaw/I6d0564ec909811ebbea4f0dc9fb69570?transitionType=Default&contextData=(sc.Default)

Guha, B., & Bandyopadhyay, G. (2016). Gold price forecasting using ARIMA model. *Journal of Advanced Management Science, 4*(2), March

Hazardous Waste (Regulation of Exports and Imports) Act 1989 - DCCEEW. (2021, October 3). https://www.dcceew.gov.au/environment/protection/hazardous-waste/about#:~:text=The%20main%20purpose%20of%20the,Australia%2C%20are%20protected%20from%20the

Investing.com. (n.d.). *Natural gas historical data*. Investing.com. https://www.investing.com/commodities/natural-gas-historical-data

Islam, M., Babikir, I., Elsaadany, M., Elkurdy, S., Siddiqui, N. A., & Akinyemi, O. D. (2023). Application of a pre-trained CNN model for fault interpretation in the structurally complex Browse Basin, Australia. *Applied Sciences, 13*(20), 11300. https://doi.org/10.3390/app132011300

Kagan, J. (2025, April 5). *Payback Period: Definition, Formula, and calculation*. Investopedia. https://www.investopedia.com/terms/p/paybackperiod.asp

Khan, M., Bery, A. A., Ali, S. S., Awfi, S., & Bashir, Y. (2024, February). Unlocking reservoir potential: Machine learning-driven prediction of reservoir properties and sweet spots identification. Paper presented at the International Petroleum Technology Conference, Dhahran, Saudi Arabia. Paper Number: IPTC-23557-MS. https://doi.org/10.2523/IPTC-23557-MS

Khan, M. I., & Islam, M. R. (2007). Types of well logging. In *Reservoir Engineering and Secondary Recovery*. In *The Petroleum Engineering Handbook: Sustainable Operations* (Section 6.3.1). Gulf Professional Publishing.

Kotu, V., & Deshpande, B. (2019). Regression Methods. In *Data Science* (2nd ed., pp. 153–180). Elsevier.

Kundu, S. N. (2023). *Geoscience for petroleum engineers*. Springer Nature Singapore. https://doi.org/10.1007/978-981-19-7640-7

Kuske, T., Le Poidevin, S., & Edwards, D. (2015). Browse Basin petroleum accumulations. *The APPEA Journal, 55*, 463. https://doi.org/10.1071/AJ14098

Lea, J. F., Jr., & Rowlan, L. (2019). Introduction. In *Gas Well Deliquification* (3rd ed.). Elsevier.

Le Poidevin, S. R., Kuske, T. J., Edwards, D. S. and Temple, P. R. 2015. Australian Petroleum Accumulations Report 7 Browse Basin: Western Australia and Territory of Ashmore and Cartier Islands adjacent area, 2nd edition. Record 2015/10. Geoscience Australia, Canberra. http://dx.doi.org/10.11636/Record.2015.010

Legislation and regulation | NOPSEMA. (n.d.). https://www.nopsema.gov.au/about/legislation-regulation-and-compliance

Natural gas futures historical prices - Investing.com. (n.d.). Investing.com. https://www.investing.com/commodities/natural-gas-historical-data

Nazlan, D. (2016, June 26). Six KO Rules to Easily Detect Oil, Gas, and Water from Well Log. *LinkedIn*.

Neal, P. R., Hou, W., Allinson, W. G., & Cinar, Y. (2010). Costs of CO_2 transport and injection in Australia. *SPE Asia Pacific Oil and Gas Conference and Exhibition*. https://doi.org/10.2118/133900-ms

Niță, C. C., Mariș, I., Munteanu, I., & Lazăr, C. (2023). Upper Eocene - Lower Oligocene stratigraphic plays in the Caswell Sub-Basin, Browse Basin (Australia). An attempt to identify new hydrocarbon reserves in a mature petroleum province. *Faculty of Geology and Geophysics, University of Bucharest; Sabba S. Ştefănescu Institute of Geodynamics of the Romanian Academy; National Institute of Marine Geology and Geo-Ecology (GeoEcoMar)*. DOI: 10.5281/zenodo.10254816

Noureldien, D. M., & Merghany, I. (2015). *Static Model QC: Technical Aspects and Practice from A to Z.* Paper presented at the SPE North Africa Technical Conference and Exhibition, Cairo, Egypt. https://doi.org/10.2118/175825-MS

Offshore drilling rigs market demand and future scope including top key players – Oil & Gas 360. (2020, March 27). https://www.oilandgas360.com/offshore-drilling-rigs-market-demand-and-future-scope-including-top-key-players/

Ogeer, N. (2022). *Field development plans: A handbook for government officials*. Commonwealth Secretariat. https://www.thecommonwealth.org

Oil & Gas Authority. (2020). *UKCS unit operating costs in 2020*. Oil & Gas Authority.https://www.nstauthority.co.uk/media/p3ed5ezn/ukcsunitoperatingcostin2020.pdf

PengTools. (n.d.). *Well Nodal Analysis*. Retrieved from https://wiki.pengtools.com/index.php?title=Well_Nodal_Analysis

Petroleum royalties. (2025, March 24). Western Australian Government. https://www.wa.gov.au/organisation/department-of-energy-mines-industry-regulation-and-safety/petroleum-royalties#:~:text=the%20Commonwealth%20website-,Royalty%20rates,for%20a%20secondary%20production%20licence.

Sea dumping - DCCEEW. (2024, August 5). https://www.dcceew.gov.au/environment/marine/sea-dumping

ScienceDirect. (n.d.). Resistivity log. In *Engineering Topics*.

Singh, H., et al. (2020). CO_2 enhanced gas recovery and sequestration in depleted gas reservoirs. *Journal of Natural Gas Science and Engineering*. Retrieved from https://www.sciencedirect.com/science/article/pii/S0920410520307518

Singh, H., et al. (2020). CO_2 enhanced gas recovery and sequestration in depleted gas reservoirs. Journal of Natural Gas Science and Engineering. Retrieved from https://www.sciencedirect.com/science/article/pii/S0920410520307518

Smyth, J., Bott, I., & McCormick, M. (2024, November 18). Offshore oil is back. At what cost? *Financial Times*. https://www.ft.com/content/5c49e3f6-474d-4fae-bcf4-7562e127e911

Wang, Y., et al. (2009). Spot Pattern - an overview. *ScienceDirect Topics*. Retrieved from https://www.sciencedirect.com/topics/engineering/spot-pattern

Ward, C. R. (2003). Neutron logging. In *Encyclopedia of Physical Science and Technology* (3rd ed.). Elsevier.

What is a good IRR in real estate? (n.d.). https://www.hellodata.ai/help-articles/what-is-a-good-irr-in-real-estate#:~:text=There%20isn't%20a%20one,look%20for%20an%20IRR%20higher

Whitson Wiki. (n.d.). *Constant composition expansion (CCE)*. https://wiki.whitson.com/phase_behavior/pvt_exp/CCE/

Yeturu, K. (2020). Principles and Methods for Data Science. *Handbook of Statistics, 43*, 123–157.

Zhang, X., et al. (2024). Research on CO_2 injection for water control and enhanced nature gas recovery. *Journal of Petroleum Science and Engineering*. Retrieved from https://www.sciencedirect.com/science/article/abs/pii/S2949891024008765

Zou, C. (2013). Oil and gas in metamorphic reservoirs. In *Unconventional Petroleum Geology*. Elsevier.

Appendices

Appendix 1. Model Calculation

Year, t	Year	Oil Production (barrel)	Oil Price ($/barrel)	Total Oil Revenue (MM$)	Annual Gas Production (MMbtu)	Natural Gas Price $/MMBtu	Total Gas Revenue (MM$)	Total Revenue (MM$)	TOTAL CAPEX (MM$)	OPEX Injection CO2(MM$)	General OPEX (MM$)	Total OPEX (MM$)	Operating Income (MM$)	Royalty (MM$)	PRPT (MM$)	EBIT (MM$)	NET INCOME (MM$)	DISCOUNTED CASH FLOW (MM$)
0	2025	25	66.908	0.001689257784	2129.616182	2.189	0.004661729822	0.006350987606	870.2121		0.00	0.00	-870.21	0.00	-348.08	-870.21	-522.12	-522.12
1	2026	921,507	67.292	62.01008225	77728863.48	2.986	232.0983864	294.1084686			20.30	20.30	273.81	29.41	97.76	273.81	146.64	133.31
2	2027	921,533	66.013	60.83314083	77730993.1	2.933	227.9850028	288.8181436			21.07	21.07	267.75	28.88	95.55	267.75	143.32	118.45
3	2028	921,533	65.604	60.45622749	77730993.1	2.528	196.5039506	256.9601781			21.84	21.84	235.12	25.70	83.77	235.12	125.65	94.40
4	2029	924,057	65.106	60.16168185	77943936.26	2.991	233.1303133	293.2919952			22.67	22.67	270.62	29.33	96.52	270.62	144.77	98.88
5	2030	921,533	64.617	59.54667477	77731011.17	2.735	212.6720466	272.2187213			23.39	23.39	248.83	27.22	88.64	248.83	132.97	82.56
6	2031	148,960	64.219	9.566062097	12564730.57	2.539	31.90185092	41.46791302		0.06	3.90	3.97	37.50	4.15	13.34	37.50	20.01	11.30
7	2032	694,306	63.808	44.30226368	58564428.29	2.605	152.5803357	196.8825994		0.06	18.78	18.85	178.01	19.69	63.33	178.01	95.00	48.75
8	2033	921,533	63.411	58.43530641	77731011.17	2.603	202.3338221	260.7691285		0.06	25.70	25.76	235.01	26.08	83.57	235.01	125.36	58.48
9	2034	924,057	63.006	58.2211489	77943954.33	2.469	192.4436232	250.6647721		0.06	26.55	26.61	224.05	25.07	79.59	224.05	119.39	50.63
10	2035	921,533	62.611	57.69808029	77730938.88	2.317	180.1025854	237.8006657		0.06	27.24	27.30	210.50	23.78	74.69	210.50	112.03	43.19
11	2036	921,533	62.267	57.38107306	84332863.49	2.467	208.0491742	265.4302473		0.06	28.02	28.08	237.35	26.54	84.32	237.35	126.48	44.33
12	2037	921,533	61.864	57.00969541	71129158.86	2.612	185.7893629	242.7990584		0.06	28.78	28.85	213.95	24.28	75.87	213.95	113.80	36.26
13	2038	924,058	61.504	56.83326332	77943918.18	2.757	214.8913824	271.7246457		0.06	29.64	29.71	242.02	27.17	85.94	242.02	128.91	37.34
14	2039	921,533	61.155	56.35632877	77731011.17	2.87	223.0880021	279.4443308		0.06	30.33	30.39	249.05	27.94	88.44	249.05	132.66	34.93
15	2040	921,533	60.805	56.03379234	77731011.17	2.944	228.8400999	284.8738892		0.06	31.11	31.17	253.70	28.49	90.09	253.70	135.13	32.35
16	2041	921,532	60.479	55.73332515	77731011.17	2.836	220.4451477	276.1784728		0.06	31.98	32.05	244.13	27.62	86.61	244.13	129.91	28.27
17	2042	924,058	60.163	55.59410154	77943918.18	2.733	213.0207284	268.6148299		0.06	32.74	32.80	235.81	26.86	83.58	235.81	125.37	24.80
18	2043	921,533	59.86	55.16294399	77730938.88	2.667	207.308414	262.471358		0.06	33.42	33.48	228.99	26.25	81.10	228.99	121.65	21.88
19	2044	921,533	59.567	54.89293493	77731083.47	2.721	211.5062781	266.399213		0.06	34.19	34.26	232.14	26.64	82.20	232.14	123.30	20.16
20	2045	921,533	59.294	54.64135652	77730938.88	2.746	213.4491582	268.0905147		0.06	34.96	35.02	233.07	26.81	82.50	233.07	123.78	18.40